

QC852
.C6
no. 457
ARCHIVE

RELATIONSHIPS BETWEEN TROPICAL CYCLONE DEEP CONVECTION AND THE RADIAL EXTENT OF DAMAGING WINDS

by Daniel N. Shoemaker

LIBRARIES
NOV 17 1989
COLORADO STATE UNIVERSITY

P.I.-William M. Gray

**Colorado
State
University**

**DEPARTMENT OF
ATMOSPHERIC SCIENCE**

PAPER NO.
457

RELATIONSHIPS BETWEEN TROPICAL CYCLONE
DEEP CONVECTION AND
THE RADIAL EXTENT OF DAMAGING WINDS

By
Daniel N. Shoemaker

Department of Atmospheric Science
Colorado State University
Fort Collins, CO 80523

October, 1989

Atmospheric Science Paper No. 457

ABSTRACT

The radial extent of damaging winds in tropical cyclones is an important problem for forecasters. With the loss of aircraft reconnaissance data in the NW Pacific, techniques are needed for forecasting these winds using satellite data. This study examines relationships between deep convective clouds (convection) and the radial extent of strong winds in tropical cyclones. Techniques are tested for determining the extent of these damaging winds using infrared data from geostationary satellites. Pixel counts at various infrared temperature thresholds and storm radii are compared with aircraft wind measurements to determine correlations between convection and the radial extent of damaging winds. Twenty-four hour running mean pixel counts for infrared cloud temperatures colder than $-25^{\circ}C$ in the 444 km (4° of latitude) radius area show an apparent correlation with both the mean radial extent and time variation of $15ms^{-1}$ winds (R15). A rapid decrease of deep convection in the 222-444 km ($2-4^{\circ}$) band offers a signal as to when maximum R15 will occur. An empirical rate of decrease of R15 from its maximum value is shown to be present. The average radius of $26ms^{-1}$ (50 knot) winds (R26) is shown to be linearly related to R15. Individual (instantaneous) measurements of convection are shown to be not well correlated with either concurrent R15 values or with time rates of R15 change. Convection asymmetries are shown to be unrelated to asymmetries of R15.

QC852
.26
no. 457
ARCHIVE

TABLE OF CONTENTS

1 INTRODUCTION	1
1.1 Goals	2
1.2 Definitions	2
1.3 Prior Work	3
1.4 Availability of New Data	5
1.5 Limitations	8
1.6 Summary	8
2 DATA	10
2.1 Aircraft Data	10
2.2 Satellite Data	12
2.3 Statistical Analysis Software	18
2.4 Summary	18
3 HYPOTHETICAL RELATIONSHIPS BETWEEN DEEP CONVECTION AND OUTER RADIUS WINDS OF TROPICAL CYCLONES	19
3.1 Convection, Wind and Surface Friction	20
3.2 Convection, R15 and Intensity	25
3.3 Summary	26
4 ASSESSMENT OF DIRECT RELATIONSHIPS BETWEEN CONVECTION AND DAMAGING WINDS	28
4.1 Relationship between R26 and R15	28
4.2 Relationships Between Intense Convection and R15	29
4.3 Relationship of Intensity to R15 and Pixel Counts	39
4.4 Effects of Inertial Stability	44
4.5 Summary	44
5 TEMPORAL ASSOCIATIONS BETWEEN CONVECTION AND THE OCCURRENCE OF MAXIMUM R15	48
5.1 Diagnosing and Forecasting the Time of Occurrence for MR15	48
5.2 Theory of Maximum R15	53
5.3 Forecasting Maximum R15	58
5.4 Forecasting Rules for Maximum R15	61
5.5 Summary	62

6	TIME VARIATION OF R15 IN RELATION TO RATES OF CONVECTION	63
6.1	Convection and R15	63
6.2	Convection and R15 Change	64
6.3	Forecasting R15 Decrease	77
6.4	Specification of R15 from Observations of Intensity and Convection	79
6.5	Summary	81
7	ASSOCIATIONS BETWEEN ASYMMETRIC CONVECTIVE BURSTS AND WIND FIELD ASYMMETRY	86
7.1	Methodology	86
7.2	Significance of Asymmetry	86
7.3	Climatology of Asymmetry	98
7.4	Summary	98
8	SUMMARY AND CONCLUSIONS	104
8.1	Summary	104
8.2	The Future	105

LIST OF SYMBOLS AND ACRONYMS

CIRA = Cooperative Institute for Research in the Atmosphere at CSU

CSU = Colorado State University

GMS = Japanese geostationary meteorological satellite

hP_a = hectopascals (1.0 mb)

hr = Hour

IR = Infrared

Ist = Inertial stability

JTWC = Joint Typhoon Warning Center

km = Kilometers

m = Meters

MOT = Coordinate system with storm motion subtracted from observations.

MSLP = Minimum sea level pressure

NAT = Natural coordinate system—with respect to the fixed Earth.

NWP = Northwest Pacific Ocean Basin

OCS = Outer Core Strength; the average wind speed within a radius extending from 111 to 333 km (or 1-3° of the TC center).

r = Correlation coefficient for linear regression

R15 = Mean radius of 15ms^{-1} (or 30 knot) winds

R26 = Mean radius of 26ms^{-1} (or 50 knot) winds

TC = Tropical Cyclone

Z = Zulu or Greenwich Mean Time (U.T.C.)

Chapter 1

INTRODUCTION

Ocean swells generated by tropical cyclone (TC) winds greatly affect maritime activity. The U. S. Navy has designated sustained winds in excess of 15 meters per second (ms^{-1}) (or 30 knots) as detrimental to shipping. Sustained winds in excess of $26 ms^{-1}$ (50 knots) are considered damaging to onshore military assets. Winds greater than $15 ms^{-1}$ may extend out to 500 kilometers (km) from the center of a large TC and $26 ms^{-1}$ winds may be found outward to 200 km. Therefore, both military and commercial interests are greatly concerned with the observation and forecasting of these potentially destructive winds.

With the loss of aircraft reconnaissance in the Northwest Pacific Ocean (NWP) in 1987, forecasters are now without their best tool for observing the outer wind structure of TCs. Satellite observations are expected to eventually fill the data gaps left by the departure of the aircraft and techniques have long been in place for estimating tropical cyclone intensity (ie., central pressure and maximum sustained wind speed) from satellite data. The most effective of these intensity estimating techniques is Dvorak's (1975) pattern matching procedure wherein the analyst attempts to match cyclone features to descriptive patterns through a decision tree. Attempts to define the outer wind structure, extending from the radius of maximum winds out to approximately 600 km, with satellite data have not had as much success. There is great need for additional research on procedures for estimating the mean radius of $15 ms^{-1}$ (R15) and $26 ms^{-1}$ (R26) winds from satellite data. Wind data from earlier, pre-1987 aircraft reconnaissance missions are used in this study to approximate surface wind profiles which are compared to various satellite derived estimates of convection over different TC radii.

1.1 Goals

The goals of this research include the investigation of possible relationships between convection and the radial extent of strong outer winds of tropical cyclones. The analyses include the development of objective techniques, using the Japanese Geostationary Meteorological Satellite (GMS), for assessing the present value and for forecasting changes of R15 and R26 so that the threat of potentially damaging winds can be managed more effectively.

1.2 Definitions

Convection: Deep convective clouds which extend to near the tropopause levels. Since most cloudiness associated with tropical cyclones is of convective origin, the extensive cirrus shield is also referred to as “convection” in this paper. For the purposes of this paper, all satellite observed cloud areas with infrared temperatures less than 0° C are referred to as “convection”.

Filling: Conditions wherein the minimum central pressure of a tropical cyclone is increasing.

Intensifying: Conditions wherein the minimum central pressure is decreasing and maximum wind speed is increasing, by their relationship.

Intensity: The Minimum Sea Level Pressure (MSLP) measured at the center of the storm in hectoPascals (hPa; equivalent to millibars). Good correlations are observed between the maximum sustained winds and MSLP and these two values are commonly used interchangeably by forecasters. In this paper, MSLP will be used as the index of intensity.

Pixel: The smallest unit of resolution in a satellite image which in this study is approximately 10 x 10 km. A brightness temperature is assigned to each pixel and the number of pixels colder than a given threshold may be referred to as either a pixel count or as a pixel area, since number of pixels times resolution is equivalent to area.

R15: The axially averaged radial extent of 15 ms^{-1} winds, measured from the TC circulation center.

R26: The axially averaged radial extent of 26 ms^{-1} winds, measured from the TC circulation center.

Strengthening: Condition wherein the radial extent of strong winds is increasing.

Weakening: Condition wherein the radial extent of strong winds is decreasing.

1.3 Prior Work

It would be convenient for tropical forecasters if the outer radius wind structure of tropical cyclones were a simple direct function of intensity. However, the relationship between intensity and values of R15 and R26 is not sufficiently reliable to be used for forecasting purposes. Merrill (1982) examined correlations between maximum sustained winds versus the radius of the outer closed isobar (similar to intensity) and obtained values of 0.32 for tropical cyclones in the NWP. Weatherford (1985) obtained correlation coefficients of -0.60 for MSLP versus R15 and -0.16 for MSLP versus R26, using a three year sample (1980-1982) of tropical storms. For the years 1983-1984, these correlation coefficients are -0.73 and -0.58 for intensity versus R15 and R26 respectively (see Figs. 1.1 and 1.2). Hence, approximately one half of the variance (correlation coefficient squared) is explained for R15 and one third for R26 in this sample.

Frank and Gray (1979) used maximum sustained wind data to separate TC intensity values into six categories. The percent of soundings with estimated surface winds greater than 15 ms^{-1} was determined for 111 km (1°) radial increments. Wind data were also stratified into left and right hemispheres (relative to the TC motion vector) and examined for wind asymmetries. Based on the maximum sustained wind values, these storms were divided into tropical storms ($18\text{-}32 \text{ ms}^{-1}$), typhoons ($33\text{-}51 \text{ ms}^{-1}$), and strong typhoons (greater than 51 ms^{-1}). The percent of estimated surface winds greater than 15 ms^{-1} in each hemisphere was determined for 111 km radial increments. A broad variation of the radial distribution of 15 ms^{-1} winds was observed for TCs of similar intensity, again demonstrating that intensity and outer wind extent are not well correlated. Merrill (1982) also encountered wide variations when using rawinsonde composites to derive graphs of the probability for encountering 15 ms^{-1} surface winds at various radii for each of eight

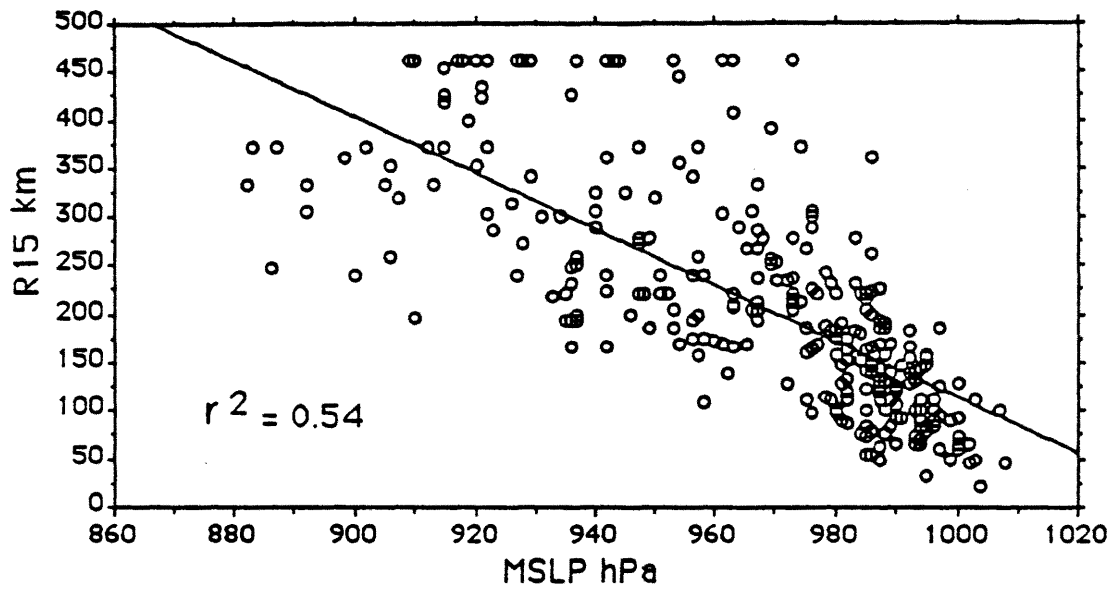


Figure 1.1: Correlation between minimum sea level pressure (MSLP) and mean radius of 15 m s^{-1} winds (R15) for the 1983-1984 storm sample.

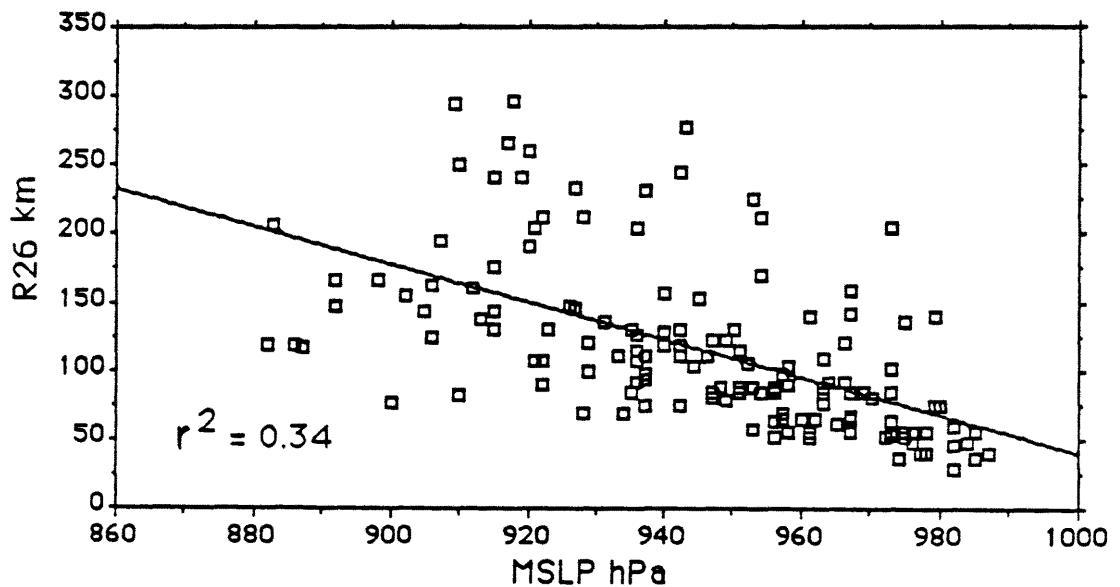


Figure 1.2: Correlation between minimum sea level pressure (MSLP) and mean radius of 26 m s^{-1} winds (R26) for the 1983-1984 storm sample.

octants of both small and large TCs. Forecasters, however, work with individual TCs and composite data do not explain how individual storms will vary from the mean. Hence, forecasters require more objective methods for determining R15 and R26.

In an attempt to relate wind structure to satellite images, Wei and Gray (1989) compared the size of cloud shields to the radial extent of 15 ms^{-1} winds. The use of satellite images for which digital satellite data were not available restricted this early work. Instead, the major and minor axes of heavy cirrus cloud shields near a TC's center were averaged. Although shield size values were not well related to maximum TC wind speeds, a modest correlation between R15 and shield size was observed. This early study showed that there was promise for inferring R15 from satellite based convection data and that these relationships should be examined further. An illustration of what Wei and Gray encountered is shown in Figs. 1.3 and 1.4. Both of these typhoons are of similar intensity, approximately 955 hPa. Whereas Typhoon Orchid (November, 1983) had an R15 value of 300 km, Typhoon Agnes (November, 1984) had an R15 of 160 km. Note the much larger overall cloud shield of Typhoon Orchid, especially for the more intense inner convective areas, as compared to Typhoon Agnes.

1.4 Availability of New Data

Infrared (IR) images taken every three hours from the Japanese Geostationary Meteorological Satellite (GMS) are now available in a digitized format which allows researchers to quickly process these data for specific needs. For example, infrared images could be enhanced (Figs. 1.3 and 1.4) and images could be animated through display of time sequences. In addition, objective, quantitative information can be extracted from digital images. Prior to this time, data images were stored on film or paper and had to be visually interpreted. Temperature thresholds could only be estimated approximately and there was no capability for reprocessing the images. Detailed descriptive information on the GMS satellite data set can be found in the World Climate Programme (1985). The present study emphasized quantifying the cloud shield as pixel counts colder than various temperature thresholds and looking for relationships with outer wind radii. One pixel

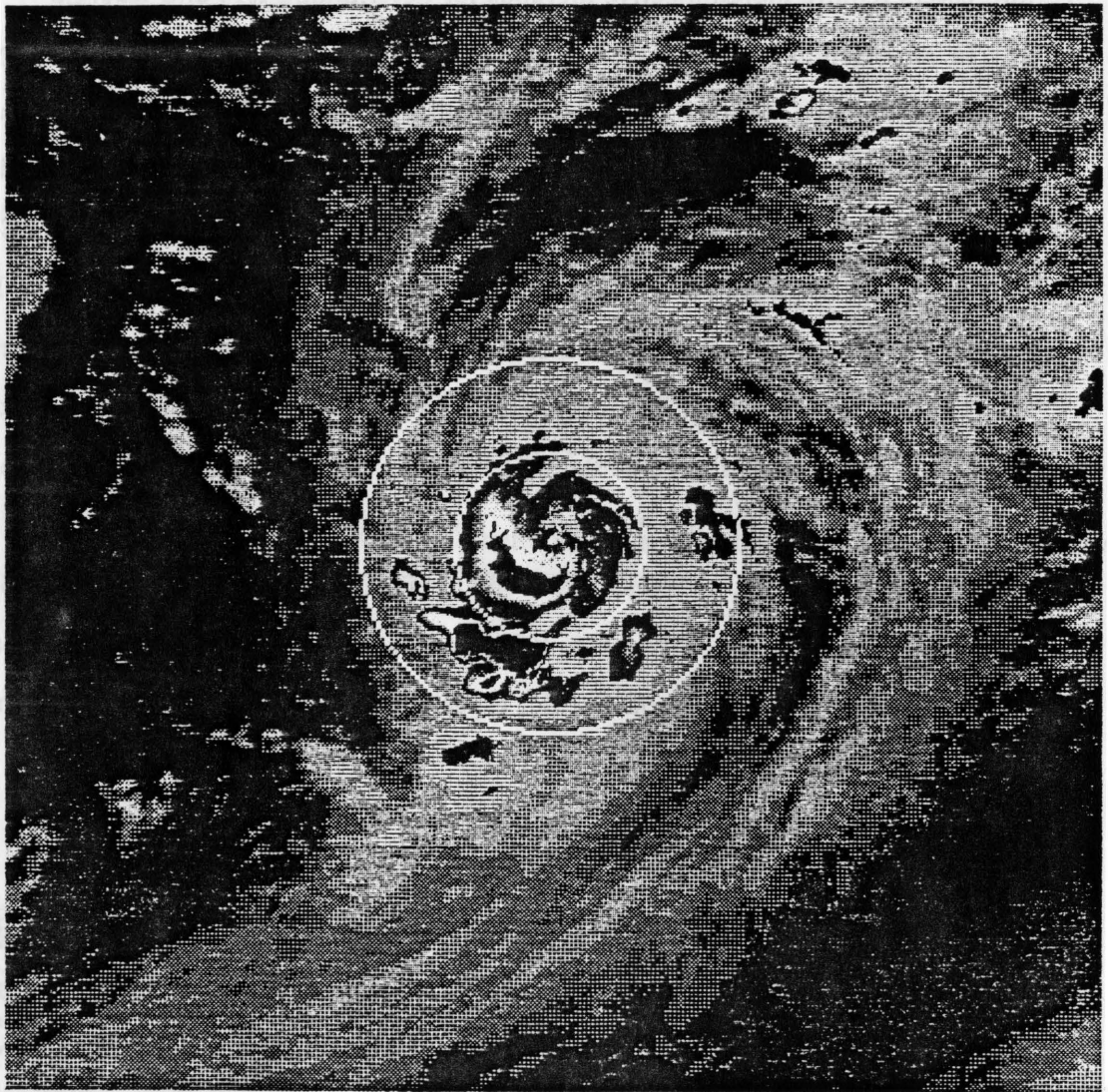


Figure 1.3: The very extensive cloud shield of Typhoon Orchid (November 1983) when (compare to Typhoon Agnes in Fig. 1.4) R_{15} was 300 km. The circles superimposed on the image are at 222 and 444 km (equivalent to 1° and 2° of latitude) from the TC center. Temperature cutoff values for the inner (dark) and surrounding enhanced areas are -80° and -65°C , respectively.

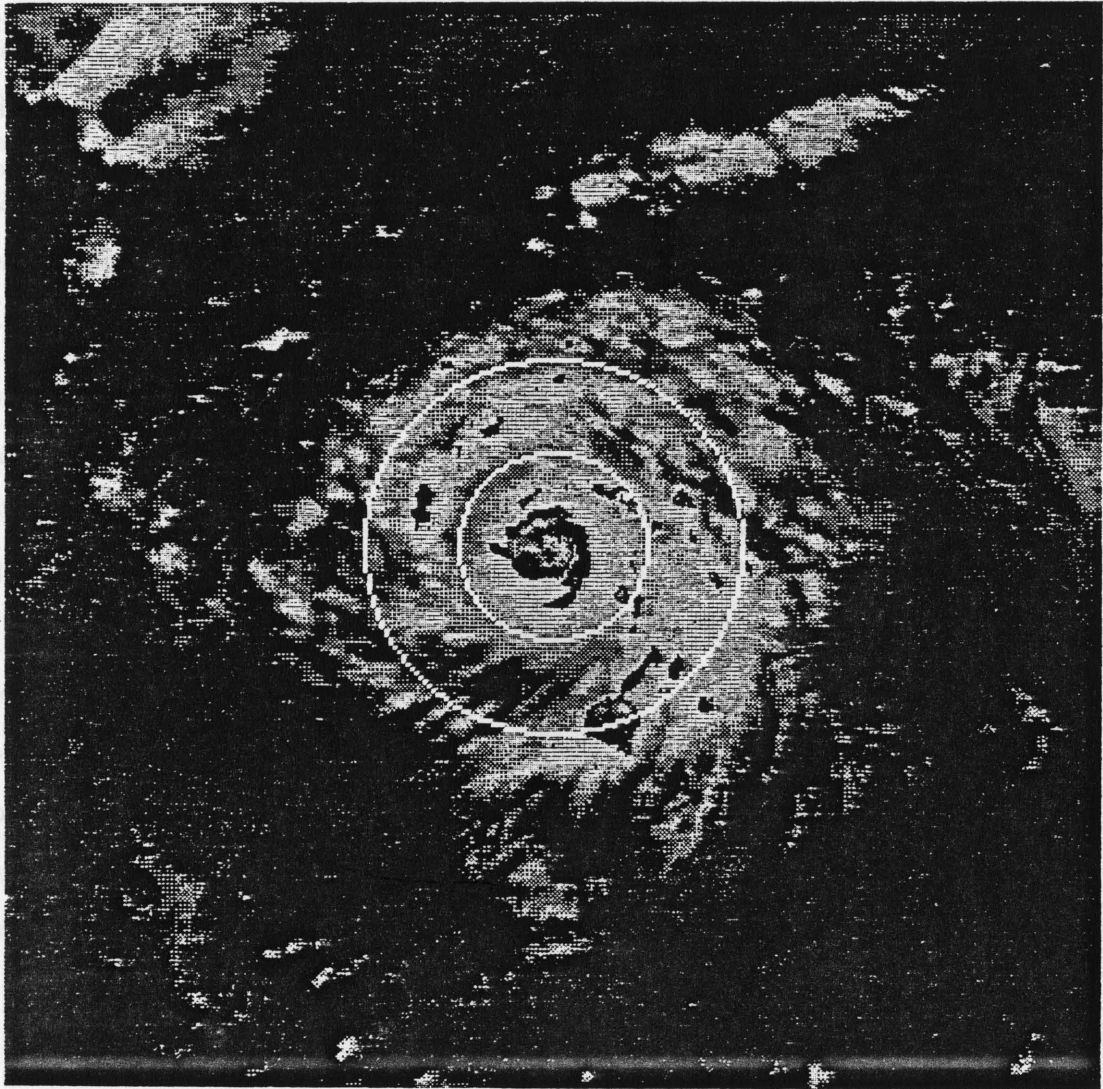


Figure 1.4: The cloud shield for Typhoon Agnes (November 1984) when R15 was 160 km. Both Agnes as shown here and Orchid in Fig. 1.3 had MSLP values of approximately 955 hPa.

was equal to approximately 100 square km. The number of pixels colder than a specified threshold is equivalent to the total cloud area colder than that threshold. The actual area can be determined by multiplying the pixel count by the pixel resolution. To emphasize this relationship, the number of pixels or “pixel count” will be used interchangeably with the term “pixel area”.

Aircraft reconnaissance observations were also available for constructing radial profiles of TC winds. These aircraft observations had been previously processed and archived digitally. The availability of both aircraft and satellite data sets allowed this research to be done.

1.5 Limitations

Two years of concurrent aircraft and satellite data were available for this study. Although aircraft measurements have been processed for the period of 1980-1985, satellite data only became available beginning with 1983 and, at the time of this study only the years 1983 and 1984 were available for research purposes. Consequently, the available data set consisted of approximately 2500 satellite images and 400 aircraft missions.

The aircraft data were taken primarily at the 700 hPa level and extrapolated to estimate values at the surface. The extrapolation procedure introduces some error into surface wind values for those cases wherein the TC is undergoing unusual shear conditions. In these few cases, flight level winds may not be precisely representative of the surface winds. However, without aircraft wind data there are no accurate methods for determining wind profiles for individual storms.

1.6 Summary

The intensity of tropical cyclones (MSLP) is not well correlated with the radial extent of damaging winds. At present there are no accurate methods for either diagnosing or forecasting R15 and R26 without aircraft reconnaissance. Previous studies have shown approximate climatological relationships between intensity and radial extent of damaging winds but these methods do not reliably explain deviations of individual storms from the

mean. Wei and Gray (1989) obtained a relationship between the size of the cloud shields of tropical cyclones and radial wind extent. New technology should now be applied to expand on this concept. This study was undertaken to search for possible relationships between convection and the extent of damaging winds so that refined techniques could be developed and applied operationally by forecasters at the Joint Typhoon Warning Center (JTWC) on Guam. This study could only have been done in the Northwest Pacific because aircraft reconnaissance measurements were routinely made out to 444 km (4° latitude or 250 nautical miles) on tracks extending to the NW, NE, SW and SE (see Fig. 1.5). Similar aircraft measurements in the Atlantic typically do not extend past 222 km (2°) radius from the cyclone centers.

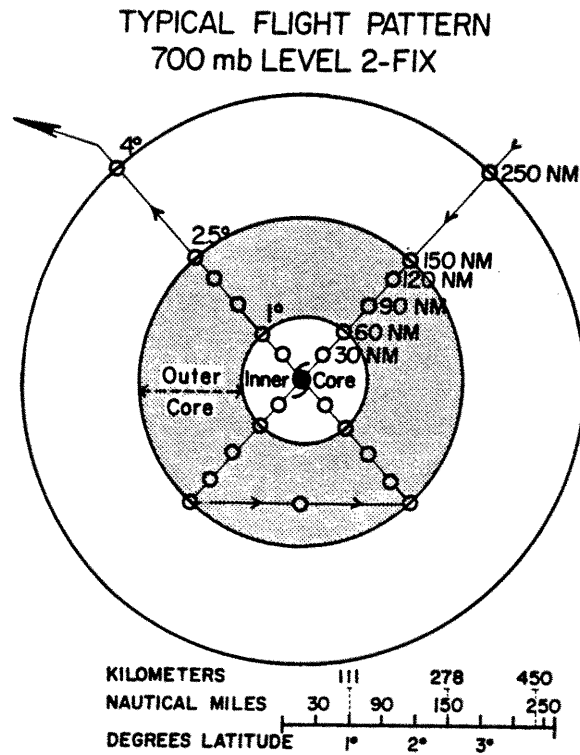


Figure 1.5: Typical 700 mb flight pattern for a single reconnaissance mission into a Northwest Pacific tropical cyclone. Circles denote required observation positions taken every $.5^\circ$ (55 km), with four additional observations taken at the radius of maximum wind. The shaded region marks the outer core (1° to 2.5° radial band) while the inner unshaded inner core is defined as the region inside 1° radius.

Chapter 2

DATA

This study encompasses a two year period (1983-1984) for which aircraft wind and pressure measurements as well as corresponding GMS IR satellite data were available for the Northwest Pacific Ocean (NWP). A description of these data sets is essential to proper understanding of the comparative techniques used in this paper.

2.1 Aircraft Data

In situ wind data for tropical cyclones were obtained from aircraft reconnaissance missions flown by the United States Air Force and included wind and pressure measurements (usually at 700 hPa) extending outward to 463 km from the TC center. These missions were flown twice a day, usually in the early morning and late afternoon and thus two complete radial wind profiles and four measurements of MSLP were obtained daily. Occasional night missions (approximately 1000Z-1400Z) were flown if JTWC determined that extra data were necessary.

MSLP values were determined by dropsonde or with established statistical correlations between MSLP and aircraft flight level pressure measurements in the TC center. The correlation between MSLP and 700 hPa height is 0.997, and hence is quite reliable (Weatherford and Gray, 1988a). Weatherford (1985) also describes details of how reconnaissance missions were flown and how meteorological data were collected and archived. Flight observations were archived and their bearing and range were navigated relative to the moving TC center throughout the mission which typically lasted approximately four hours. If storm relative navigation were not done, winds at the end of the mission could be referenced to a TC center position 100 km or more from the actual current position of the storm. Wind speed and direction were plotted in a natural (NAT) Earth relative

coordinate system because it is these actual wind speeds relative to the surface, rather than the TC-relative winds, that cause damage and which are included in tropical cyclone warnings. Plots of flight level winds as shown in Fig. 2.1 were then generated for each mission.

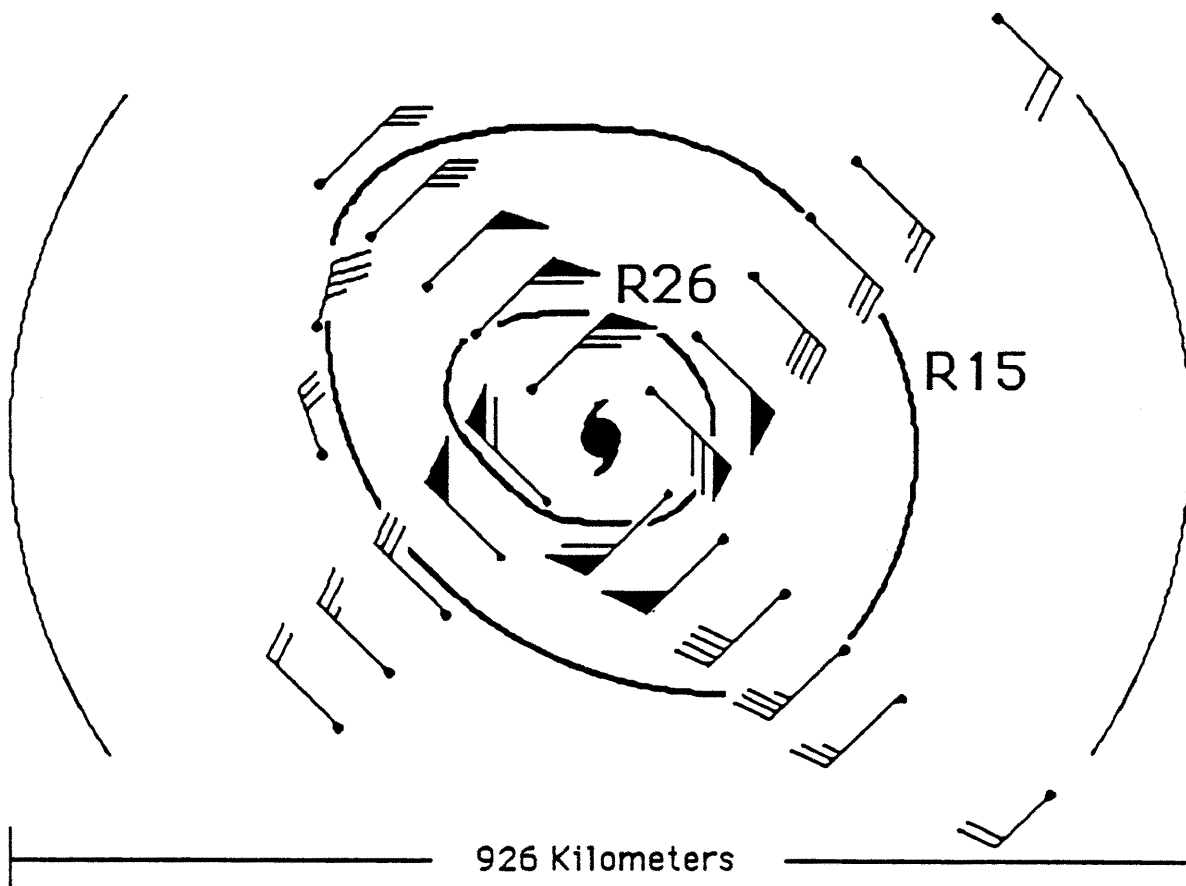


Figure 2.1: Example of aircraft reconnaissance data for a mission flown at 700 hPa. Values for R15 and R26 are calculated from the four quadrant average of the extent of 18 and 30 ms^{-1} winds (at 700 mb). Winds shown here are in knots with pennants representing 50 knots, full barbs representing 10 knots, and half barbs representing 5 knots. One knot equals $0.5144 ms^{-1}$

Forecasters at the Joint Typhoon Warning Center (JTWC) on Guam are operationally concerned with the radial extent of 15 and 26 ms^{-1} surface winds. Various agencies in the Department of Defense as well as civilian governments in the NWP area need information on winds exceeding these thresholds of destruction. To extrapolate surface wind speeds from aircraft reconnaissance data, surface speeds were presumed to be 85 percent of the 700 hPa speeds as indicated in Fig. 2.1 (Powell, 1982; Shea and Gray, 1973; Jorgensen,

1984; Frank, 1977; Frank and Gray, 1980). Hence, the R15 and R26 profile for each mission was analyzed using the 18 m s^{-1} and 30 m s^{-1} winds at 700 hPa to represent the 15 m s^{-1} and 26 m s^{-1} surface winds. The original wind data set was measured in knots (1 knot = 0.5144 m s^{-1}) so that in actual practice, profiles of 35 and 59 knot winds were drawn. The original aircraft observations (Air Weather Service forms 35, 82, and 82b) were consulted for remarks which might provide additional insight when needed. For occasional low-level missions (below 500 m), or when low level observations were taken during a combined low-level and 700 hPa mission, the flight level winds were considered to be representative of the surface winds.

Mission plots of R15 and R26 radii were analyzed to determine the extent of 18 m s^{-1} and 30 m s^{-1} 700 hPa winds. These radial values were then measured and averaged over four quadrants to calculate the R15 and R26 for each mission (see Fig. 2.1). All R15 values greater than 463 km (250 nautical miles) were recorded as 463 km since aircraft observations typically did not extend beyond this radius.

Because of this truncation, a few TCs with very large circulations exhibit constant R15 values of 463 km even though R15 actually extended farther out. Figure 2.2 shows an example of a TC with a large R15.

The two-year aircraft data set contained a wide distribution of R15 and R26 values as can be seen in Figs. 2.3 and 2.4. The bar graphs in these figures represent the number of R15 and R26 values observed within each of ten 50 km radial bands referenced to the TC center. The high frequency of R15 values located in the 450 km to 500 km radius in Fig. 2.3 is due to the grouping of truncated R15 values larger than 463 km into that band.

2.2 Satellite Data

The satellite data set consists of infrared data taken by the Japanese GMS at three hourly intervals over the NWP area. There were a few TCs early in the 1984 season for which images were available only every six hours. However, this deficiency does not affect the results of this study. Resolution of the satellite data at satellite sub-point is 10 km (each pixel equals 100 km^2) for full-disk images which are stored digitally on magnetic tape.

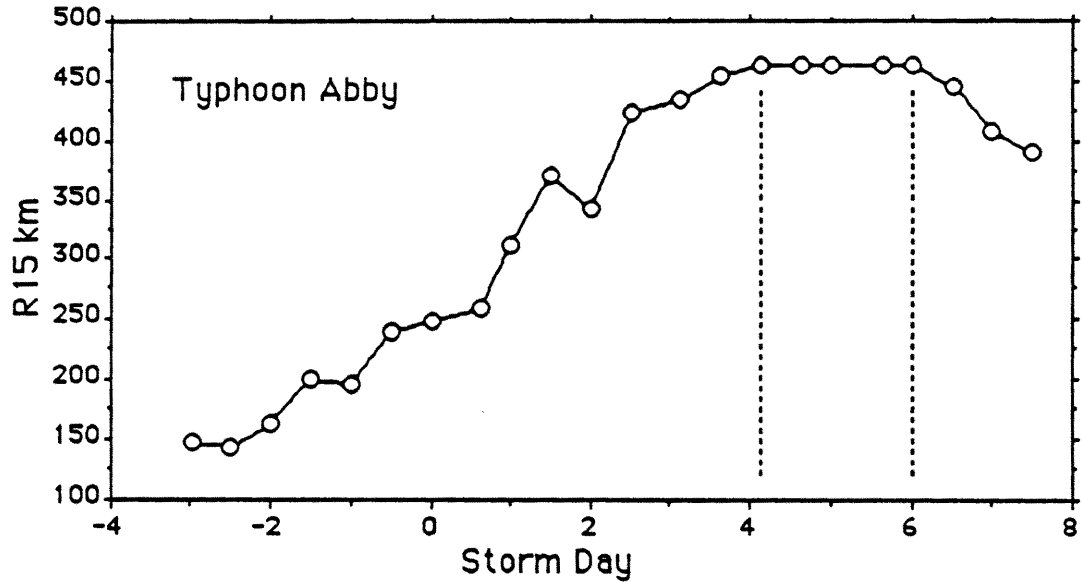


Figure 2.2: Time variation of R15 for Typhoon Abby over a 12 day period. Although R15 extended past 463 km for approximately two days (time between vertical dashed lines), it was recorded and displayed as 463 kilometers (see text). Storm day on the abscissa is referenced from the time of maximum intensity which is designated as zero.

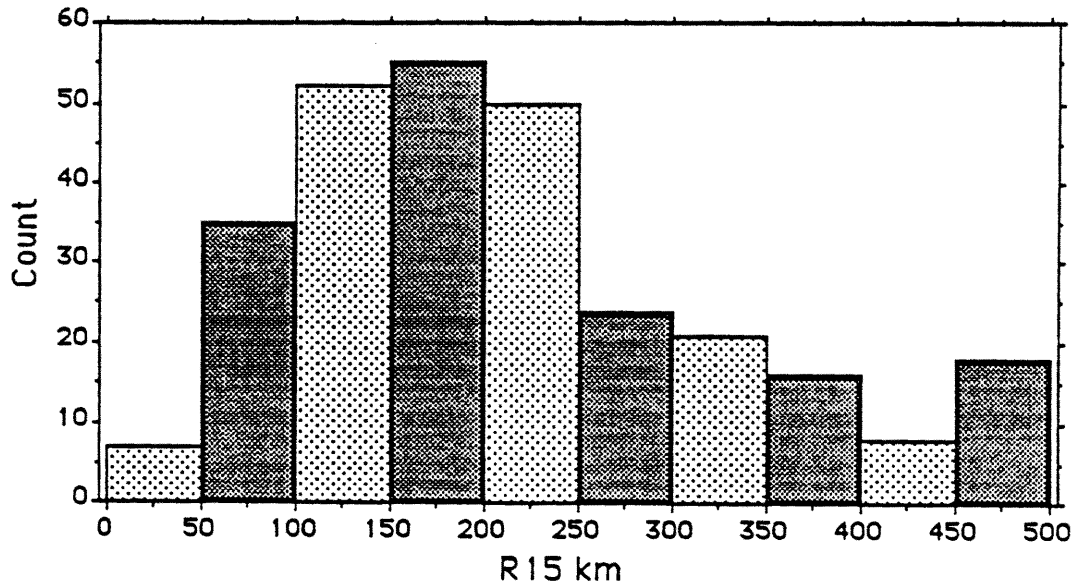


Figure 2.3: Frequency distribution of R15 for the 1983-1984 aircraft data set. Values of R15s greater than 463 kilometers were coded as 463 km.

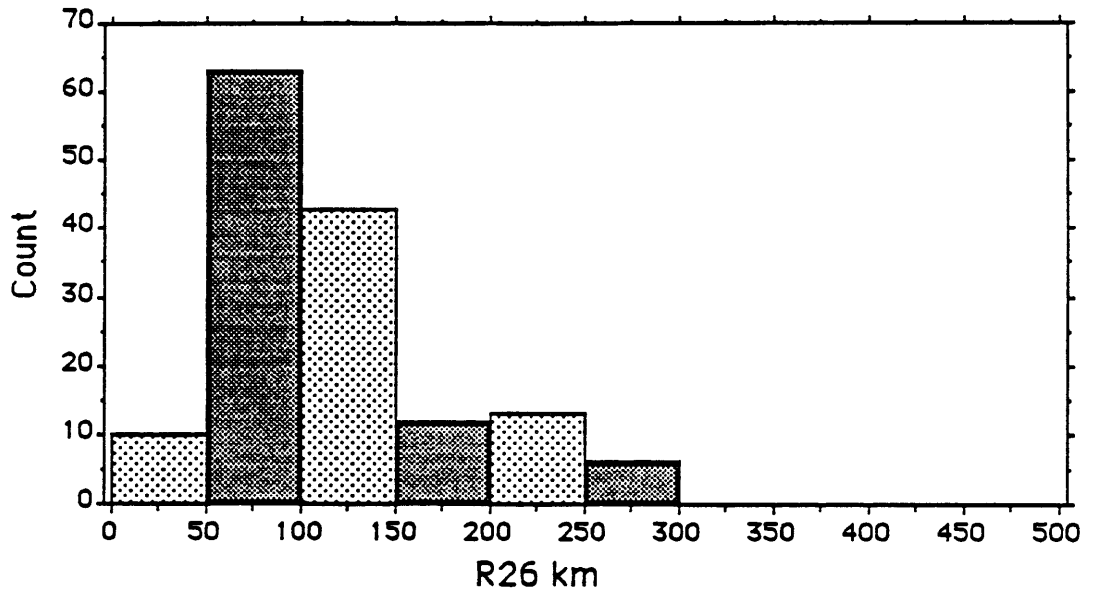


Figure 2.4: Same as Fig. 2.3 except for R26.

These images were archived for cloud climatology purposes and have been made available for other research (World Climate Programme, 1985). Computer programs for navigating the images to TC centered coordinates were provided by the Cooperative Institute for Research of the Atmosphere (CIRA) at CSU.

To avoid possible bias due to geometric foreshortening effects in the satellite imagery, no TC data were included for storm centers which were more than 28° from the satellite subpoint. This constraint meant that images for TC centers farther north than 28°N latitude, west of 112°E longitude, or east of 168°E longitude could not be used. However, this restriction generally only excluded data for recurving TCs which typically travelled north of 28°N while recurving.

Four temperature thresholds were used for counting pixels. These included temperature values less than 0°C , -25°C , -50°C , and 75°C , respectively. As there was no a priori way to anticipate what temperature thresholds might be important for associations with R15 and R26, it was assumed that useful information would be obtained by examining a range of thresholds. This range of thresholds permitted the measurement of not only deep convection, but also of the extensive cirrus cloud shield. All TC images for 1983 and 1984 which corresponded to times of concurrent aircraft reconnaissance missions were processed

for radii extending from 0 to 444 km (4 degrees of latitude). Correlations between individual measurements of satellite observed convection and radial wind extent could then be examined.

Twelve TCs in the 1983-1984 data set (Table 2.1) had good continuity for both satellite images and aircraft reconnaissance observations. These twelve were generally both more intense and longer lived than average which probably accounts for the good continuity of aircraft reconnaissance data. The data set for these cyclones is also favorable for this study in that the more intense storms generally have larger R15 values and create the most concern for potential damage in the NWP. Tropical Storm Wynne remained below typhoon intensity and Typhoon Ike transited the Philippine Islands which altered its convection and wind profiles.

Table 2.1: Twelve TCs used for extensive analysis in this study.

1983	1984
Supertyphoon Abby	Supertyphoon Bill
Typhoon Ellen	Typhoon Cary
Supertyphoon Forrest	Typhoon Clara
Supertyphoon Marge	Typhoon Doyle
Typhoon Orchid	Typhoon Ike
	Supertyphoon Vanessa
	Tropical Storm Wynne

The satellite data were examined closely at seven different concentric radii for all four temperature thresholds. Table 2.2 lists the dimensions of these radii and the total number of pixels (proportional to total area) in each annulus. This analysis procedure yielded a good mix of data for both inner and outer convection and permitted the exclusion of either the inner or outer convection when selectively testing for correlations.

Convection in four storm quadrants was analyzed out to 444 km. These quadrants, labeled north (N), south (S), east (E), and west (W), were obtained by dividing the images diagonally along lines crossing the storm center at the 45° and 135°. This stratification was done to permit the analysis of asymmetries in convection as described below in Chapter Eight.

Table 2.2: Radii (expressed in km and as degrees of latitude) and equivalent pixel counts for the seven annuli used for the analysis of GMS data.

Kilometers	Total Pixels
0-111 (1°)	380
0-222 (2°)	1520
0-444 (4°)	6082
0-667 (6°)	13977
111-444 (1-4°)	5702
222-444 (2-4°)	4562
222-667 (2-6°)	12457

Pixel areas from preceding and subsequent images were averaged to obtain interpolated data for the occasional missing images. This interpolation procedure helped to keep time continuity intact and eliminated several data gaps from the plots.

In the course of this study it became apparent that the recent (time averaged) history of convection would be a useful index of convective activity. Running means of convection, as defined in Fig. 2.5, were calculated for 24, 48, and 72 hour periods. These running mean values were then compared to current values of R15, as well as the prior and subsequent time rate of change of R15. Figure 2.5 defines and illustrates each of these quantities and Fig. 2.6 gives an example of the time variation of instantaneous pixel area measurements and of 24 hour running mean pixel areas.

Instantaneous and running mean pixel areas were processed for comparison with aircraft data. Each data point was identified by time using a Julian Hour calendar referenced to the start of 1983. Data for each TC were also identified by "storm day", which was referenced to the day and hour of maximum intensity for each storm. This storm day designation allowed different TCs to be compared for similar stages of their life cycle in relation to maximum intensity.

Time series plots of R15, R26, and MSLP for each storm were generated for analyses of time variations of wind radii and intensity. Figure 2.7 shows examples of R15 and MSLP plots for Typhoon Abby. Data were also stratified for various other considerations including intensification, filling and time of day. Convection changes were determined over

24 hour intervals rather than over shorter periods, so as to avoid the possible effects of diurnal convection variation (Zehr, 1987).

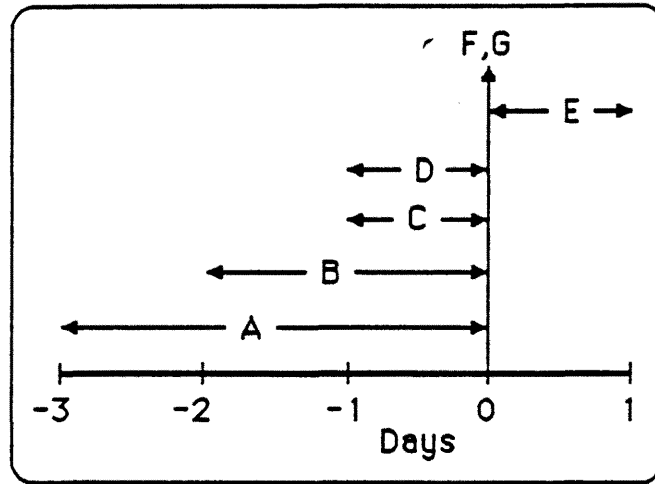


Figure 2.5: Definitions of measurements A-G referenced to time of maximum intensity are as follows: A, prior 72-hour running mean of convection; B, prior 48-hour running mean of convection; C, prior 24-hour running mean of convection; D, prior 24-hour change of R15; E, subsequent 24-hour change of R15; F, current R15; and G, current pixel area.

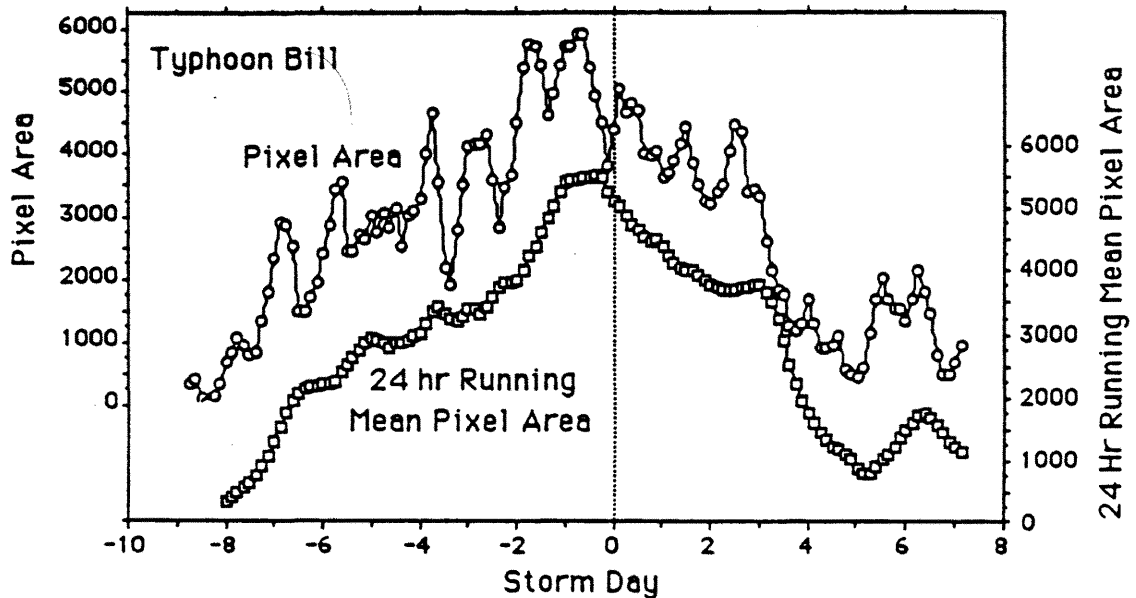


Figure 2.6: Illustration of “instantaneous” (left ordinate scale) and 24 hour running mean (right ordinate scale) pixel areas for convection colder than -25°C . Ordinates are in pixel counts, hence multiply by 100 to get area in square km. Note the smoothing of the diurnal variation in the mean plot. The vertical scales have been offset to prevent overlap.

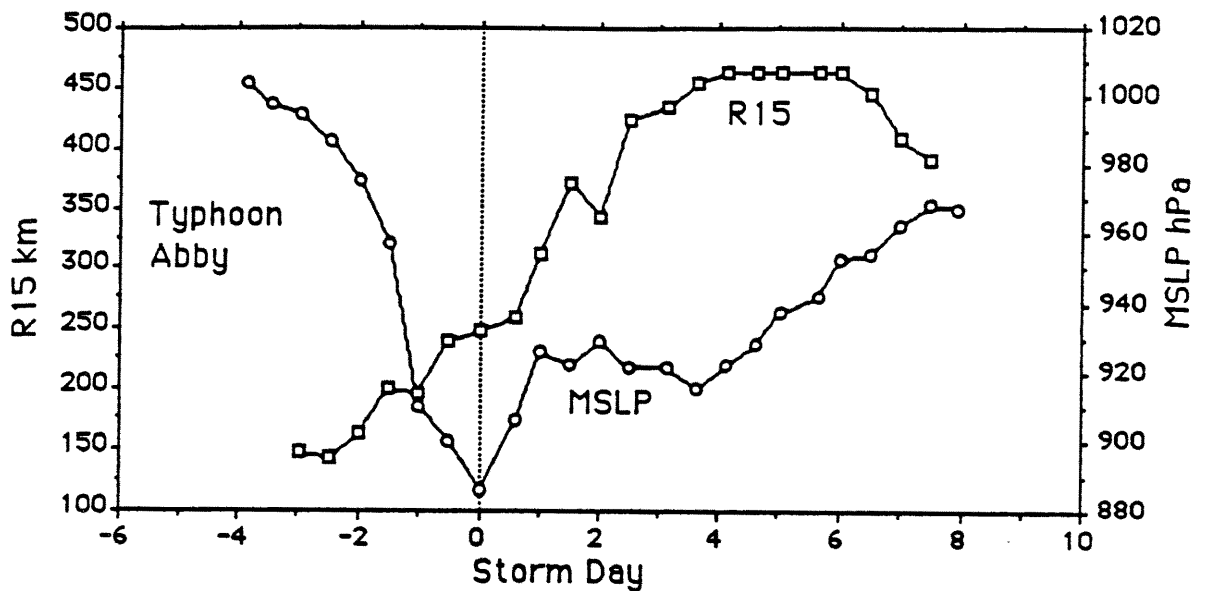


Figure 2.7: Time plot of R15 and MSLP for Typhoon Abby. Storm day is referenced from time of maximum intensity.

2.3 Statistical Analysis Software

Statistical analyses used in this paper were performed using prepackaged statistical analysis software. Documentation on the statistical analysis schemes can be found in the Macintosh Statview 512 Manual (1986). This software facilitated the analysis by allowing graphs to be generated using numerous stratifications and also by calculating correlation coefficients, running means, and fitted curves.

2.4 Summary

The data sets for this study included airborne weather reconnaissance observations of tropical cyclones, generally at 700 hPa, consisting of winds and pressure. The 700hPa wind speed values were adjusted to a factor of 0.85 to approximate surface wind speeds. Values of R15 and R26 were obtained from analyses of reconnaissance mission plots. The satellite data set consists of three hourly digital images navigated to TC centered coordinates. Cloud areas were computed by the number of pixels colder than each of four temperature thresholds at seven different radii.

Chapter 3

HYPOTHETICAL RELATIONSHIPS BETWEEN DEEP CONVECTION AND OUTER RADIUS WINDS OF TROPICAL CYCLONES

As a tropical cyclone develops into an intense vortex, its net tropospheric tangential momentum increases (Fig. 3.1), while continually giving up tangential momentum to the ocean below (Fig. 3.2). For a TC to maintain itself against frictional dissipation at the air-sea interface, there must be a continuous in-up-and-out (i.e., radial) circulation which acts to enhance tangential winds and balance frictional dissipation.

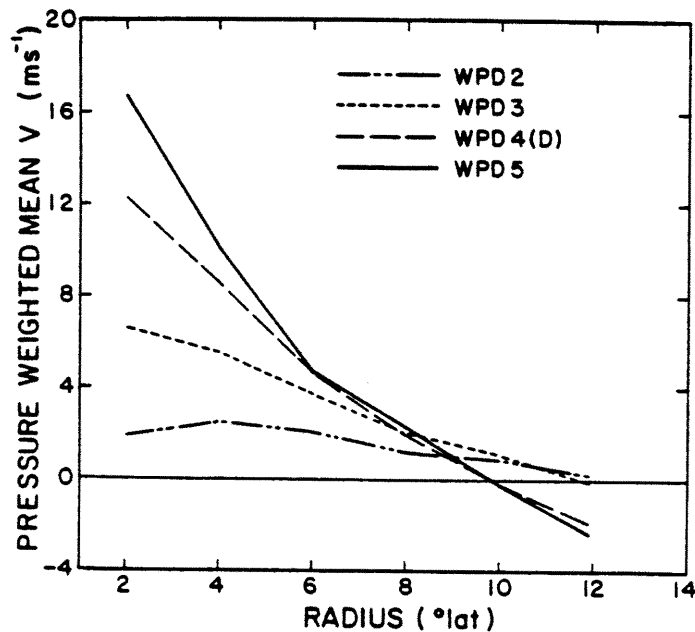


Figure 3.1: Vertically averaged radial profiles of V_T for developing tropical cyclones in the northwest Pacific. The WPD (acronym for West Pacific Developing) numbers signify cyclones of increasing intensity wherein 2 is a developing cyclone, 3 a cyclone of tropical storm strength, 4 a cyclone of typhoon strength, and 5 a supertyphoon. (From Holland, 1983).

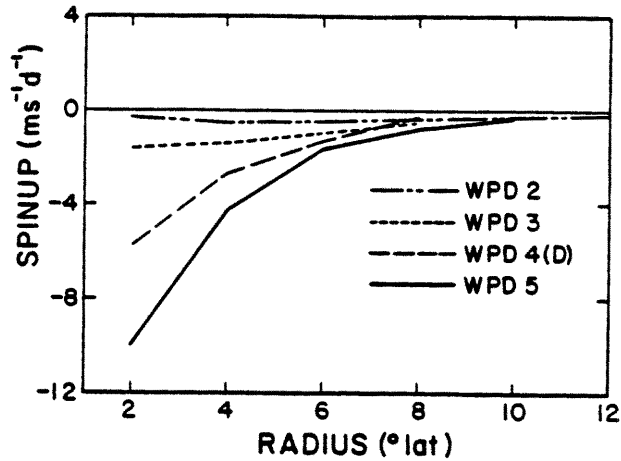


Figure 3.2: Negative spin-up due to surface frictional dissipation for cyclones of different intensity. (From Holland, 1983).

A hypothesis was formulated as to how convection, transverse circulation and the radial extent of strong winds in tropical cyclones are related. These concepts are presented below in a series of illustrations and as a set of simplified equations. These hypothetical concepts will then be tested and forecasting rules will be developed using the data sets described previously.

3.1 Convection, Wind and Surface Friction

As shown in Fig. 3.3, the wind field of a tropical cyclone in cylindrical coordinates can be decomposed into tangential (V_T) and radial (V_r) components. Equation 3.1 expresses the time rate of change of V_T as a function of V_r , relative vorticity ζ (which increases tangential winds when there is inflow of cyclonic vorticity) and tangential friction F_T (which always works to diminish V_T).

-A- -B- -C-

$$\int_A \int_P \frac{\partial V_T}{\partial t} \frac{dAdp}{g} = \int_\ell \int_P r\zeta(-V_r) \frac{d\ell dp}{g} + \int_A \int_P F_T \frac{dAdp}{g} \quad (3.1)$$

The factor $(\frac{dAdp}{g})$ represents the incremental portion of mass of the vortex. Also, $A = 2\pi r_o^2$, and P extends from the surface to 100 mb, $\ell = 2\pi r$.

Note that term A in Eq. 3.1 is influenced by both R15 (ie., the OCS) and by changes in MSLP. In this case, closer in convection will relate more closely to MSLP while farther

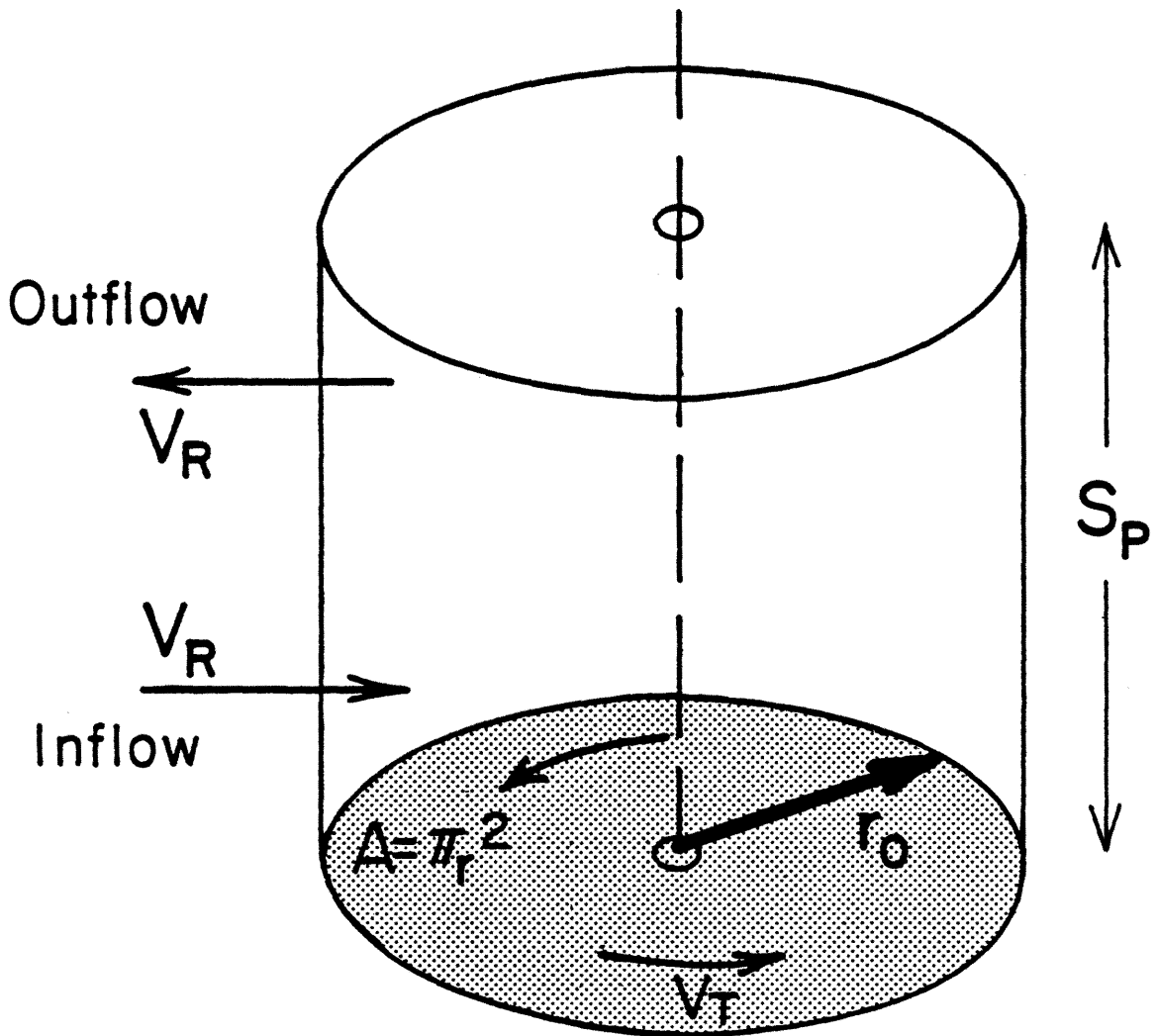


Figure 3.3: Conceptual representation of a tropical cyclone in cylindrical coordinates. The cyclone is assumed to extend from the surface to 100 mb. The area (A) lies within a specified radial distance (r_0). V_T and V_R are the tangential and radial winds, respectively.

out convection should be more closely relate to R15. When integrated over the depth of the troposphere, the source term (ie., term B) in Eq. 3.1 yields the net inflow of tangential momentum. Inflow occurs in the lower troposphere where relative vorticity is high (see Fig. 3.4). Outflow, as shown in Fig. 3.3, occurs aloft where absolute vorticity may approach zero (Fig. 3.4). Therefore, a net increase of tangential wind (spin-up) occurs, provided the transverse (radial) circulation importing tangential momentum (term B of Eq. 3.1) exceeds the frictional effects (term C).

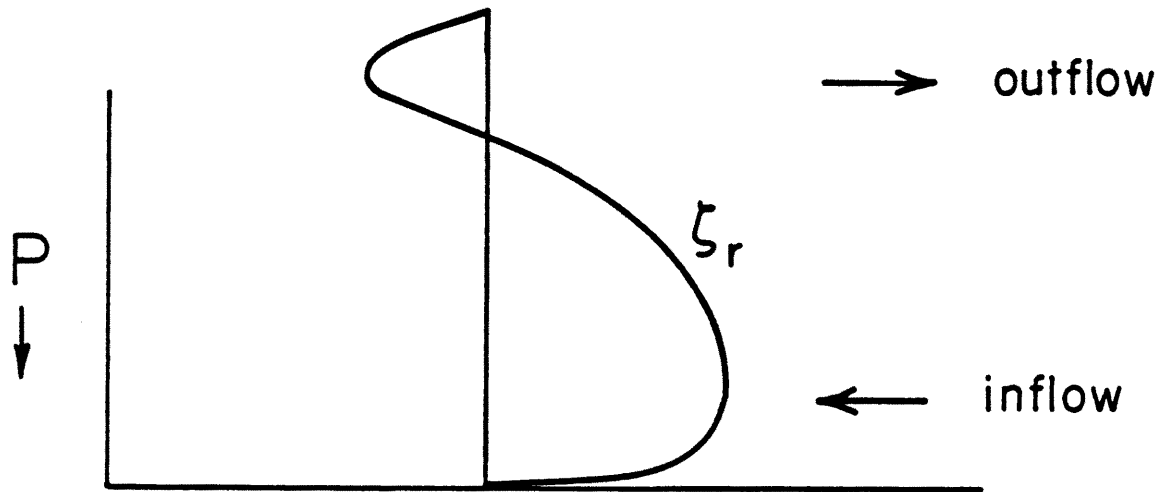


Figure 3.4: Conceptual illustration of the typical vertical distribution of relative vorticity (ζ_r) of a tropical cyclone at 3-4° radius.

Radial velocity is related to divergence and vertical motion through simple continuity concepts. It is vertical motion which is indirectly estimated in GMS data as areas of intense convection. Hence, sustained deep convection signifies sustained vertical motion, low level convergence, and consequently, the spin-up of TC winds. This spin-up process will continue to increase the tangential winds until balanced by frictional effects. In the most basic sense, the research described here seeks to determine if GMS imagery can be used to make reliable estimates of Term B, and thereby gain improved quantitative estimates of Term A and hence, of time varying outer radius wind strength.

Deep convection also causes warming aloft which acts hydrostatically to lower surface pressure near the TC center. This reduced central pressure and associated pressure gradi-

ent accelerates boundary layer winds towards the TC center through Ekman convergence. Tangential winds then intensify following Eq. 3.1. As convection in the core area continue to cause warming aloft, the pressure gradient, V_r and V_T , all continue to increase.

The effects of friction in the boundary layer are represented by Eq. 3.2, wherein V_T is assumed to represent the average wind speed at 10 m height over the ocean and C_D is a drag coefficient.

$$\bar{F}_T \approx \frac{-g}{\Delta p} C_D V^2 T_o \quad (3.2)$$

For a given rate of convection, maintained over time, an equilibrium condition will eventually develop. Friction in Eq. 3.2 increases approximately as the square of the wind speed. Hence, tropical cyclones cannot intensify indefinitely because of the non linear increase of the effects of friction with speed. The TC will intensify when convection is strong enough to maintain a large in-up-and-out circulation which causes the tangential winds to increase faster than frictional dissipation. When there is less convection than is needed to maintain the TC against frictional decay, filling and/or generally weaker tangential winds will result. There is greater net frictional dissipation in a large, intense typhoon than in a small, minimal tropical storm. Therefore, the amount of convection which will allow winds in a large storm to weaken, might also cause a minimal tropical storm to strengthen.

Merrill (1982) made an analysis of tropospheric Relative Angular Momentum (RAM) budgets for tropical storms (TS) and typhoons (TY) of different size. Storm size was defined by the radius of the outer closed isobar. The larger cyclones in Merrill's work were found to have stronger 0-4° tangential wind fields. There was little variation of central pressure values among storms which were within either the TS size groups or within the TY size groups. However, values for the net tangential relative angular momentum ($\int_A \int_P r V_T \frac{\delta A \delta p}{g}$) and friction dissipation ($\int_A \int_P r F_T \frac{\delta A \delta p}{g}$) of the larger sized cyclones were considerably greater than for the smaller sized cyclones (see Figs. 3.5 and 3.6). Despite the weaker outer radius winds (in comparison with inner radius speeds) angular momentum dissipation is concentrated at the outer radius because of the area relationship.

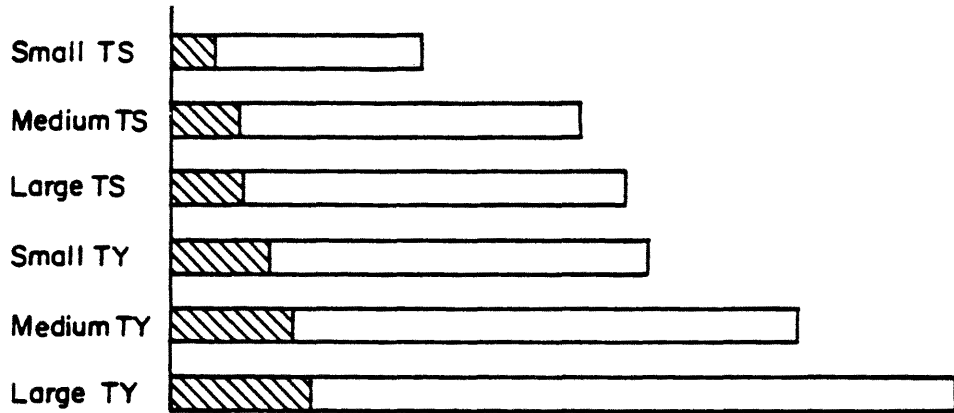


Figure 3.5: Integrated Relative Angular Momentum (RAM) from $0^\circ - 4^\circ$ latitude radius and 950 mb to 100 mb for Atlantic and Pacific tropical cyclone composites. The shaded area is the RAM estimated for the $0^\circ - 2^\circ$ region using the fitted modified Rankine vortex approximation. (From Merrill, 1982.)

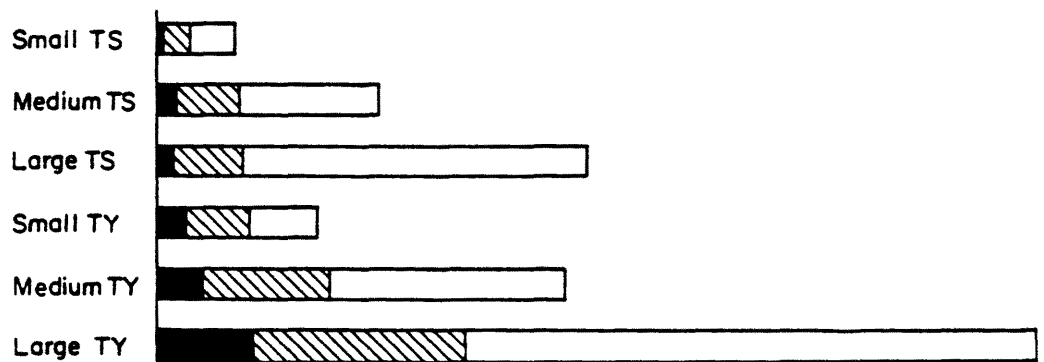


Figure 3.6: Integrated surface sink of cyclone RAM from $0^\circ - 8^\circ$ latitude radius of Atlantic and Pacific tropical cyclone composites. The black area corresponds to surface losses in the area within 2° latitude radius of the center, the hatched area from 2° to 4° , and the remainder from 4° to 8° . (From Merrill, 1982.)

Given the greater frictional dissipation for the larger sized tropical cyclones shown in Fig. 3.6, it is to be expected that the maintenance of large storms with stronger outer radius winds requires larger in-up-and-out radial circulations in the outer radius area. The associated deep convection must also be considerably greater than for the smaller cyclones. The larger cyclones in Merrill's study also had a substantially greater 300 mb vertical velocity inside the 4° radius than did the smaller cyclones. If this were not the case, then the outer circulation wind fields of the large-scale cyclones would have to rapidly weaken as Term C, integrated over 24 hours, would be larger than term B. By contrast, a very large amount of deep convection associated with a stronger than usual radial circulation would cause term B to be larger than term C and lead to a spin-up of the outer-circulation.

Since deep convection undergoes very large diurnal variations without concurrent diurnal changes in outer radius vortex strength, it is implicit that the relationship expressed by Eq. 3.1 can not apply for instantaneous observations. Rather, when Eq. 3.1 is integrated over time, say for a 24-hour period or longer, this relationship appears to offer a reasonable estimate of the expected changes in tangential winds over outer radius winds.

Figure 3.7 gives a conceptual representation of the relationship between running average convection and R15. The heavier curved line represents a balance between the three terms in Eq. 3.1. If the rate of convection falls in the area above this line, R15 should increase and likewise, R15 should decrease if convection falls below the line. The rate of R15 increase or decrease should also be proportional to the excess or deficit of convection for a given R15 value.

3.2 Convection, R15 and Intensity

The strength of the circulation in the outer radius of a tropical cyclone (and hence of R15) is well correlated with the overall tangential wind strength in the $0-3^\circ$ radius vortex but not with intensity (MSLP) (Holland, 1982; Merrill, 1984; Weatherford and Gray, 1988a, 1988b). Specifically, Merrill (1982) found that the mean radius of the outer closed isobar was correlated with MSLP at a value of 0.3 and Weatherford and Gray found that

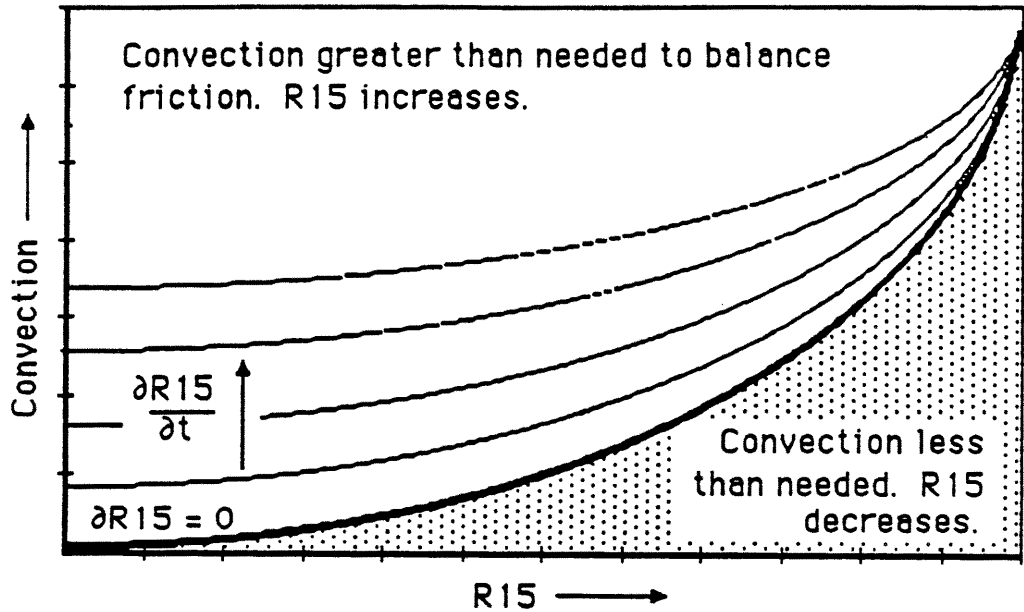


Figure 3.7: Idealized representation of how convection is related to R15. The balance (heavy) line is curved because friction increases non-linearly. If convection is greater than needed to sustain a given R15, then R15 should increase and the amount of R15 increase should be proportional to the distance above the balance line for different $\partial R15/\partial t$ values.

variations in R15 explained only about one third of the variance of MSLP. All of these studies dealt exclusively with NWP storms.

For the present study, the concept illustrated in Fig. 3.7 relating R15 and convection was expanded to encompass relationships between intensity and convection. It was postulated that a certain amount of convection should sustain a certain storm intensity and, if observed convection was in excess of what was needed to maintain that intensity, the extra energy should manifest itself in the wind field (ie., as R15). Figure 3.8 shows an idealized rendering of this hypothetical relationship between convection and intensity wherein variable values of R15 would be the anticipated result.

3.3 Summary

Radial wind is a major factor governing variations of the tangential wind through the conservation of angular momentum. Convection is related to radial winds through continuity. Hence, there may then be relationships between either the intensity of current convection or the mean level of prior sustained convection and variations of R15. Running mean and current (instantaneous) measurements of convection, inferred from satellite

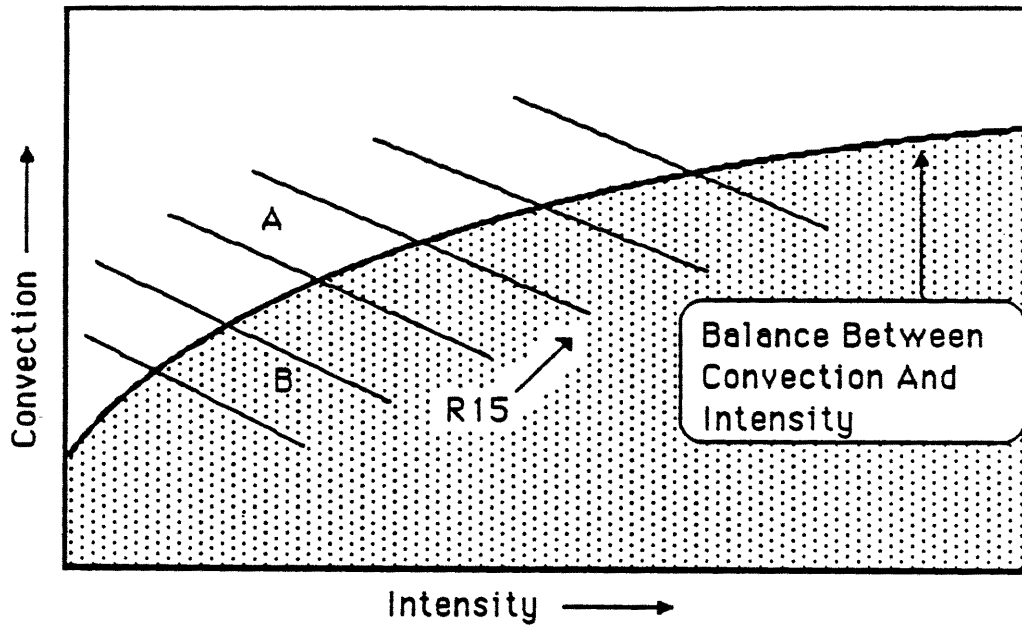


Figure 3.8: Idealized representation of the hypothesized relationship between convection and intensity (MSLP). For a given intensity, convection greater than needed to balance friction should serve to increase tangential winds. Intensity is similar at points (A) and (B), but R15 is greater for point (A).

based radiance data, are used to test this inference in the following chapters. Also, the possibility of a relationship between TC intensity and rates of convection will also be examined.

Chapter 4

ASSESSMENT OF DIRECT RELATIONSHIPS BETWEEN CONVECTION AND DAMAGING WINDS

The first step in testing the hypothetical associations discussed in Chapter Three was to look for relationships between values of R15 or R26 and concurrent convection. Values of R15 and R26 for each mission were compared to concurrent pixel counts at four temperature thresholds within the 0 to 444 km radius. Because poor correlations were obtained for these tests, no additional radii were examined for relationships of this sort. Results for these tests are included here to illustrate the nature of the relationships which were observed between convection and radial extent of winds and to document their apparent lack of usefulness to forecasters. Note the difference in the ordinate scales for Figs. 4.1 and 4.2, illustrating the substantial size differences between these (and other) storms. Similar differences in pixel counts between different storms and especially for different temperature thresholds further necessitated the use of variable ordinate scales. The reader is advised to note these scale differences carefully in making comparisons between various figures.

4.1 Relationship between R26 and R15

Changes in the value of R26 for a given storm tend to follow concurrent changes in the value of R15. Examples of these changes (for typhoons Abby and Clara) are shown in Figs. 4.1 and 4.2. These plots suggest that R26 and R15 should both exhibit similar relationships with convection. Because values for R26 are smaller than R15 values, a forecaster may determine R15 through synoptic analysis but not know R26.

Values for R26 were compared to R15 and a linear regression equation relating the two was developed. This relationship is given in Eq. 4.1 and shown graphically in Fig. 4.3. Because of these similarities R26 will not be discussed separately from R15.

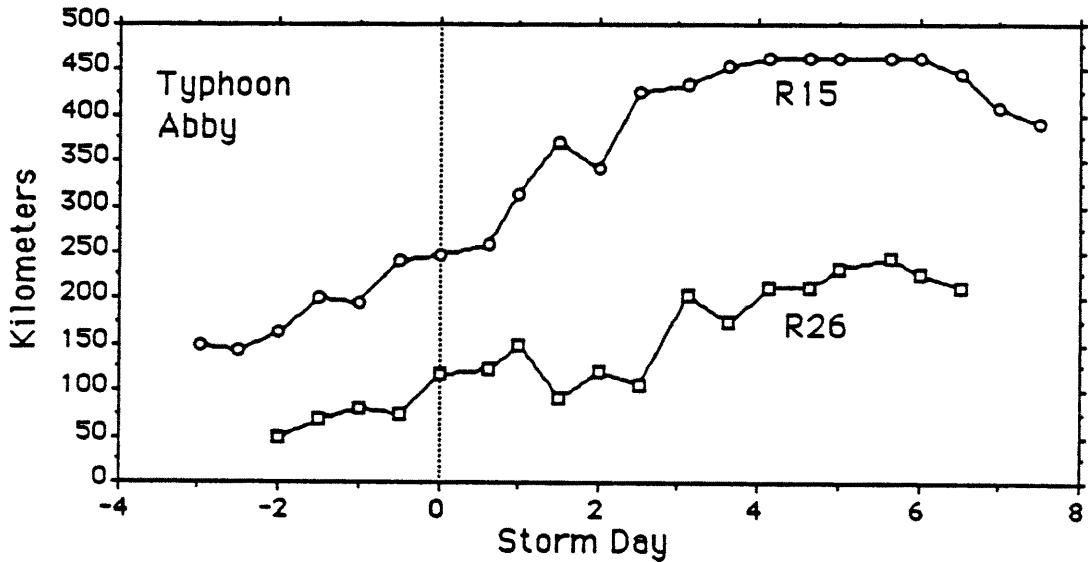


Figure 4.1: Time plot of R15 and R26 for Typhoon Abby. Time on the abscissa scale is plotted in days relative to the time of maximum intensity (minimum SLP) which is represented as the vertical dashed line of day -0. Note that R26 closely parallels R15. Small fluctuations in R15 and R26 are likely due to uncertainties of measurement.

$$R26 = 0.5 \cdot R15 - 20(km) \quad (4.1)$$

4.2 Relationships Between Intense Convection and R15

No strong correlations were observed between R15 and concurrent instantaneous pixel counts at the four temperature thresholds as shown in Figs. 4.4 through 4.7. When the data were stratified so as to include only intensifying TCs (Figs. 4.8–4.11), some trend towards convection being associated with R15 values can be observed by inspection although less than 20 percent of the variance was explained. Similar relationships (not shown) were obtained for filling TCs.

Zehr (1987, 1989) and McBride and Gray (1980a,b) have shown that tropical cyclones have a diurnal cycle of convection. Greater amounts of very cold clouds tend to occur in

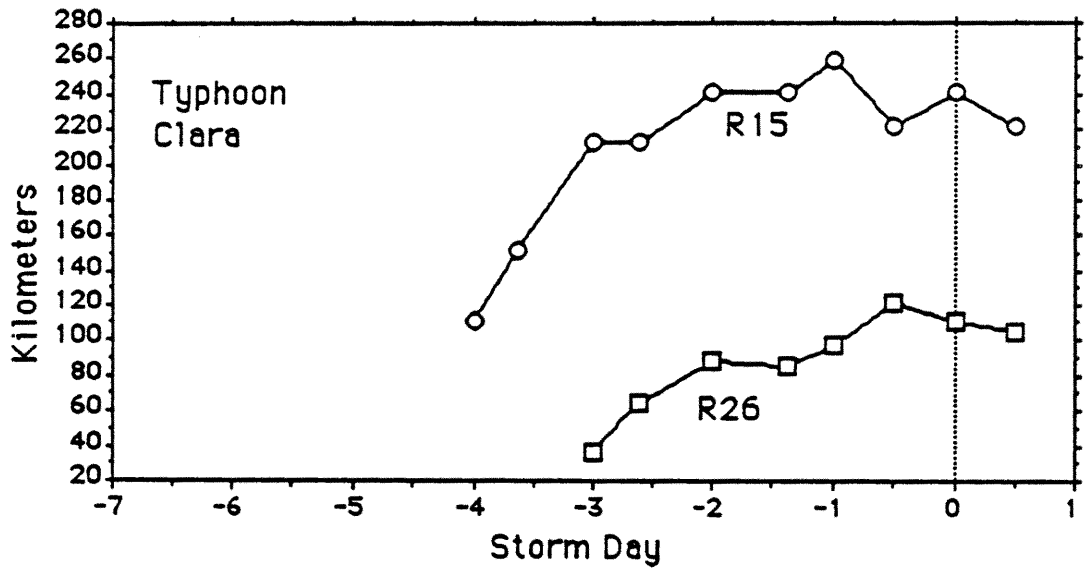


Figure 4.2: As in Fig. 4.1 but of R15 and R26 for Typhoon Clara.

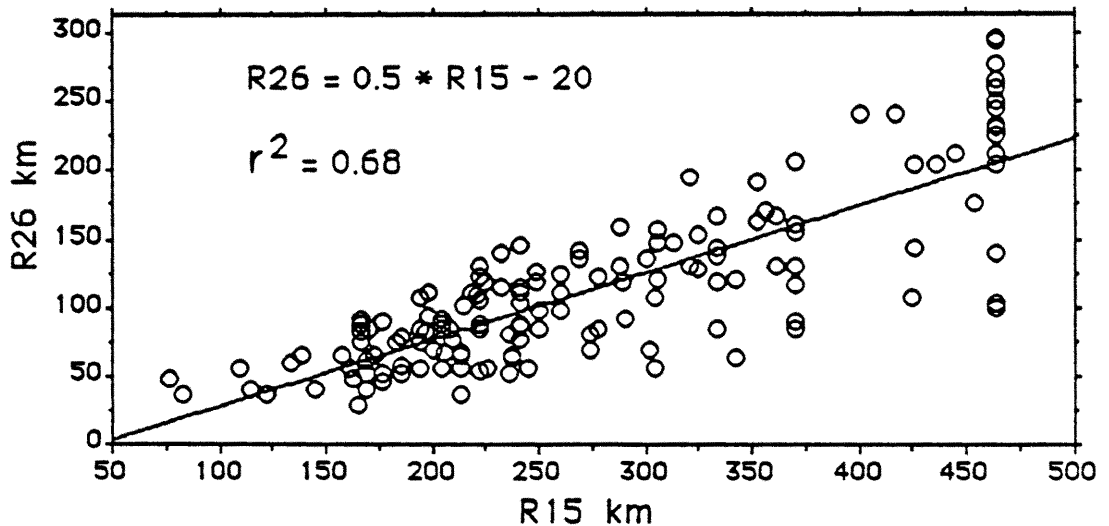


Figure 4.3: Linear regression between R26 and R15. Approximately two-thirds ($r^2 = 0.68$) of the variance is explained by this relationship. R15s greater than 463 km are truncated to values of 463 km (Chapter 2), thus explaining the clustering at the right of the chart.

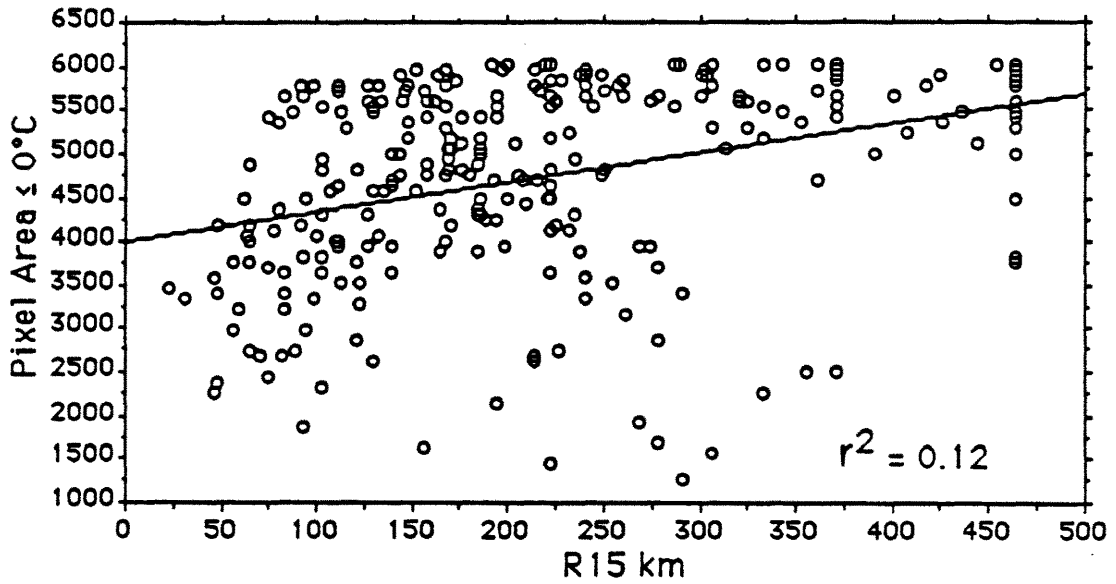


Figure 4.4: Pixel counts (ordinate) for areas of convection colder than 0°C versus R15 (abscissa) for all storms. The value of r^2 represents the amount of the variance explained (correlation coefficient squared).

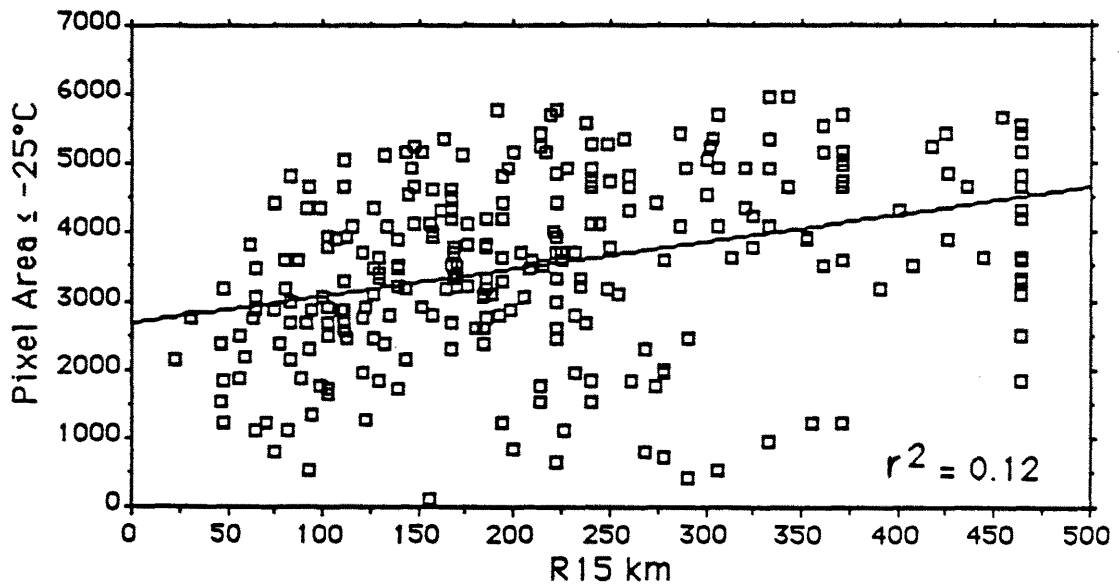


Figure 4.5: As in Fig. 4.4 except for the -25°C temperature threshold.

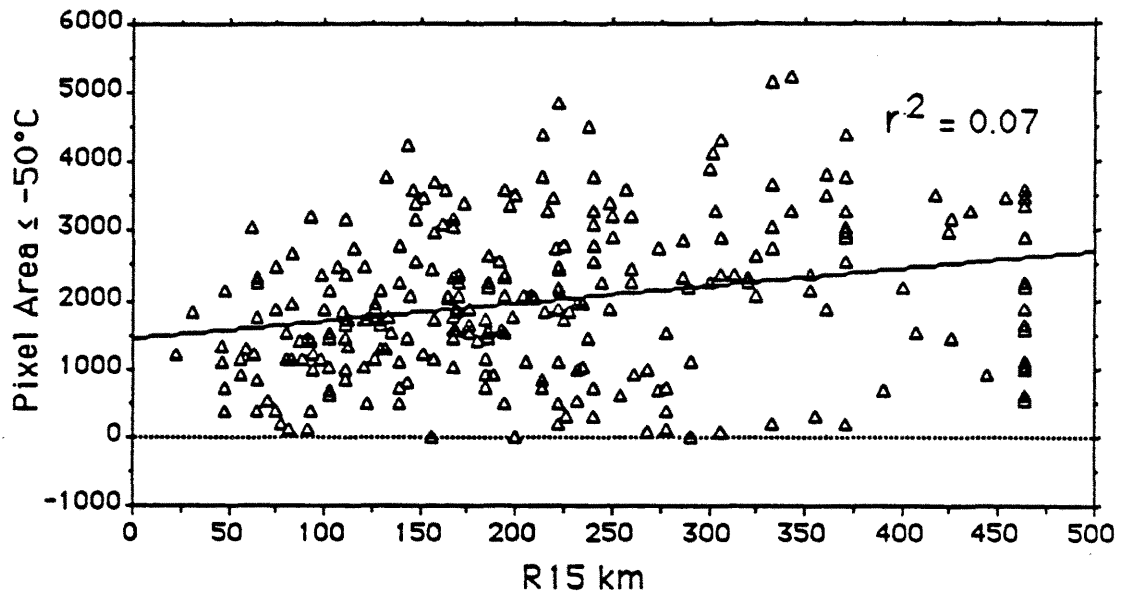


Figure 4.6: As in Fig. 4.4 except for the -50°C temperature threshold.

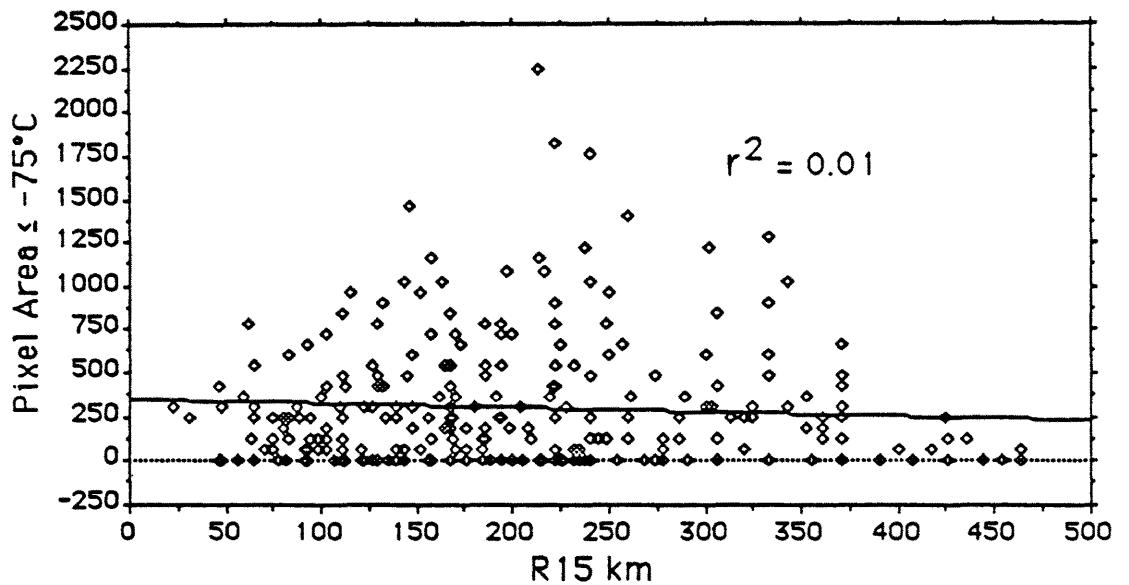


Figure 4.7: As in Fig. 4.4 except for the -75°C temperature threshold.

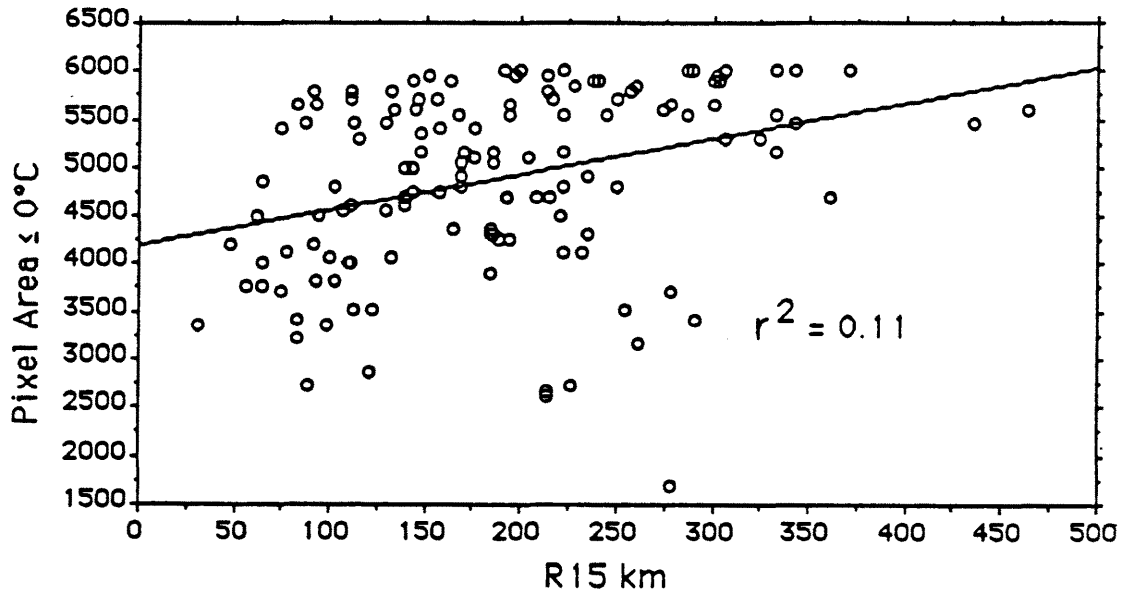


Figure 4.8: As in Fig. 4.4 (all convective areas with temperatures below 0°) but for intensifying storms only.

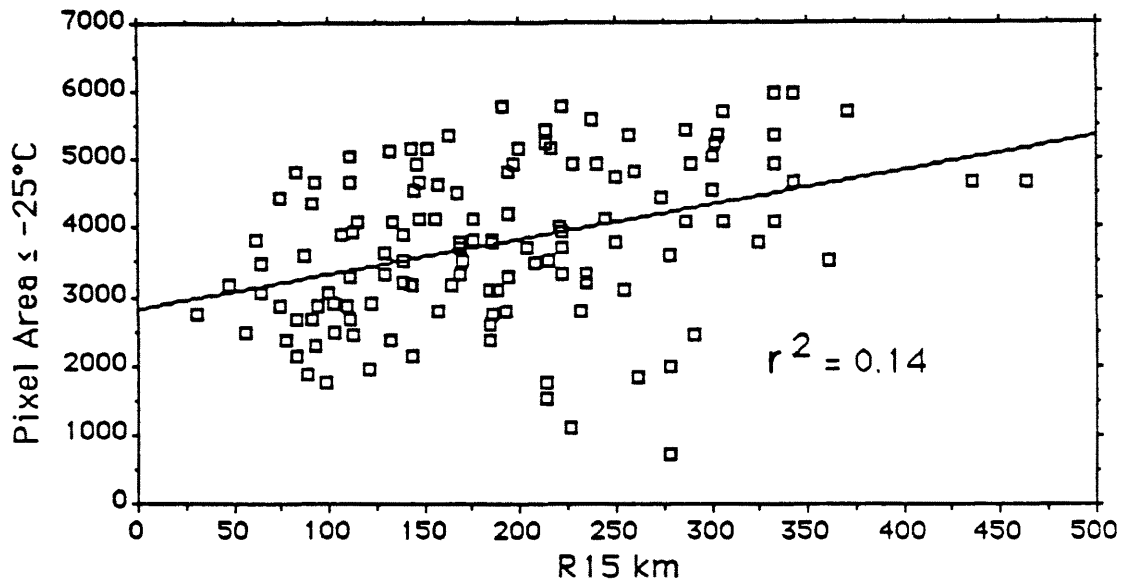


Figure 4.9: As in Fig. 4.8 except for the -25°C temperature threshold.

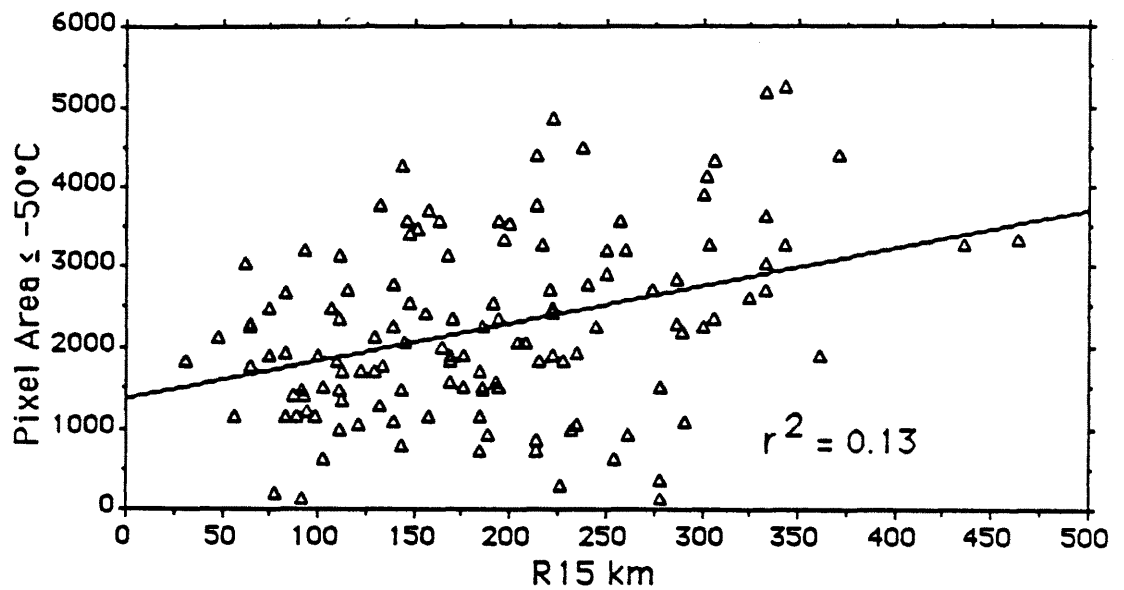


Figure 4.10: As in Fig. 4.8 except for the -50°C temperature threshold.

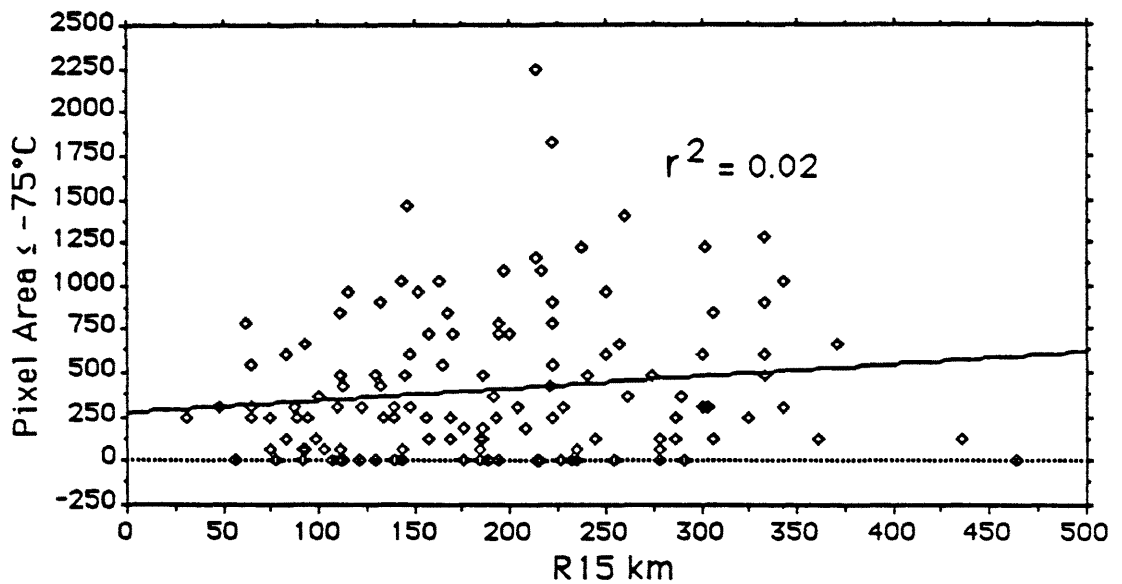


Figure 4.11: As in Fig. 4.8 except for the -75°C temperature threshold.

the morning hours with a maximum around sunrise. Separating morning and evening data to remove the effects of this diurnal variability of convection and comparing to R15 values for intensifying TCs also revealed no strong correlation. Results for correlations between morning data from intensifying TCs are shown in Fig. 4.12–4.15. Correlations for evening data from intensifying TCs were slightly weaker than for the morning, and are not shown. For filling TCs (intensity decreasing), neither morning nor evening satellite observations yielded good correlations with R15.

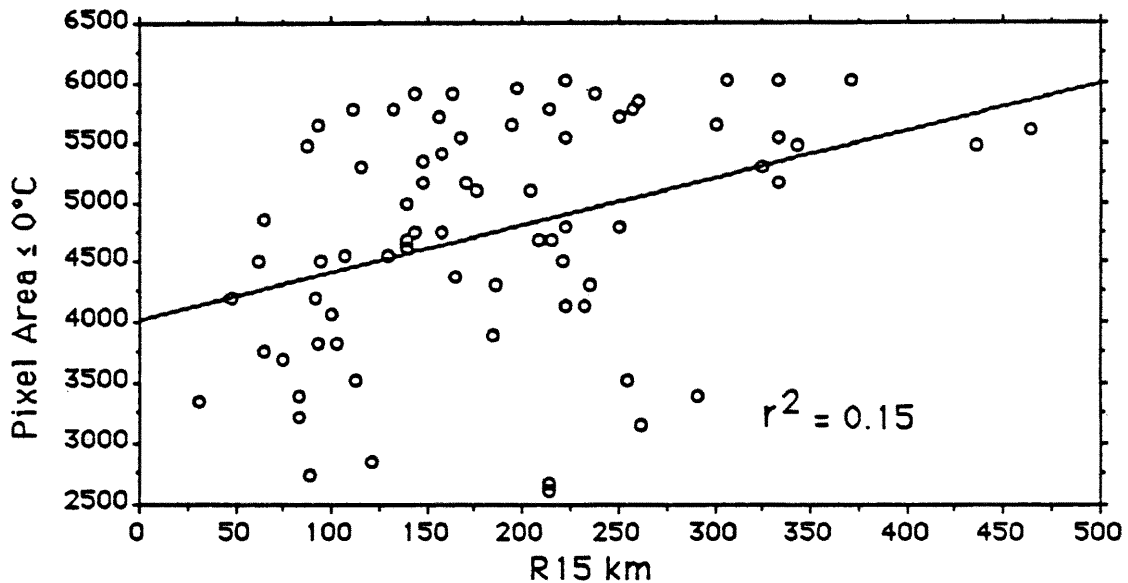


Figure 4.12: As in Figs. 4.4 and 4.8 (convective temperature threshold is 0°C) but for morning pixel counts for intensifying storms only.

The possibility that an increase in pixel count correlates with an increase in R15 was tested by first removing the diurnal variability of convection by comparing 24 hour pixel count changes with 24 hour changes of R15. When this is done the resulting distribution appears random (Figs. 4.16-4.19) with no apparent relationship. The correlation was also poor when stratified into intensifying and filling classes. When the convection is increasing, R15 may increase or decrease, although there appears to be a slight bias towards an increasing R15 for intensifying TCs. When a TC is filling, either convection and/or R15 may continue to increase (Weatherford, 1985) and no relationship observed between convection change and R15 change.

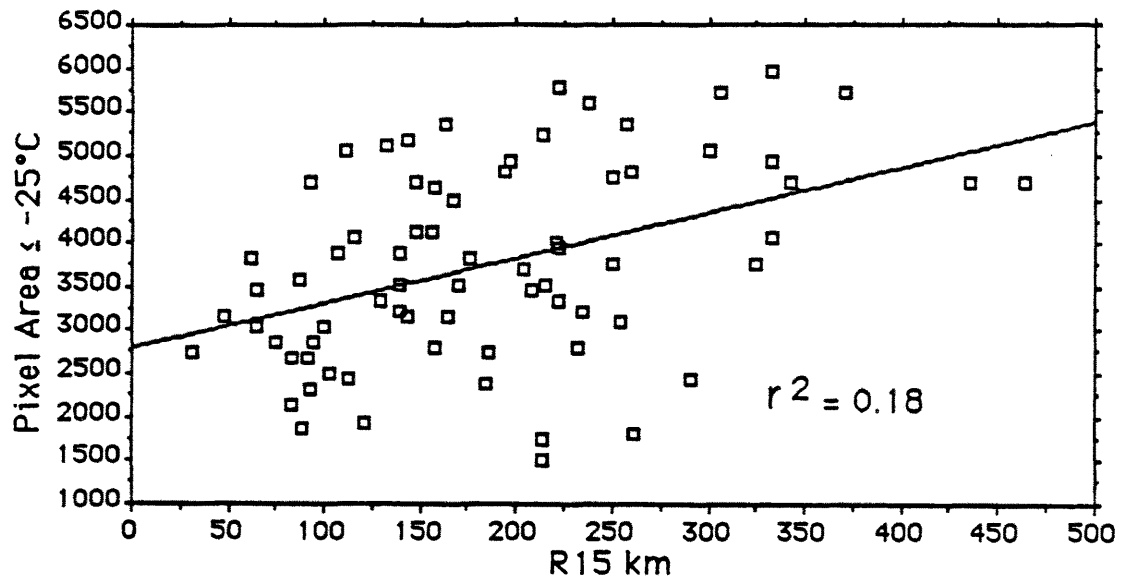


Figure 4.13: As in Fig. 4.12 except for the -25°C temperature threshold.

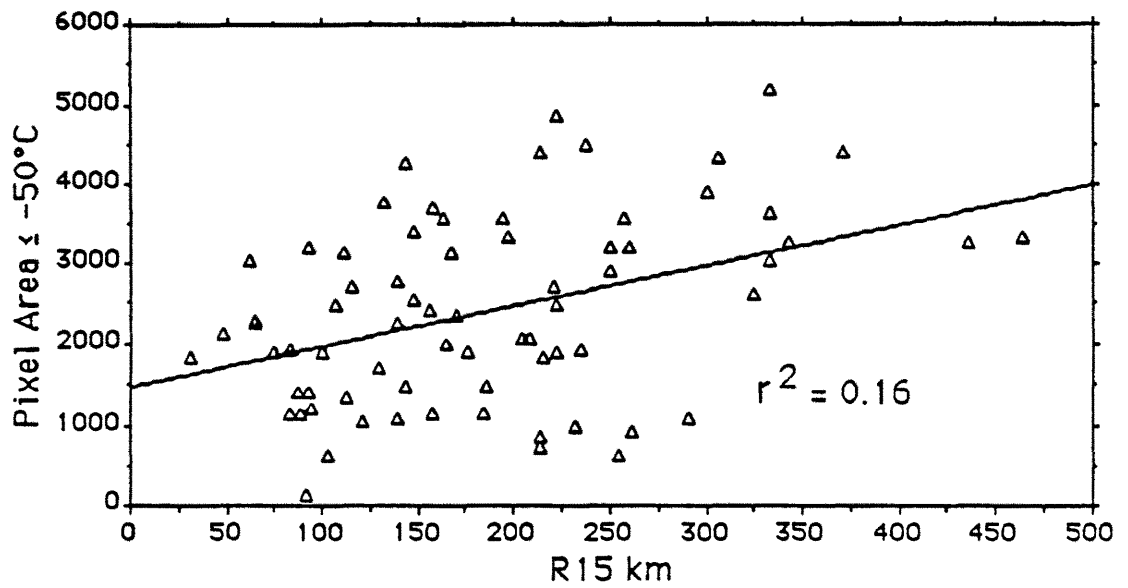


Figure 4.14: As in Fig. 4.12 except for the -50°C temperature threshold.

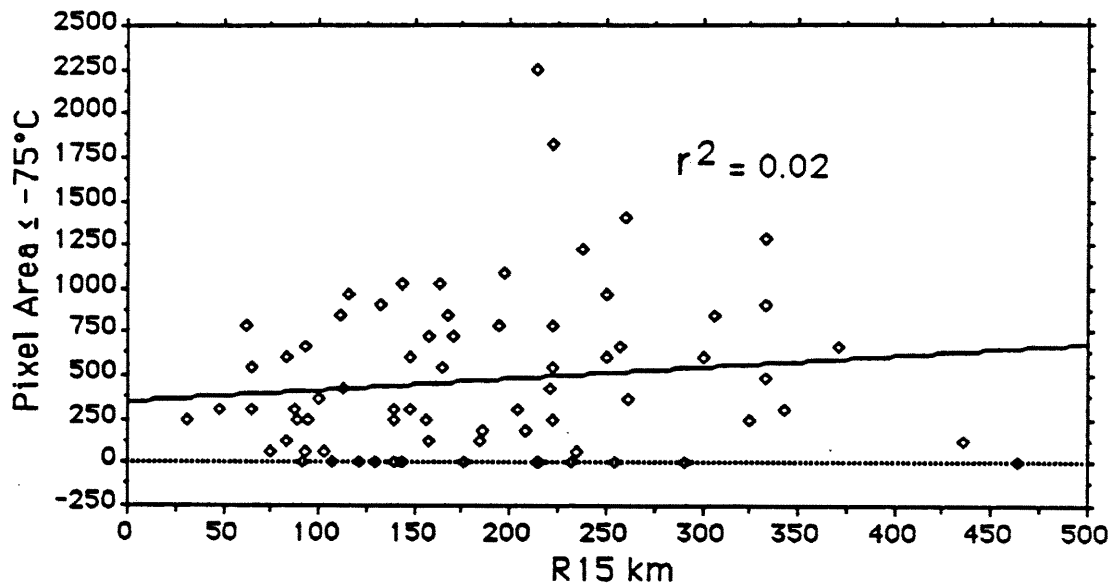


Figure 4.15: As in Fig. 4.12 except for the -75°C temperature threshold.

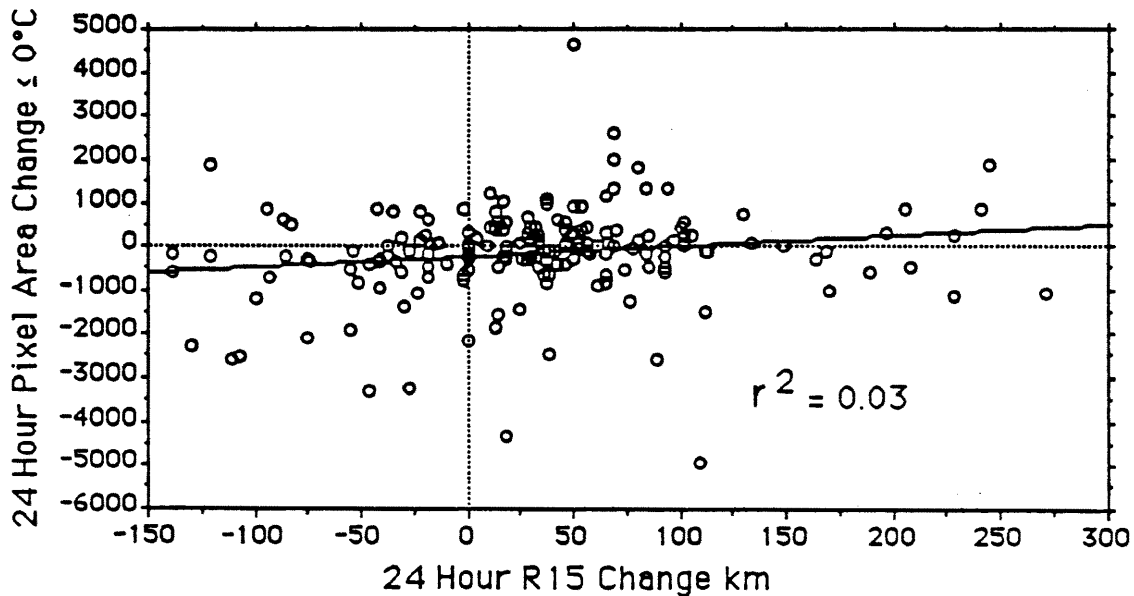


Figure 4.16: Twenty-four hour change of ($\leq 0^{\circ}\text{C}$) convection for all storms compared to change of R15. Results were similar for intensifying and filling TCs.

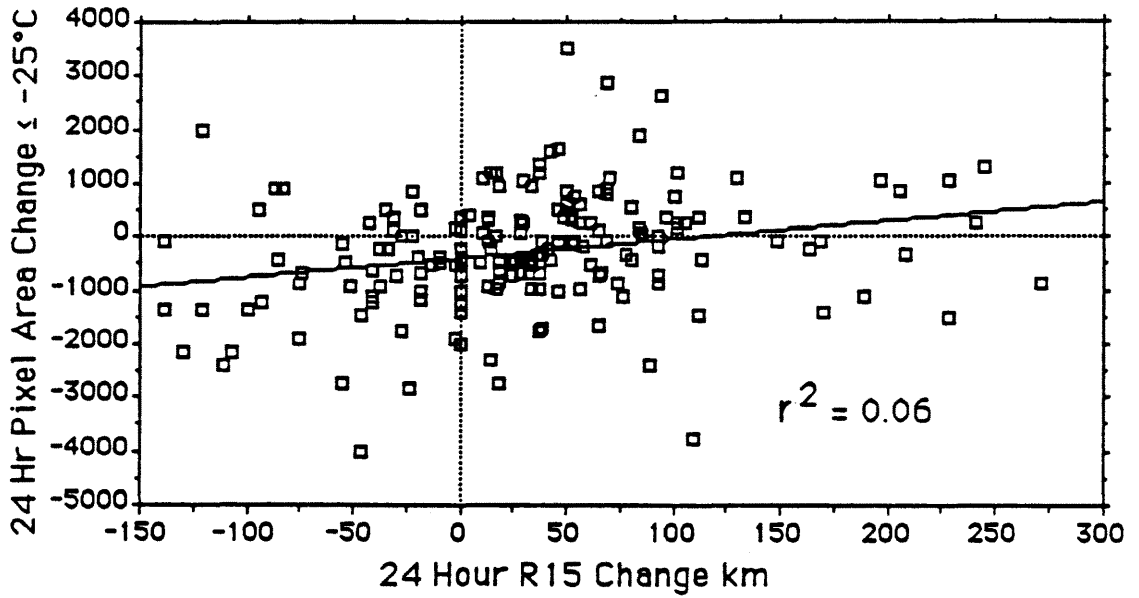


Figure 4.17: As in Fig. 4.16 except for the -25°C temperature threshold.

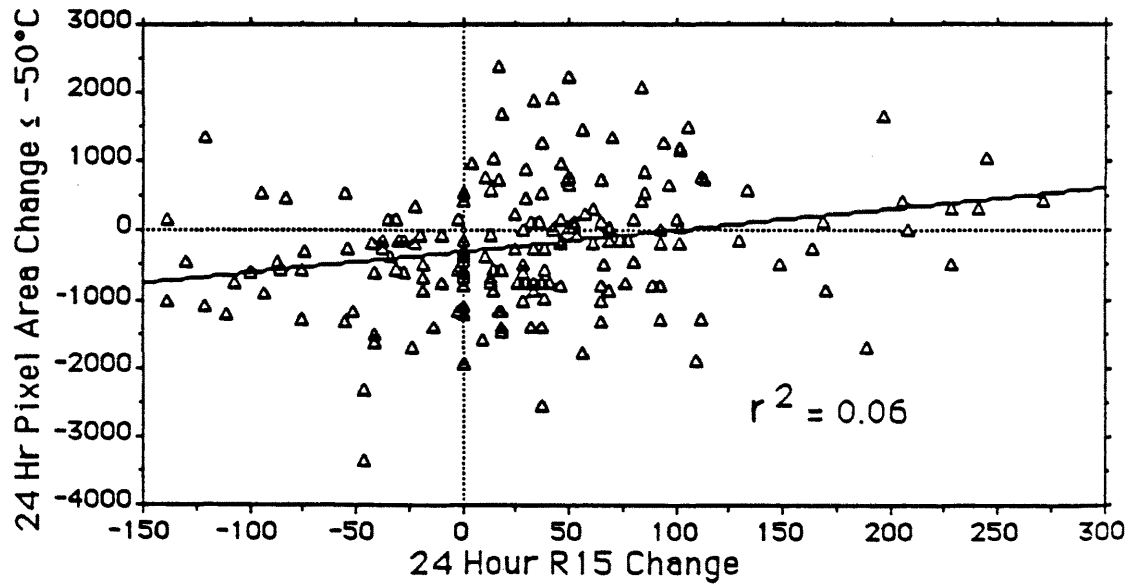


Figure 4.18: As in Fig. 4.16 except for the -50°C temperature threshold.

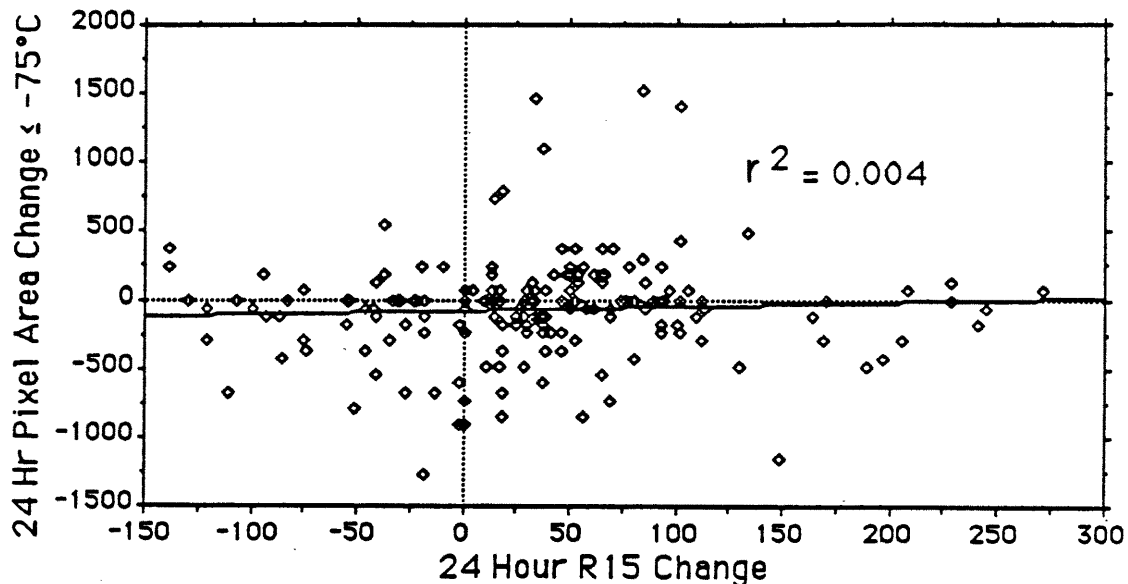


Figure 4.19: As in Fig. 4.16 except for the -75°C temperature threshold.

4.3 Relationship of Intensity to R15 and Pixel Counts

As stated in Chapter 1, variations in MSLP (intensity) accounted for approximately one half of the variance of R15 (Fig. 1.1) for the 1983-1984 data set. This relationship was also examined for TCs which had been stratified according to whether they were intensifying or filling to see if improved correlations between convection and R15 could be obtained. It is reasonable to expect a filling TC to have a greater R15 at a similar MSLP value than an intensifying TC. This difference is attributable to longer spin up time for its outer regions of filling TCs. The MSLPs for intensifying TCs versus R15 and R26 are compared in Figs. 4.20 and 4.21. These results show values of 52 and 39 percent of variance explained for R15 and R26 respectively. For filling TCs, 48 and 27 percent of the variance is explained for R15 and R26 respectively (see Figs. 4.22 and 4.23). Although these findings show that more intense TCs tend to have larger R15 values, there is appreciable scatter and forecasters would not know what R15 to forecast based on intensity alone.

An interesting relationship between convection and MSLP is shown in Figs. 4.24-4.27 for filling storms. Up to 60 percent of the variance of MSLP is explained by the amount of convection colder than either -25°C or -50°C (Fig. 4.25). The amount of convection

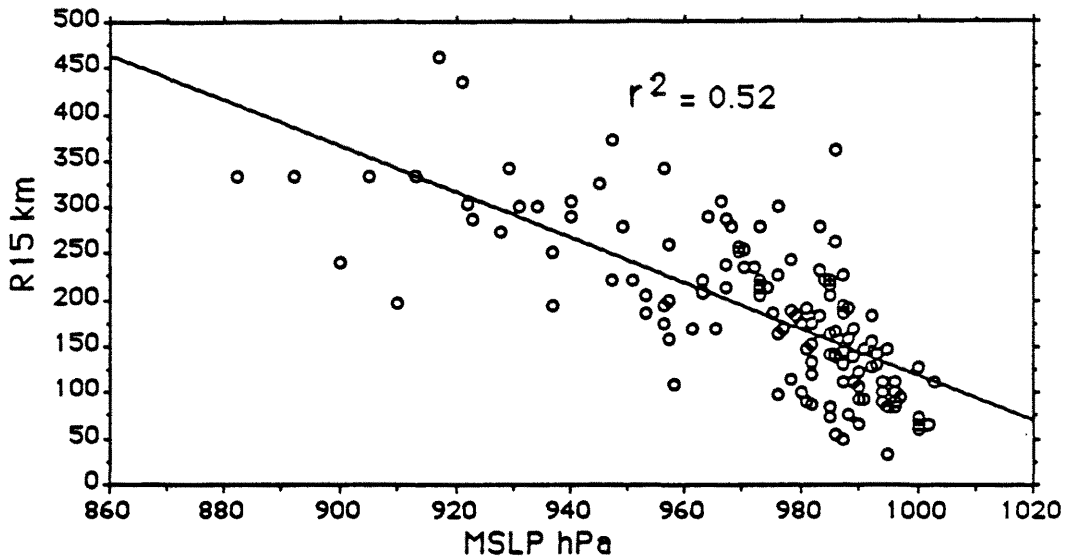


Figure 4.20: Comparison of MSLP and R15 for intensifying storms. Fifty-two percent of the variance of R15 is explained by MSLP.

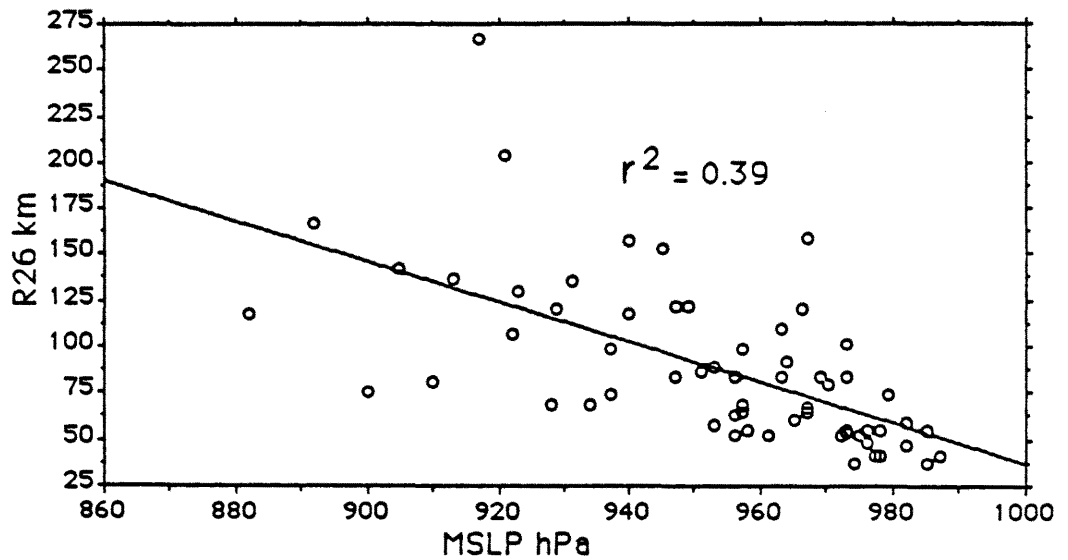


Figure 4.21: As in Fig. 4.20 but for MSLP and R26 for intensifying storms.

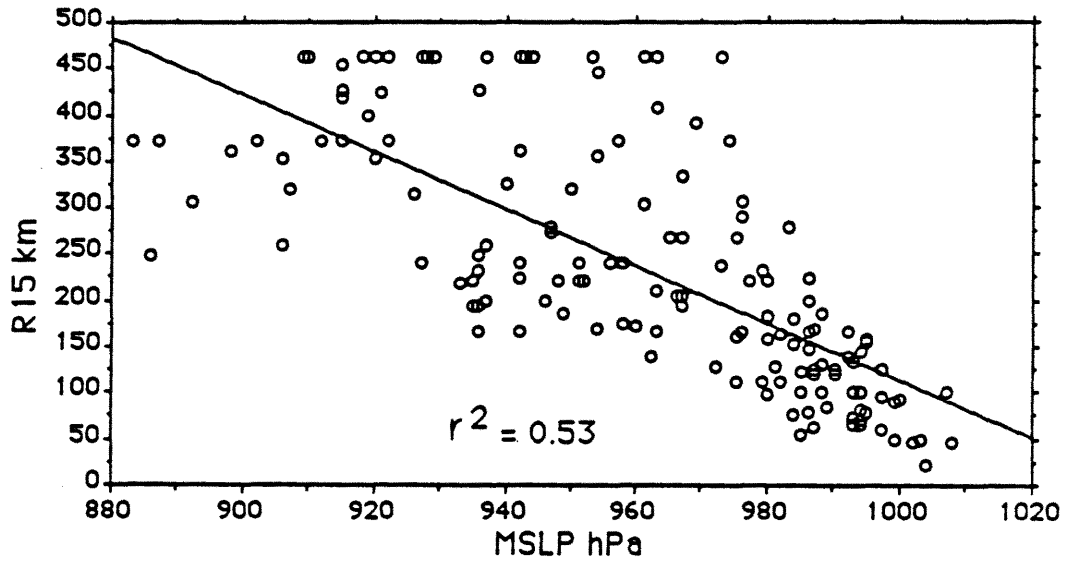


Figure 4.22: As in Fig. 4.20 but for MSLP and R15 for filling storms.

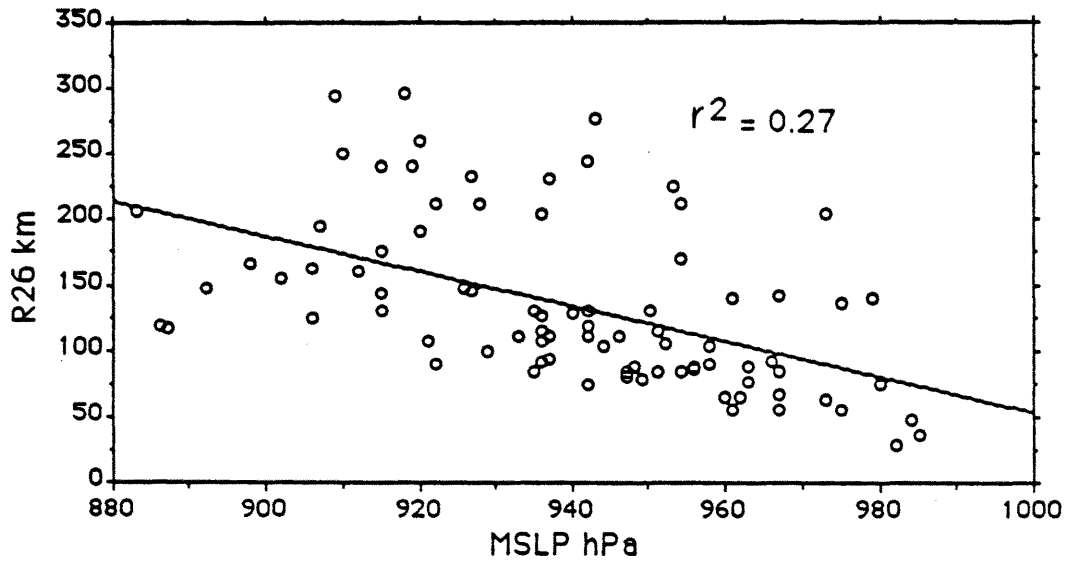


Figure 4.23: As in Fig. 4.20 but for MSLP and R26 for filling storms.

in a filling TC could be used to estimate a range of probable MSLPs. However, this association is not particularly helpful to forecasters because of the availability of more accurate intensity measurement schemes (Dvorak, 1975, 1984).

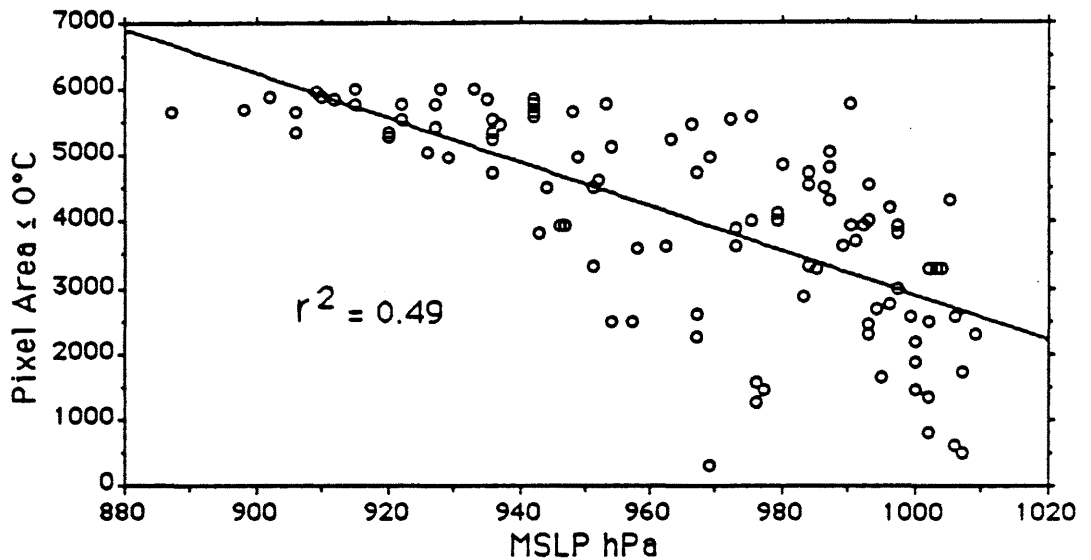


Figure 4.24: Pixel counts for convection colder than 0°C compared to intensity for filling storms. It appears that as storms fill, they lose convection.

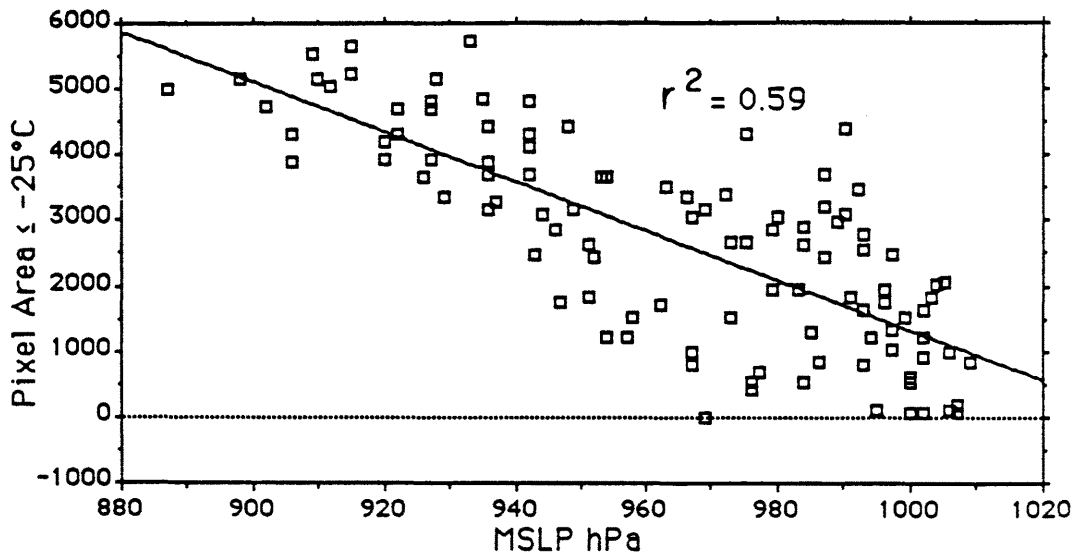


Figure 4.25: As in Fig. 4.24 except for -25°C threshold. Fifty-nine percent of the variance is explained.

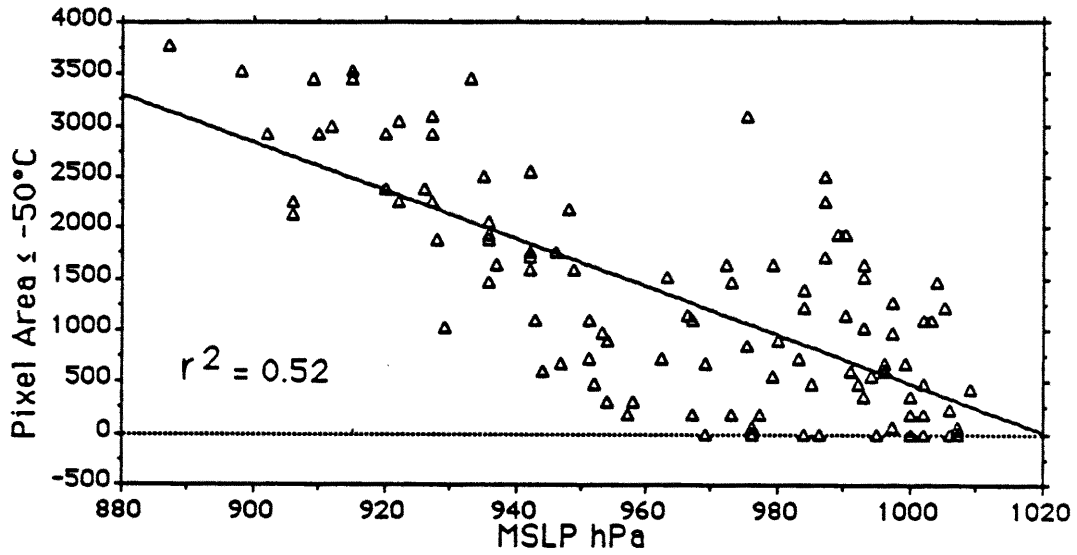


Figure 4.26: Same as Fig. 4.24 except for threshold of $\leq -50^{\circ}\text{C}$.

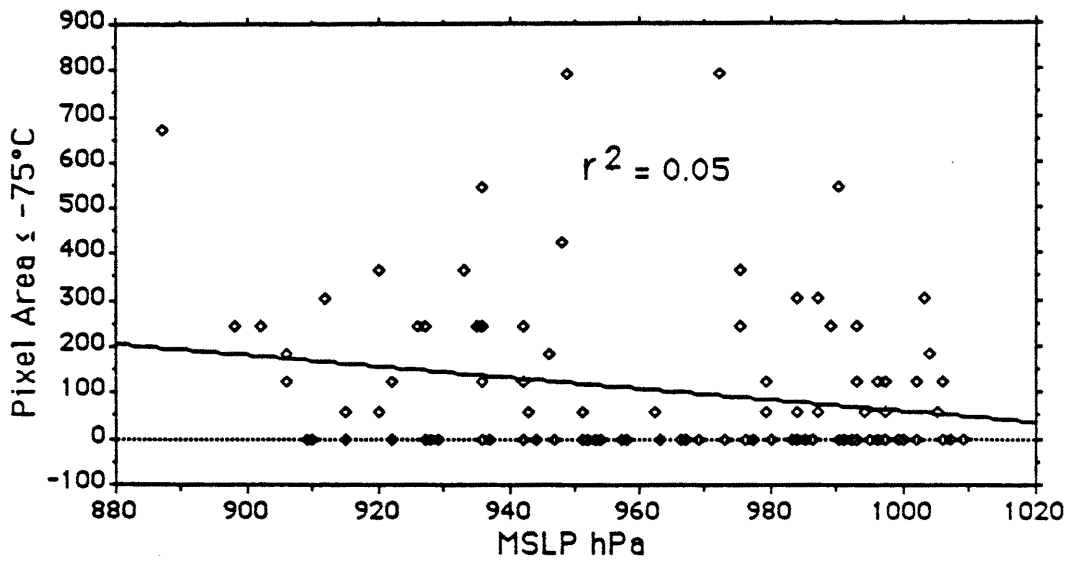


Figure 4.27: Same as Fig. 4.24 except for threshold of $\leq -75^{\circ}\text{C}$.

4.4 Effects of Inertial Stability

It can be assumed that a tropical cyclone with a large areal extent of winds greater than 15 ms^{-1} would have greater inertial stability, I^2 , [or $\zeta_a(\frac{V_T}{R} + f)$] than a small TC with spatially confined winds. It is also possible that pixel counts do not correlate well with R15 change because of the effects of I^2 . Specifically, a TC with a given amount of convection would show less R15 change for large I^2 situations than for small I^2 . Pixel counts divided by I^2 yield numbers which are larger if inertial stability is small. This number might then correspond to a larger R15 increase since the convection can have a greater net effect on winds. It was decided to initially examine a quick measure of inertial stability and see if promising results might be obtained in normalizing for its effects. More precise values for inertial stability could be calculated later from aircraft observations if appropriate. For the purpose of initial testing, an approximate measure of inertial stability was estimated from the ratio $R15/(1009 - \text{MSLP})$. The average sea level pressure of the undisturbed deep tropics (approximately 1009 mb) is included in the denominator so as to keep the values of this approximation greater than zero.

If two TCs with identical MSLPs were compared, the TC with the greater R15 would have greater inertial stability. For a given amount of convection or convection change, a TC with less inertial stability would be expected to have a greater R15 change. When pixel areas divided by I^2 were plotted against R15 change, as in Figs. 4.28–4.31, the graphs show that there is little correlation between the amount of convection normalized by I^2 and changes in R15. Twenty four hour convection change normalized by I^2 correlates poorly to R15 change and graphs are essentially the same as Figs. 4.28 to 4.30. Hence I^2 does not look promising for forecasting R15 and detailed integrated inertial stability values were not calculated from the aircraft mission data.

4.5 Summary

The rather simplistic tests described here failed to yield direct quantitative relationships which might be useful for relating values of tropical cyclone intensity, instantaneous convection and R15 in a way that would allow forecasters to better assess and predict the

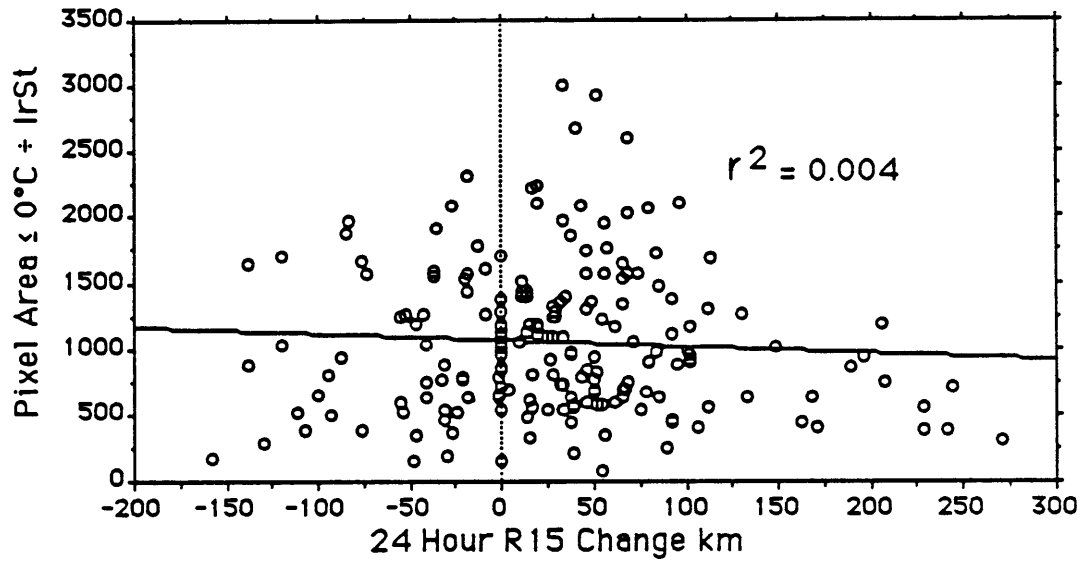


Figure 4.28: Convection normalized by “inertial stability” compared to 24 hour R15 change. Threshold is $\leq 0^\circ\text{C}$.

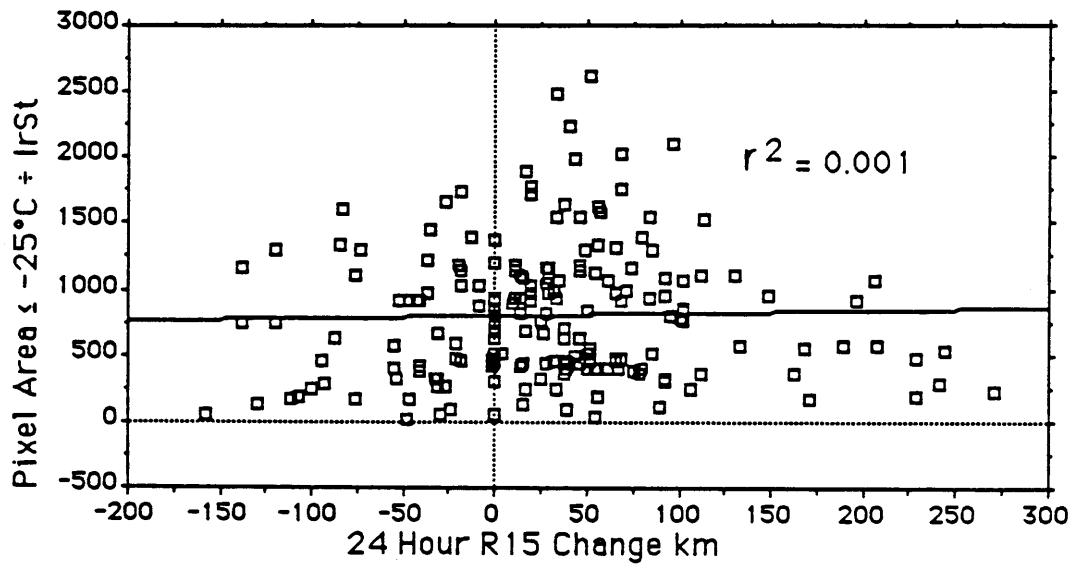


Figure 4.29: Same as Fig. 4.28 except for threshold of $\leq -25^\circ\text{C}$.

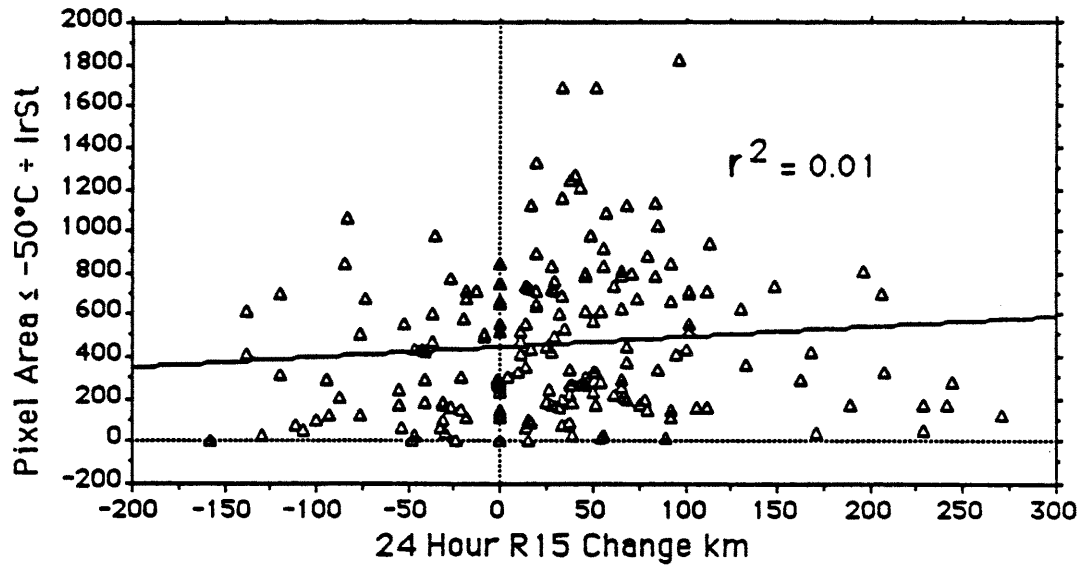


Figure 4.30: Same as Fig. 4.28 except for threshold of $\leq -50^{\circ}\text{C}$.

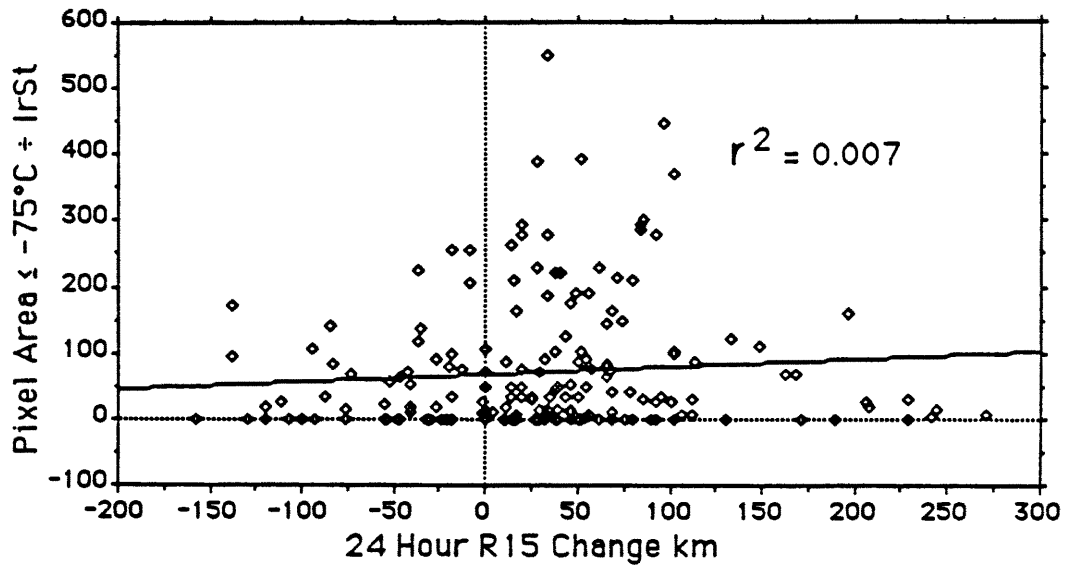


Figure 4.31: Same as Fig. 4.28 except for threshold of $\leq -75^{\circ}\text{C}$.

evolution of the wind structure of tropical cyclones. Although there is a fairly strong correlation between convection colder than -25° and MSLP for filling TCs, this relationship does not improve on techniques already available to forecasters. In the past, direct measurement of winds by aircraft was the only accurate method for determining R15. There are apparently no simple satellite based replacements to be found and more sophisticated schemes must be pursued.

Chapter 5

TEMPORAL ASSOCIATIONS BETWEEN CONVECTION AND THE OCCURRENCE OF MAXIMUM R15

Inspection of the time variation of pixel counts for temperatures colder than -75°C (also termed -75°C convection) at various radii reveals a steady increase in deep convection, followed by a rapid drop off which persists until the TC dies. This large decrease of deep convection generally occurs after maximum intensity is attained and a point is reached where deep convection stops completely and remains stopped as the TC dies. This sequence of development and dissipation is plausible because filling TCs have less deep convection than intensifying TCs and because it corresponds well with the theory advanced previously.

5.1 Diagnosing and Forecasting the Time of Occurrence for MR15

Maximum R15, or MR15, is defined as the greatest extent of R15 occurring during the lifetime of a tropical cyclone. When comparing pixel counts to plots of R15 for the twelve TCs in Table 2.1, a tendency emerges suggesting that in general, -75°C convection in the 222 to 444 km ($2\text{-}4^{\circ}$ annulus stops before the MR15 is reached. However, this tendency is not observed in all TCs and close examination showed that there appear to be two classes of TCs with very different MR15 characteristics; there also appears to be a signal in deep convection at radius 222 to 444 km that may precede MR15 by up to two days.

The relationship wherein the end of deep convection precedes MR15 by approximately two days occurs in six of the twelve TCs. Cyclones which definitely show this relationship include Abby (Fig. 5.1), Forrest (Fig. 5.2), and Vanessa (Fig. 5.3). Typhoons Cary (Fig. 5.4), Ellen (Fig. 5.5), and Marge (Fig. 5.6) also appear to show this relationship to some extent just prior to either making landfall or moving north of 28°N latitude and hence

beyond the domain of this study. Although deep convection in all seven annuli in each of these cyclones showed this trend, -75°C convection in the radius between 222 and 444 km showed the most contrast and the best lead time between convection and MR15.

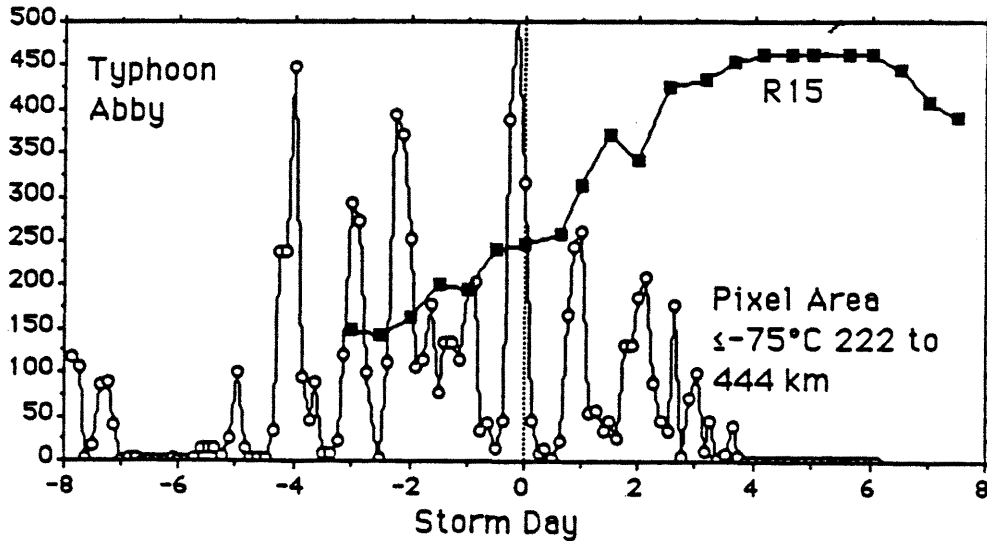


Figure 5.1: Time variation of instantaneous pixel counts and R15 (km) for Typhoon Abby. Deep convection ends on day (plus) three and R15 reaches a maximum approximately two days later. The vertical dotted line (day 0) indicates the time of minimal SLP.

Typhoon Ike (Fig. 5.7) and Tropical Storm Wynne (Fig. 5.8) do not show this time delay between the end of convection and the occurrence of MR15. Typhoon Ike was still intensifying when it crossed the Philippine Islands which interfered with the normal progression of convection and R15. Ike began to reintensify over the South China Sea until making landfall in Southern China. Tropical Storm Wynne made landfall before intensifying to typhoon strength. Thus, both TCs were still in their intensifying and strengthening stage when impeded by the influence of land surfaces.

The other four TCs in the twelve storm sample exhibited no significant lead time between the end of deep convection and the occurrence of MR15. These four were a significant percentage of the sample and were examined to determine why they behaved so differently. Figures 5.9 through 5.12 show the relationship between -75°C convection and R15 for these four, which include Typhoons Bill, Clara, Doyle, and Orchid, respectively. No systematic delay between the end of deep convection and MR15 is apparent. Note

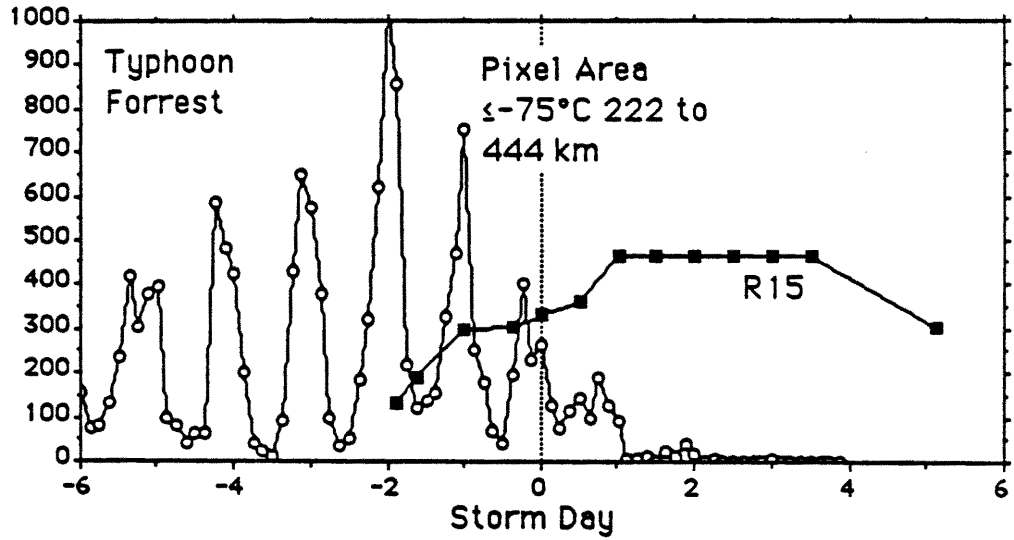


Figure 5.2: As in Fig. 5.1 except for Typhoon Forrest. Note that ordinate scale is two times that for Typhoon Abby (in Fig. 5.1) and more than three times that for Typhoons Carry, Ellen and Ike in Figs. 5.4, 5.5 and 5.7, respectively.

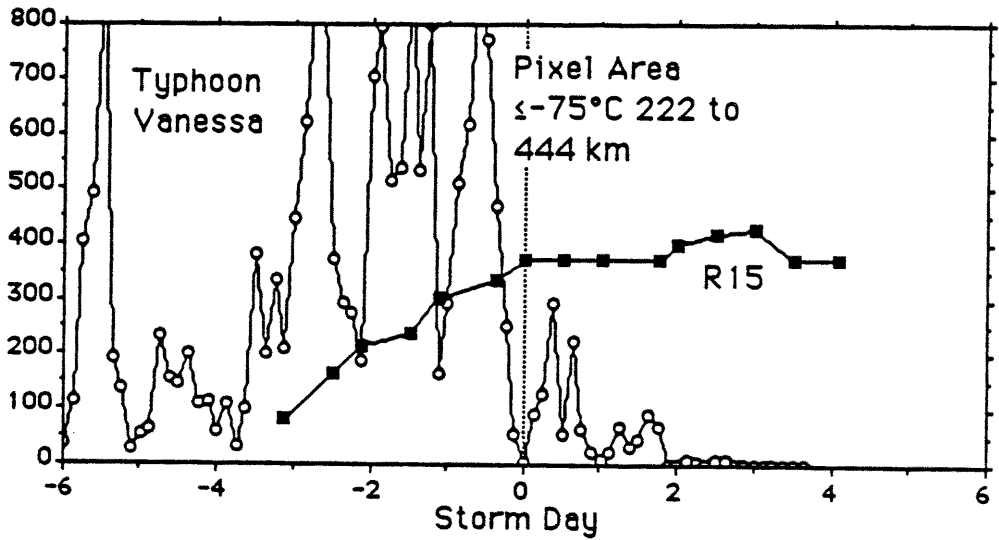


Figure 5.3: As in Fig. 5.1 except for Typhoon Vanessa.

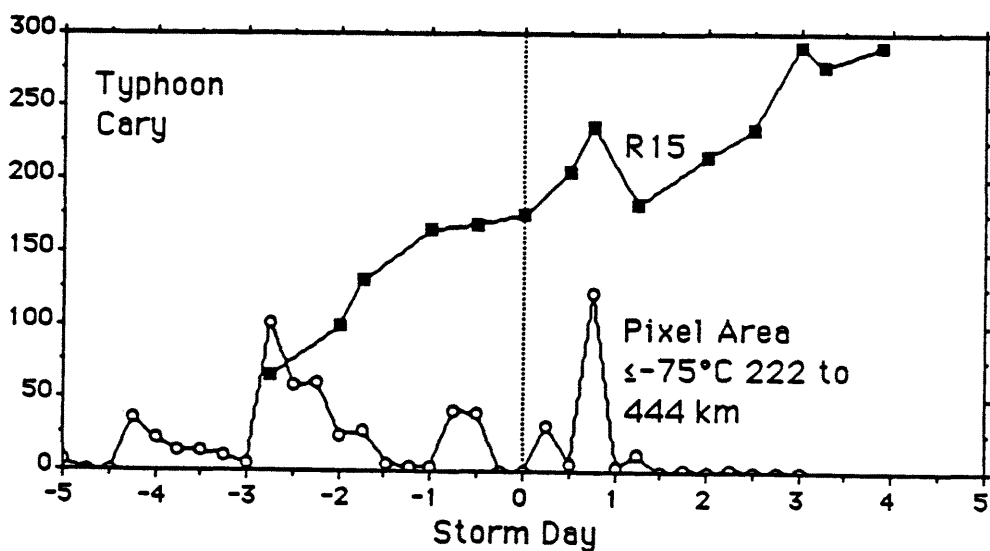


Figure 5.4: As in Fig. 5.1 except for Typhoon Cary. Images were available at six hour intervals for this storm.

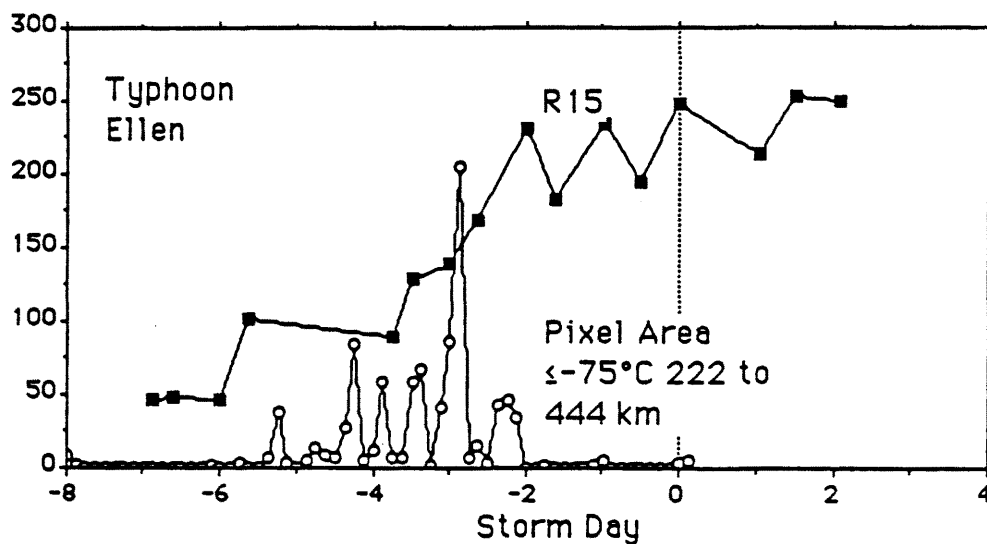


Figure 5.5: As in Fig. 5.1 except for Typhoon Ellen.

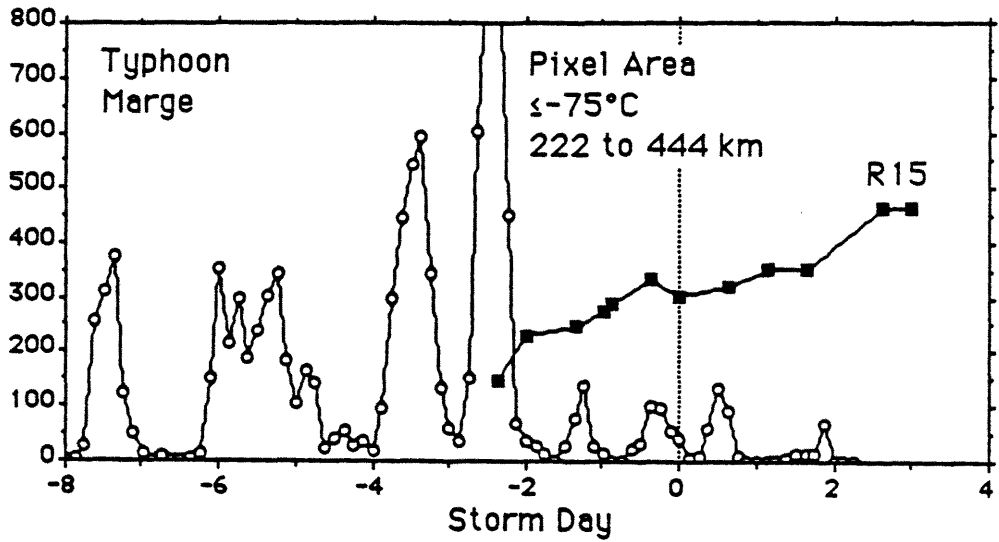


Figure 5.6: As in Fig. 5.1 except for Typhoon Marge.

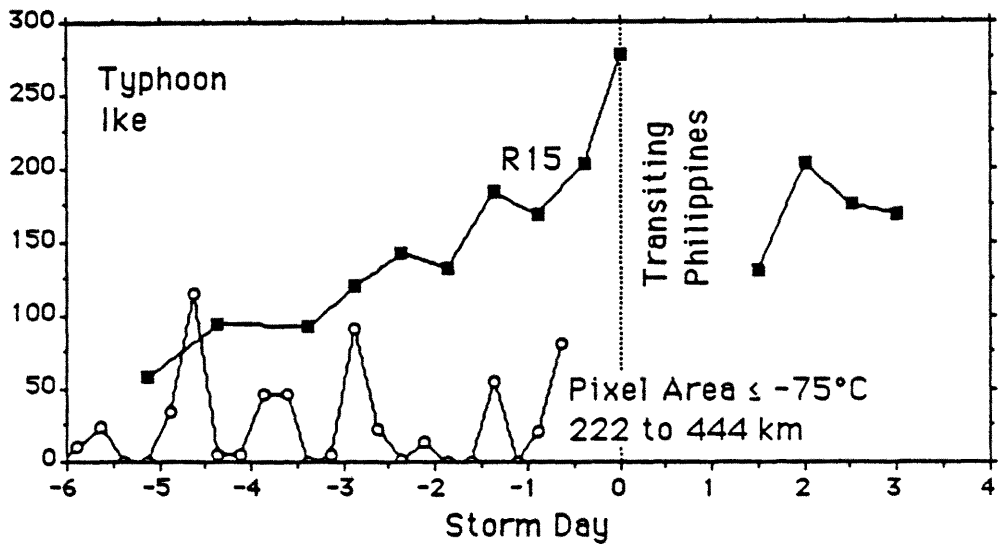


Figure 5.7: As in Fig. 5.1 but for Typhoon Ike. Convection and the wind profile in Ike were disrupted as it transited the Philippines.

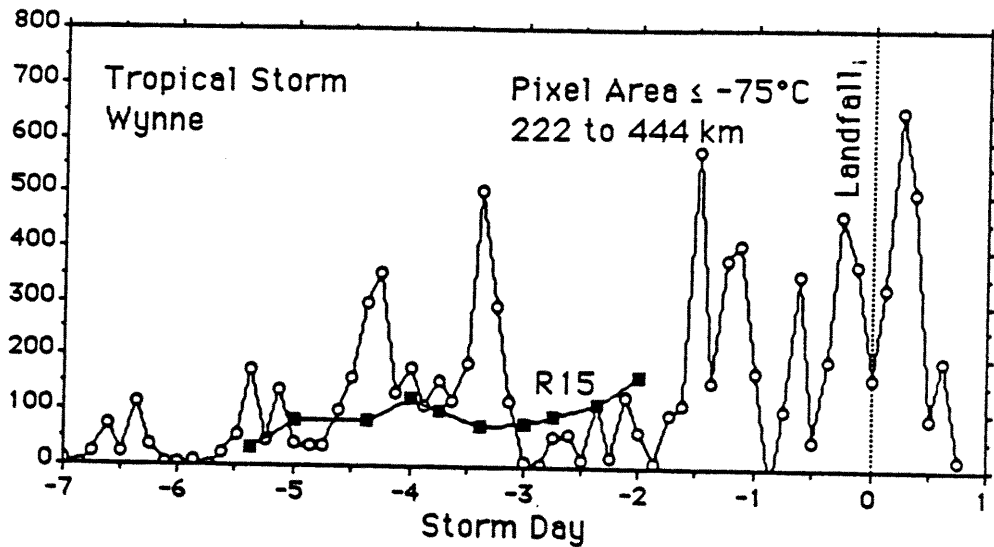


Figure 5.8: As in Fig. 5.1 but for Tropical Storm Wynne which made landfall in southern China before maximum intensity.

that although MR15 occurred up to two days after the end of deep convection, there are no cases among these four wherein deep convection in the 222 to 444 km radius occurs more than twelve hours after MR15.

5.2 Theory of Maximum R15

Weatherford (1989) proposed that, in general, R15 keeps increasing after maximum cyclone intensity is reached and continues to increase until approximately that time when there is no longer an eye in the storm. Weatherford defines Outer Core Strength (OCS) as the average wind from 111 to 278 km radius and shows that OCS values correlate well with R15. Dunn and Miller (1960) and Riehl (1979) divide Atlantic Hurricanes into four idealized stages which parallel Weatherford's findings. These stages are,

1. The formative stage including the time from when the TC initially develops until it reaches hurricane intensity;
2. The immature stage wherein intensification proceeds with little change in OCS. This period ends when the cyclone reaches maximum intensity;

3. The mature stage wherein intensity no longer increases but OCS grows;
4. The decaying stage wherein OCS begins to collapse.

This sequence of stages applies to the six TCs which exhibited a two day lead time between convection and MR15 (Figs. 5.1-5.6). All six are filling when MR15 is reached (maximum OCS) and thus appear to fit the description of a typical TC. In this paper, these typical storms will be characterized as “delayed” TCs since MR15 is delayed following the end of maximum intensity.

In the four TCs with no lead time between the end of -75°C convection (in radius 222 to 444 km) and MR15, the MR15 value is reached within approximately twelve hours of maximum intensity (Figs. 5.9-5.12). Hence, MR15 occurs almost simultaneously with maximum intensity, and also with the end of deep convection. These four storms are termed as “simultaneous” TCs. These TCs have a distinctly different wind distribution over their lifetimes when compared to delayed TCs. Examining the deep convection from 0 to 222 km for the four simultaneous TCs shows that although the deep convection from 222 to 444 km has stopped, deep convection from 0 to 222 km persists and TCs are still active.

Figure 5.13 shows a comparison of the convection in these two annuli for Typhoon Orchid, a simultaneous TC. In the delayed TCs, convection in both annuli stops at approximately the same time as shown in Fig. 5.14 for Typhoon Abby. Thus it appears that when simultaneous TCs reach maximum intensity, they immediately begin the process of decay, skipping step three (maturing) of the Dunn and Miller TC cycle. When a delayed TC reaches maximum intensity, it adjusts outward and, although maximum intensity has been reached, the OCS continues increasing and deep convection near the TC's center persists as the TC strengthens during that time.

The cause of this difference will possibly be found in the large scale influences. The delayed TCs may be entering a more favorable synoptic environment such as one wherein vorticity near the outer radius increases due to the influence of the subtropical ridge. The comparative climatological characteristics of delayed and simultaneous TCs provide

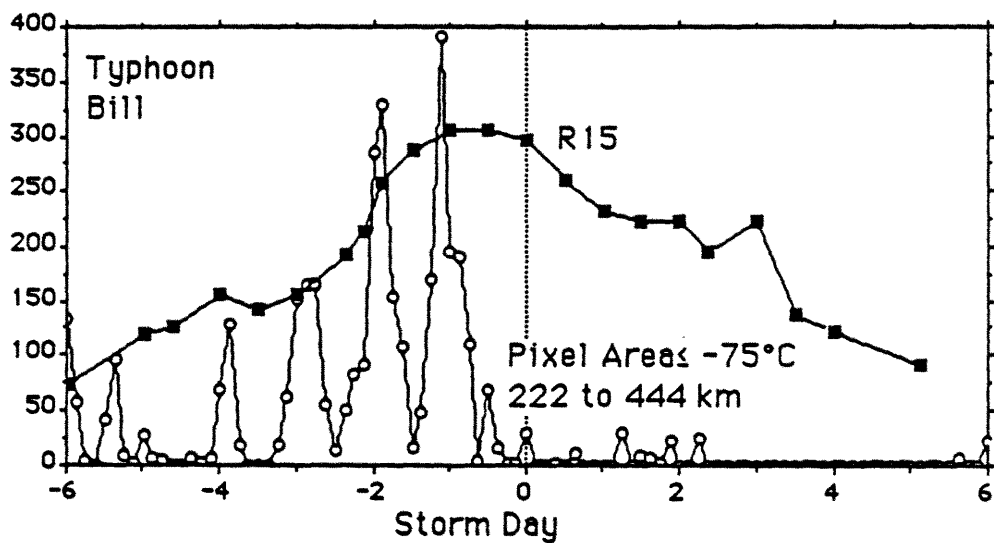


Figure 5.9: As in Fig. 5.1 but for Typhoon Bill. Deep convection ended at approximately the same time as R15 reached maximum which also corresponded to the time of maximum intensity.

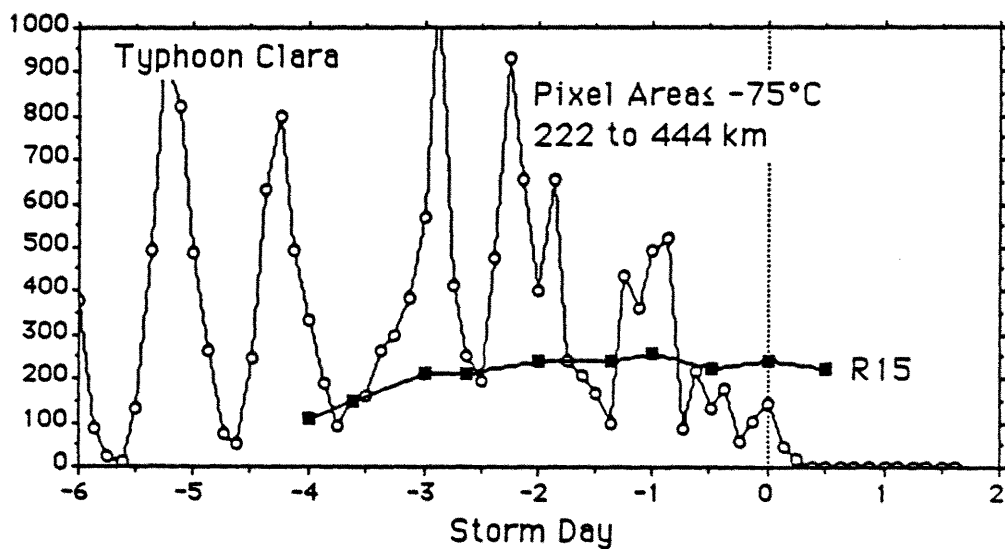


Figure 5.10: As in Fig. 5.9 except for Typhoon Clara.

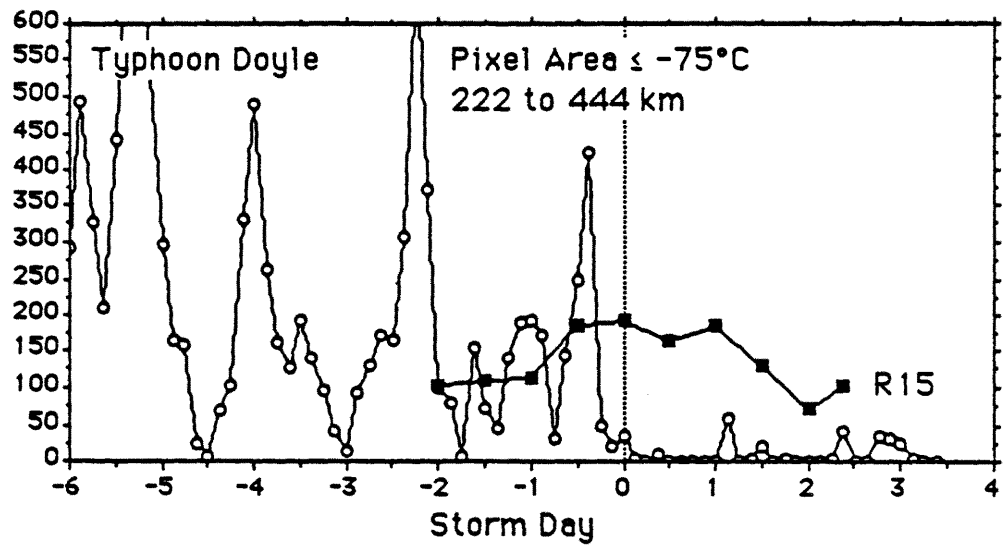


Figure 5.11: As in Fig. 5.9 except for Typhoon Doyle.

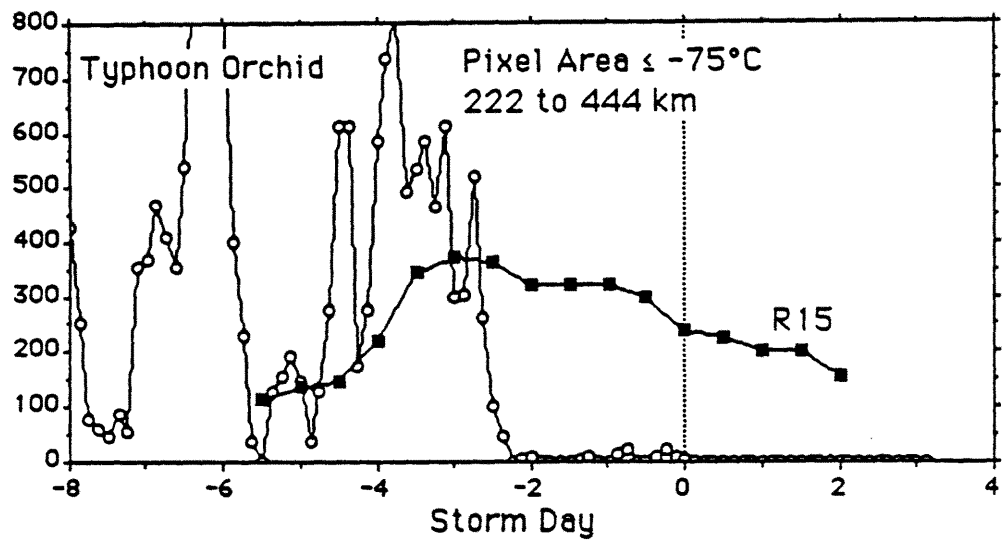


Figure 5.12: As in Fig. 5.9 except for Typhoon Orchid.

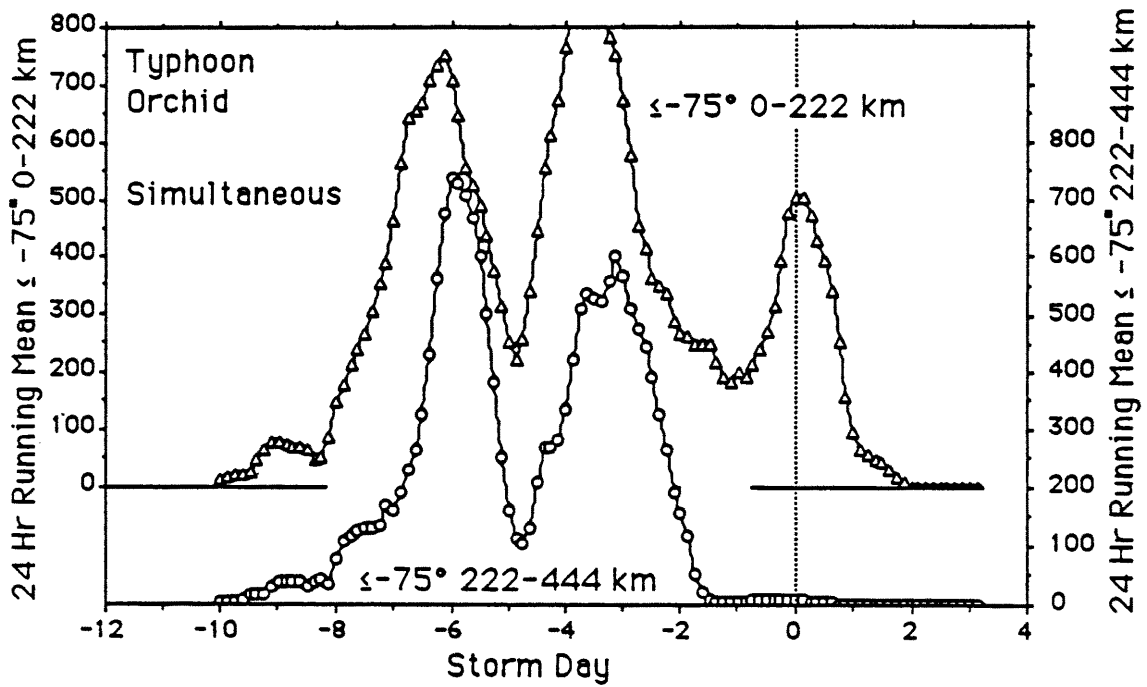


Figure 5.13: Deep (-75°) convection in Typhoon Orchid for the 0-222 km annulus. Convection over 0-222 km continues for approximately three days after the deep convection in the 222-444 km annulus ends (heavy dashed line). This sequence is typical of simultaneous TCs.

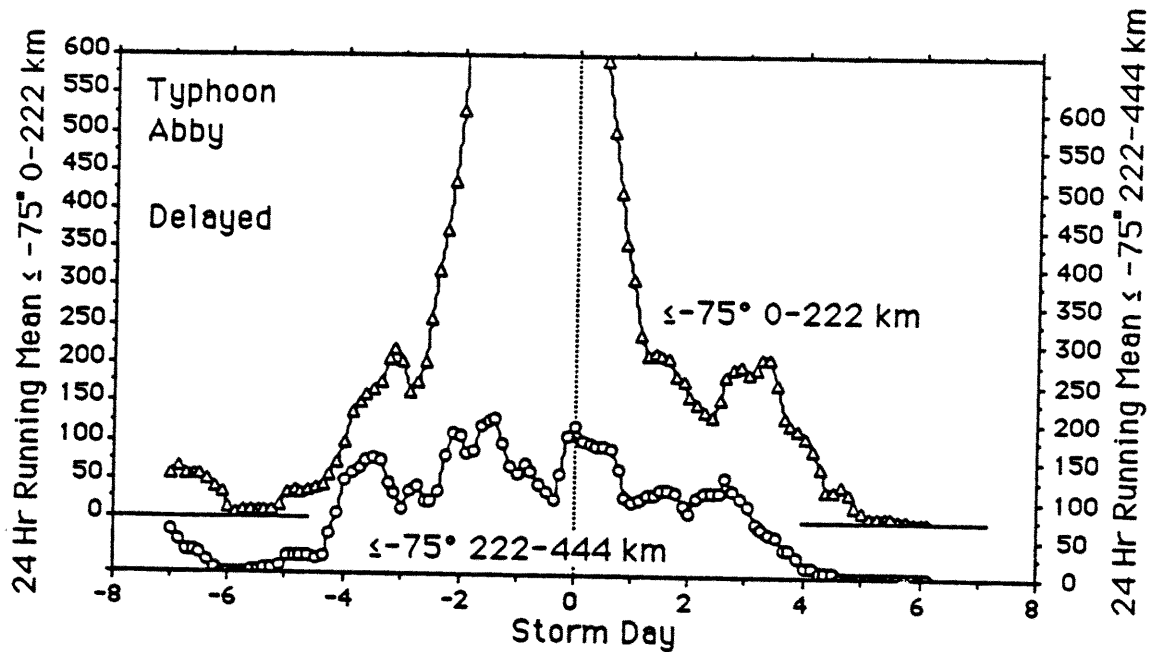


Figure 5.14: Deep convection in Typhoon Abby for both the 0-222 km and 222-444 km annuli. Convection ends in both annuli within one day of each other. This is typical of delayed TCs.

hints as to possible differences in their life cycles. The six delayed TCs occurred in July, August, September (2), October, and November. The four simultaneous TCs occurred in November (3) and December. This time distribution may indicate a seasonal effect, as the large scale influences may not be as favorable in the latter part of the TC season in comparison to the early fall. Recurvature seemed to not be a factor in differentiating between simultaneous and delayed TCs in that two of the simultaneous TCs recurved and two did not. Of the delayed TCs, five recurved and one did not. Presently, the seasonal effects appear to be more important in determining TC type.

5.3 Forecasting Maximum R15

Important considerations for forecasting MR15 include any clues which indicate in advance which TCs are simultaneous and which are delayed. Aircraft reconnaissance measurements of eye sizes might provide such a clue. Eye size data, which were part of the reconnaissance data set, were collated for the six delayed and four simultaneous TCs.

Figures 5.15 and 5.16 show the variation in time of mean eye sizes relative to the time of the first appearance of the eye for both delayed and simultaneous TCs.

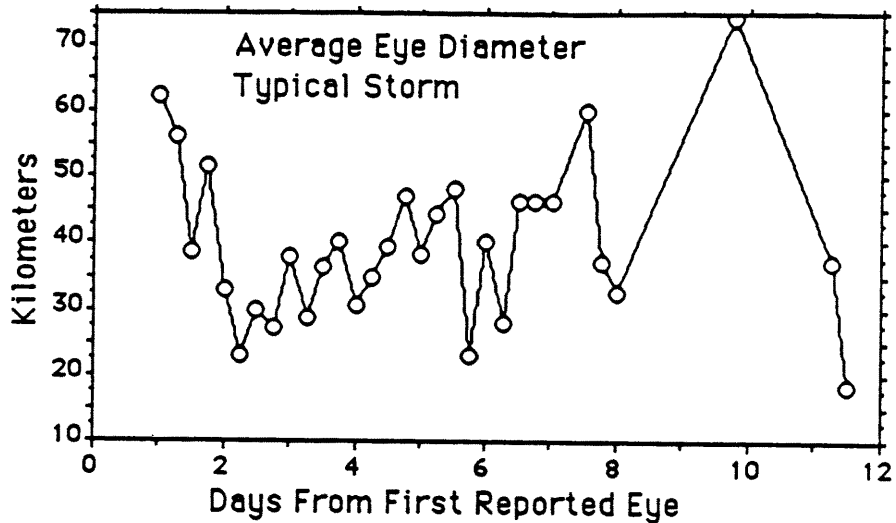


Figure 5.15: Time variation of delayed TC eye diameters in relation to the time of the first reported eye size. Eyes appear to grow slowly over time beginning on day 3.

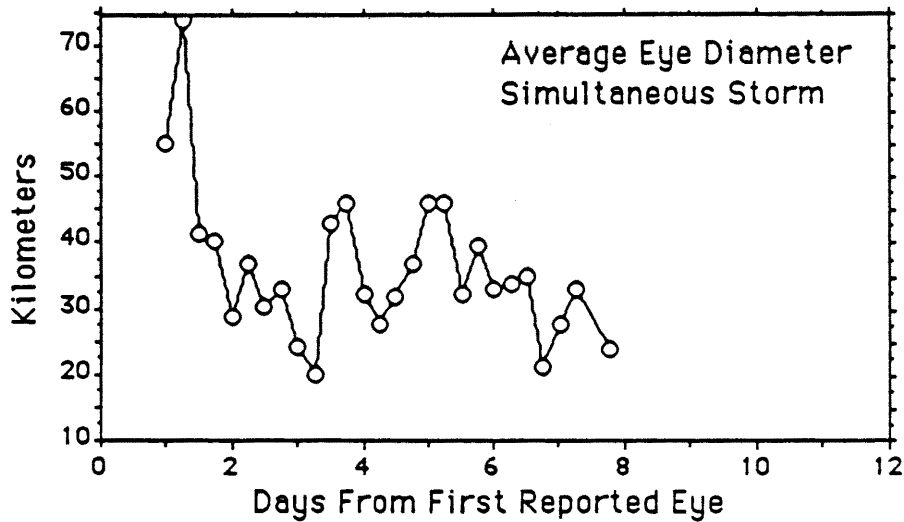


Figure 5.16: Time variation of averaged eye diameters of simultaneous storms shown in relation to the time of the first reported eye. A slight contracting trend is evident beginning on day 5.

No trends became evident when viewing these plots. It was then decided to examine the time variation of eye size in relation to the time of maximum intensity. Time of

maximum intensity was defined as day zero for each TC life cycle and eye sizes were first averaged and then plotted. Figures 5.17 and 5.18 reveal distinct differences between the two TC types. Whereas the eyes of delayed TCs tend to decrease until maximum intensity is reached and then tend to increase again, the eyes of simultaneous TC tend to remain at approximately the same size and may decrease slightly after maximum intensity. Also, following maximum intensity, the eyes of simultaneous TCs did not persist for as long as those of delayed TCs.

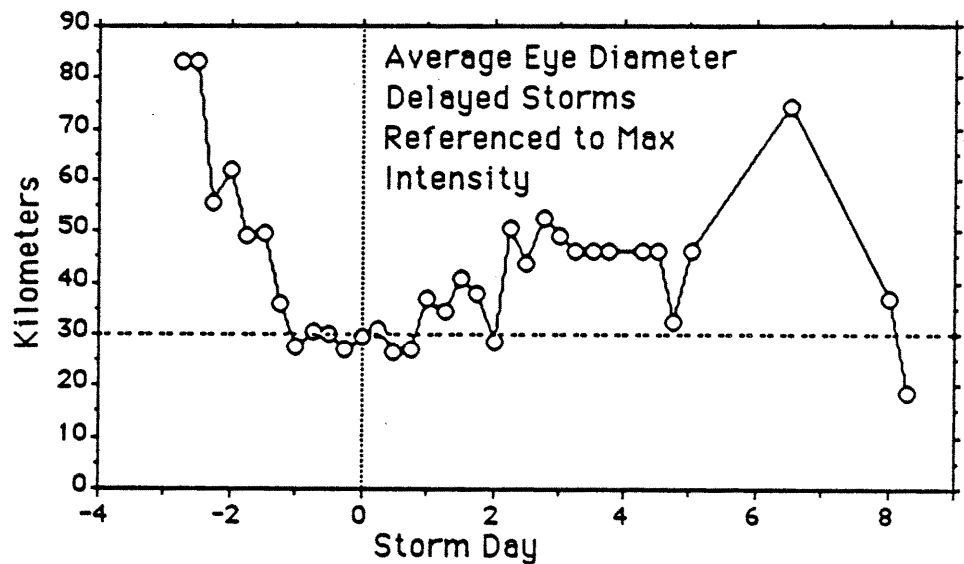


Figure 5.17: Time variation of averaged eye diameters for delayed storms in relation to time of maximum intensity (day 0). Note how eye shrinks until maximum intensity is reached and then expands. Large variability at the start and end of the time series is due to small sample sizes.

These differences in eye characteristics combined with the differences in convective characteristics seems to suggest that fundamental differences may exist between these two types of TCs. In delayed TCs, R15 continues to increase and the eye grows larger, even though maximum intensity has been reached. Deep convection continues on a broad area around the TC after maximum intensity. In simultaneous TCs, MR15 occurs at about the same time as maximum intensity and subsequent deep convection becomes confined to the area near the center of the TC (0 to 222 km). Thus, delayed TCs, after reaching maximum intensity, appear to adjust outward, “maturing” as their OCS increases. Simultaneous

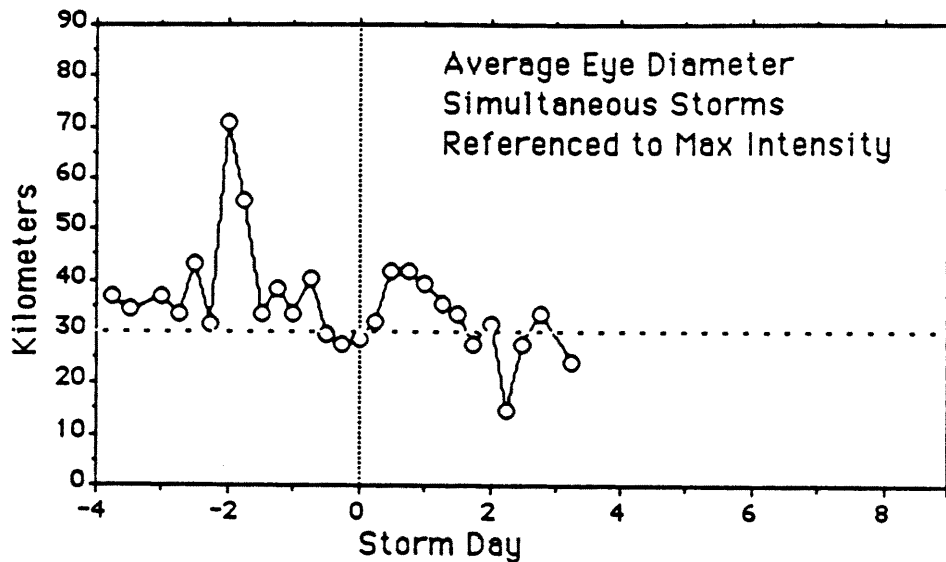


Figure 5.18: Time variation of average eye diameters for simultaneous storms. Eyes appear earlier in the storm's life cycle, do not last as long after maximum intensity, and neither decrease nor expand after maximum intensity is reached.

TCs remain compact, and do not grow in radial extent after maximum intensity; rather, they reach maturity at the same time as maximum intensity. After maximum intensity is reached, the OCS of simultaneous TCs decreases as these TCs weaken.

Although the sample size used to compute mean eye diameters for this analysis is small, the results are interesting and are presented primarily in consideration of future research. Also, because values for the time variations of eye size are too small to measure with present satellite technology, techniques for using eye sizes to forecast TC type are not presently applicable.

5.4 Forecasting Rules for Maximum R15

Useful "rules of thumb" are needed for forecasters to differentiate between delayed and simultaneous TCs and to forecast the time of MR15. Presently these rules include the following:

1. If -75°C convection occurs over more than two percent of the annulus spanning 222 to 444 km for more than twelve hours after maximum intensity has been reached:

- This is a delayed TC.
 - Maximum R15 will occur approximately two days after -75°C convection in the 222 to 444 km annulus reaches a value of less than two percent of the area.
2. If maximum intensity has either not yet been reached or was reached within twelve hours of -75°C convection in the 222 to 444 km annulus falling below two percent of the area:
- This is a simultaneous TC.
 - Maximum R15 occurred or will occur within twelve hours of the decline of deep convection in the 222-444 km radius.
 - Maximum intensity occurred or will occur within twelve hours of the end of deep convection in that radius.

5.5 Summary

It is now possible to estimate when MR15 will occur with a modest degree of skill. Two distinct modes for wind development in tropical cyclones became apparent when looking at twelve selected TCs in 1983 and 1984: the OCS may either continue to increase after maximum intensity has been reached, (delayed TCs), or the OCS may follow intensity and begin to decrease immediately after maximum intensity has been reached (simultaneous TCs). Diminished rates of deep convection in the 222 to 444 km annulus ends are a signal that MR15 will be reached approximately two days later in delayed TCs, or that the MR15 and maximum intensity have already occurred or will occur within twelve hours for simultaneous TCs. These forecasting tools are objective and the signal is a change in the convection data which is easily observed.

Chapter 6

TIME VARIATION OF R15 IN RELATION TO RATES OF CONVECTION

6.1 Convection and R15

It was shown in Chapter 5 that temporal trends in convection offer some insight as to when R15 has reached its maximum value. This association suggests that convection might also be useful for predicting changes of R15 with time. The hypothesis discussed in Chapter 3, that the amounts of convection should correlate with R15 and/or its variation with time, was examined to see if the rate of change for R15 could be determined from the current R15 value and the recent history of convection. Running mean values for 24, 48, and 72 hour average convection within a 444 km radius were computed for each day, along with current values for R15 and prior and subsequent rates of change of R15. These values were computed over the entire life cycle of each of the twelve cyclones studied here. The observations were then compared graphically to determine if useful relationships might exist.

Running mean values of convection for 24, 48, and 72 hour periods for temperature thresholds of -25°C and -50°C were compared to values of R15. Correlation statistics for a polynomial regression were also computed. Figures 6.1 through 6.6 show the relationships obtained in these tests. For the best of these results (Fig. 6.3), 51 percent of the variance of R15 was explained by the 72 hour running mean -25°C (and colder) convection. When R15 values were less than 300 km, there was a tendency for increased convection to correspond to increased values of R15. However, for R15s greater than 300 km, similar amounts of convection were observed for a large range of R15 values. Note that the difference between the figures shown here (Figs. 6.1 through 6.6) versus Figs. 4.4 through

4.15 is the use of running mean rather than instantaneous values of convection in Figs. 6.1-6.6.

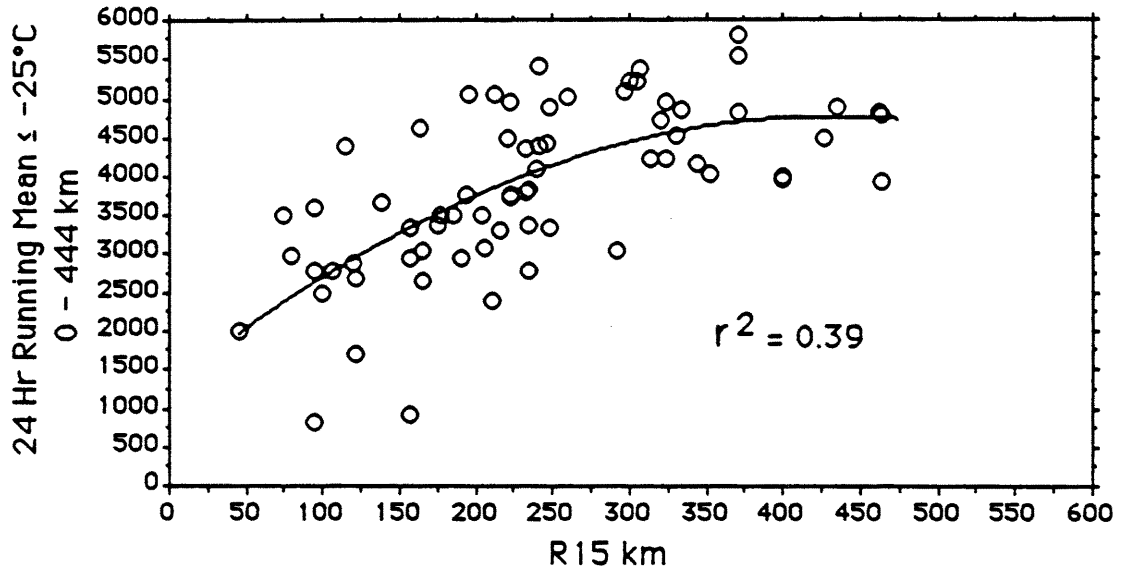


Figure 6.1: Twenty-four hour running mean pixel counts for convective cloud top temperatures less than -25°C in the 0 to 444 km radius area compared to subsequent R15 values observed for the end of the averaging period. The best fit routine uses a polynomial regression of order two.

6.2 Convection and R15 Change

Temporal associations for various time varying values of R15 were illustrated in Fig. 2.5. Figure 3.7 presented an idealized hypothetical relationship between R15, R15 change, and convection. In this section the possibility that changes of R15 can be determined from such a relationship is examined. Initially, all observations were stratified according to whether R15 was increasing or decreasing and then compared to see if a curve similar to that in Fig. 3.7 could be observed. The best results obtained in this test were obtained for the -25°C threshold, which are shown in Figs. 6.7 through 6.12. There is considerable overlap between the increasing and decreasing R15 groups and many of the observations with decreasing R15 were associated with greater convection than were observations with R15 increasing. This overlap also occurred for both prior and subsequent changes of R15

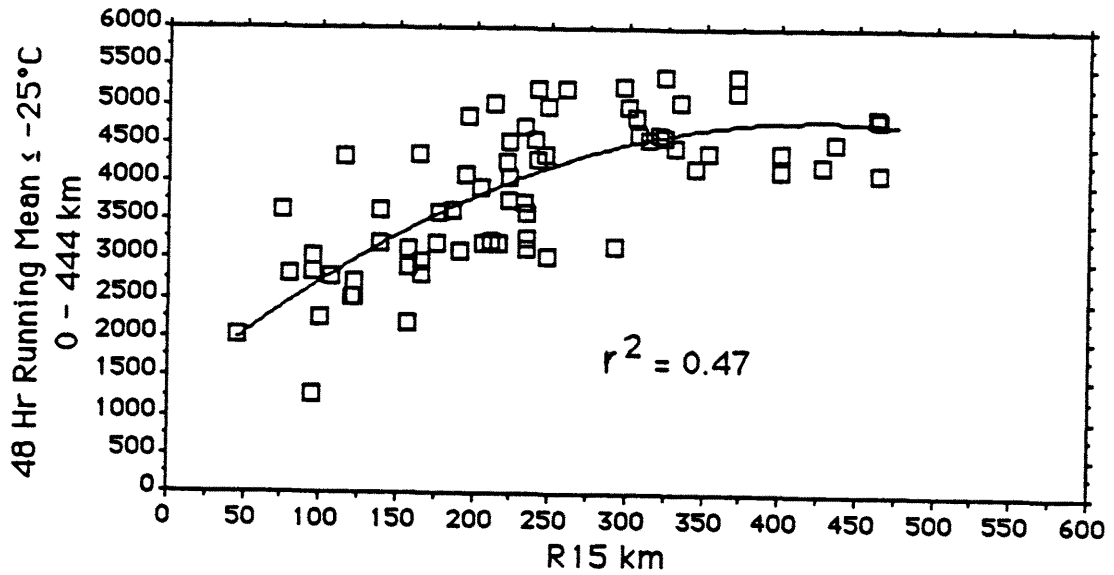


Figure 6.2: Forty-eight hour running mean pixel counts for -25°C convection compared to subsequent R15 values.

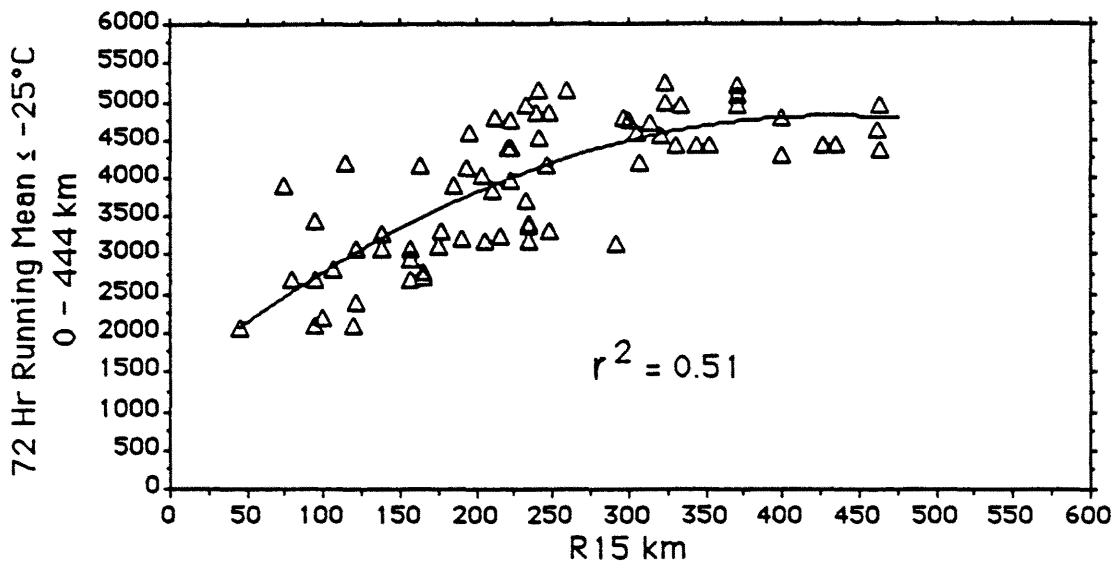


Figure 6.3: Seventy-two hour running mean pixel counts for -25°C convection compared to subsequent R15 values.

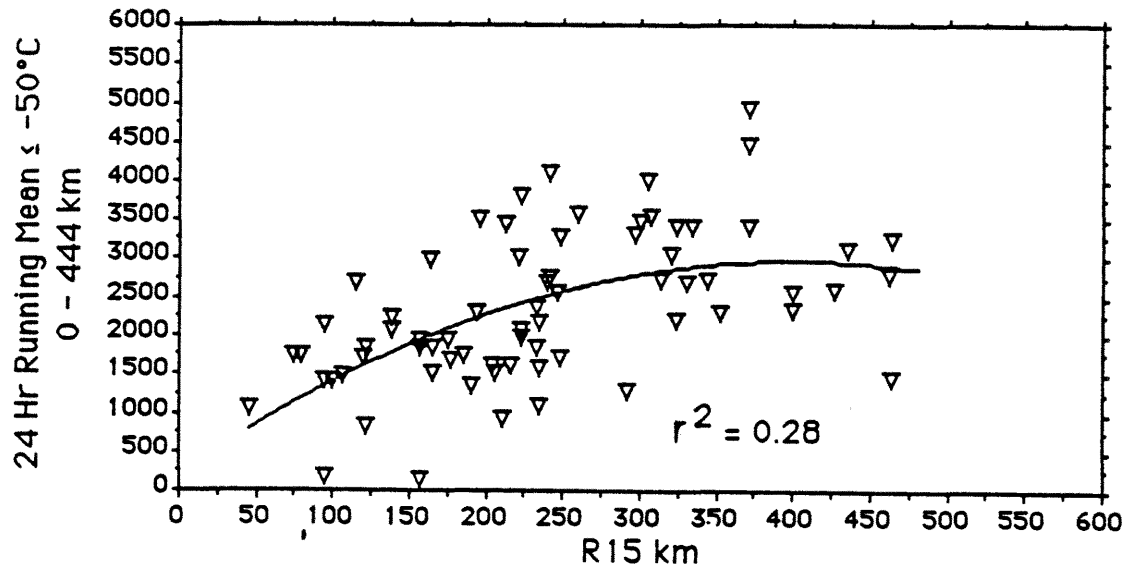


Figure 6.4: Twenty-four hour running mean pixel counts for -50°C convection compared to subsequent R15 values.

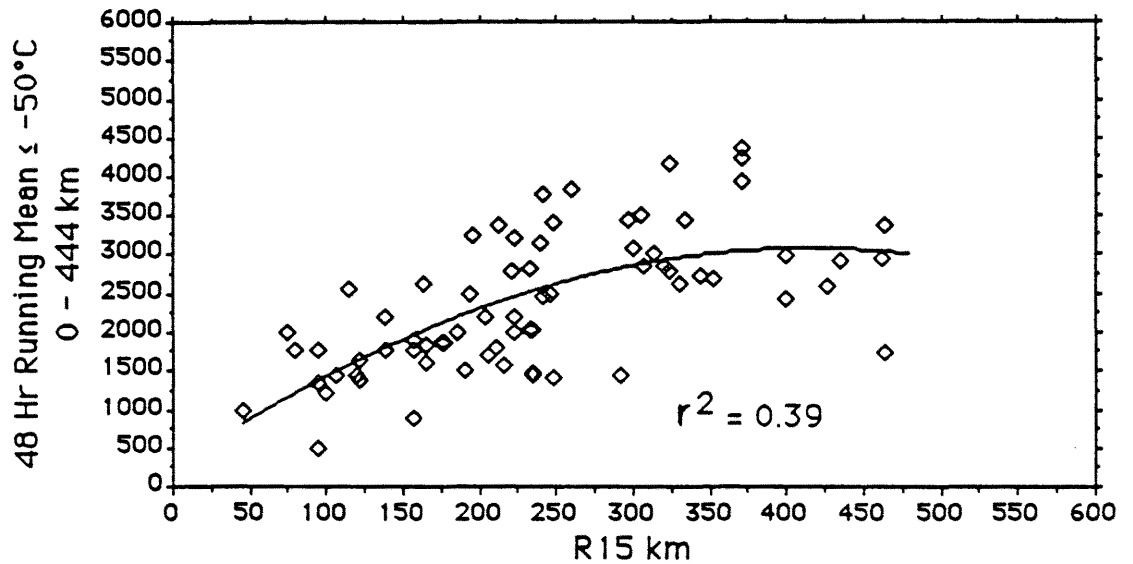


Figure 6.5: Forty-eight hour running mean pixel counts for -50°C convection compared to subsequent R15 values.

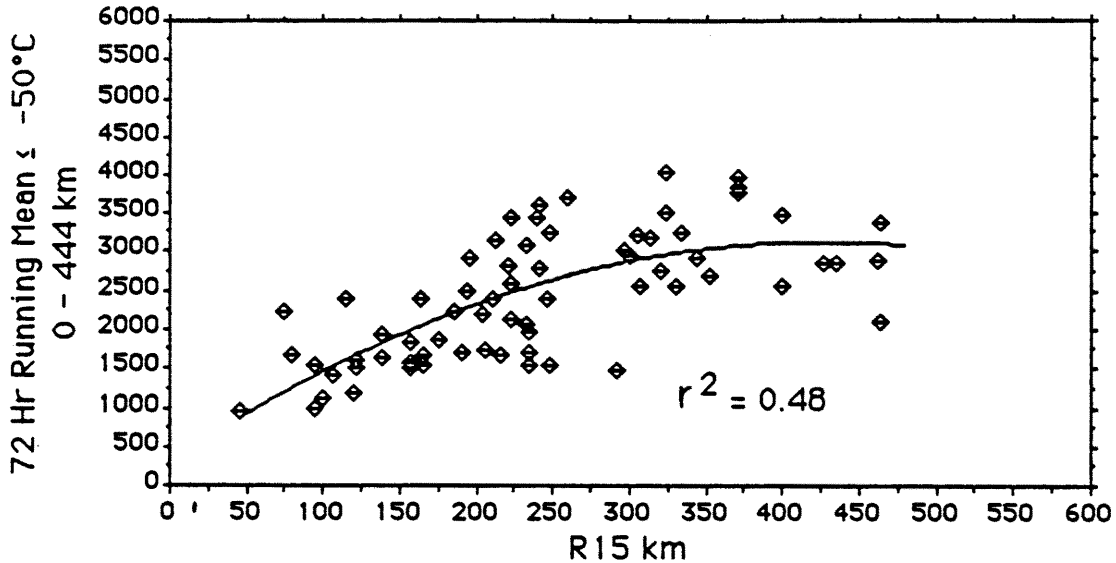


Figure 6.6: Seventy-two hour running mean pixel counts for -50°C convection compared to subsequent R15 values.

in relation to the convection averaging period (see Fig. 2.5 for definitions of “prior” and “subsequent” 24-hour changes of R15).

It was thought that because the data sample in Fig. 6.7 contained both delayed and simultaneous TCs, the wind profiles of each, following maximum intensity, might be the cause of the overlap. The comparison in Fig. 6.7 was redone using only observations from intensifying TCs and results of these tests are shown in Figs. 6.13–6.18. For subsequent future changes of R15 (Figs. 6.16–6.18), a reasonable distinction emerges, separating the samples wherein R15 was increasing from those where it was decreasing. When TCs are intensifying, there indeed appears to be a certain level of convection which, if exceeded, will result in an increase of R15. This finding confirms the hypothesis stated in Chapter 3 that convection should correlate with radial wind extent, allowing for noise in the sample caused by other influences including variable large scale processes. When restratified and omitting all R15 changes smaller than 20 km, the level of noise is reduced considerably (Figs. 6.19 through 6.21).

Values for subsequent increases and decreases of R15 were stratified for intensifying TCs to see if, as hypothesized, larger R15 changes will be found farther (above or below)

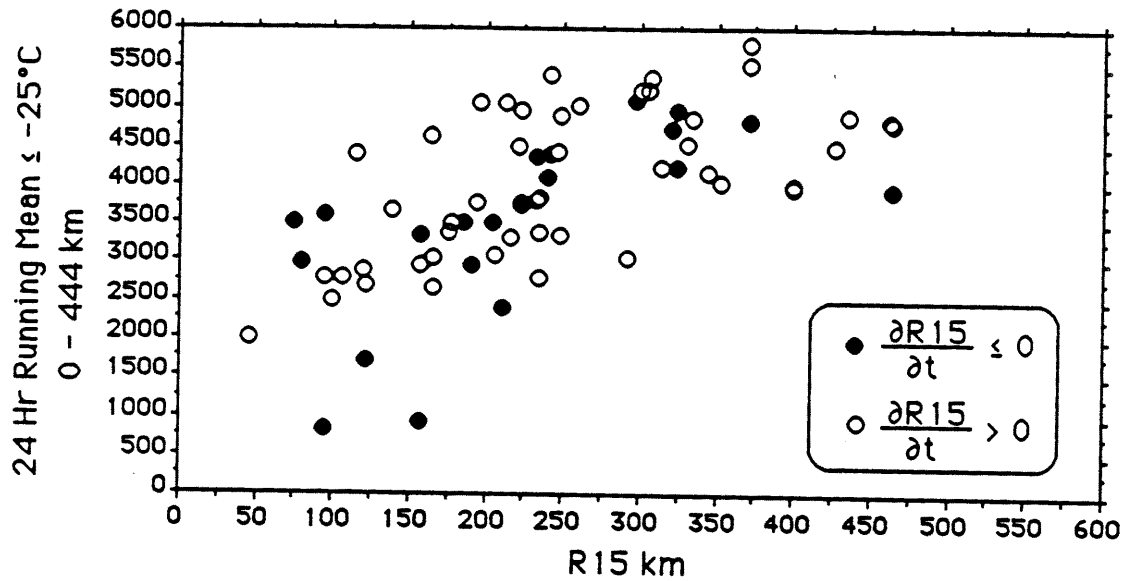


Figure 6.7: Cases of increasing and decreasing 24 hour changes of R15 compared to the prior 24 hour running mean -25°C convection. Note the considerable overlap between observations where R15 was decreasing (solid) and increasing (open circles).

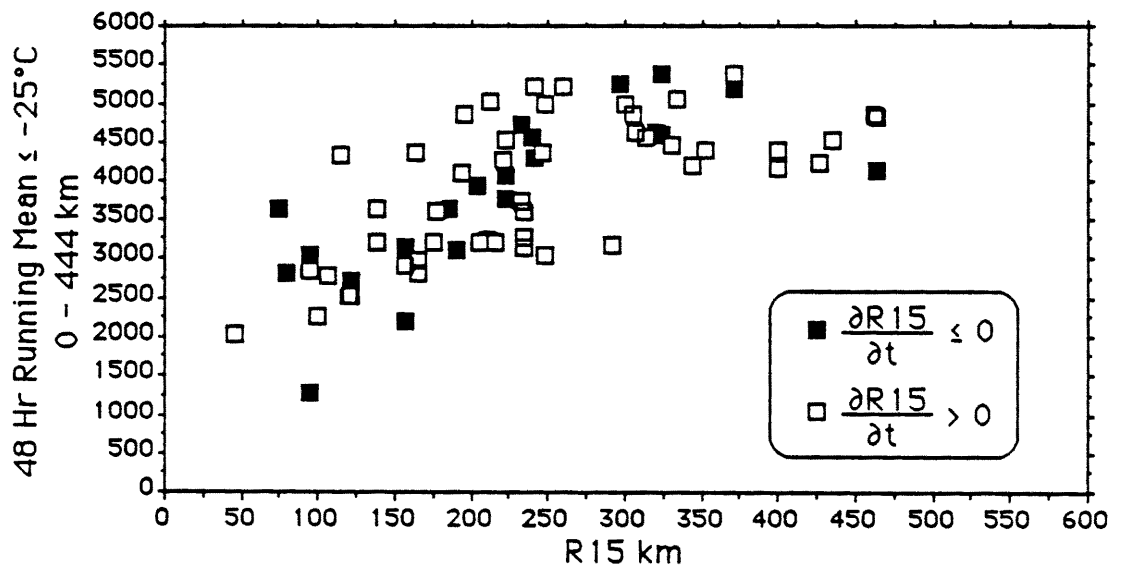


Figure 6.8: Same as Fig. 6.7 except for running mean -25°C pixel areas over the prior 48 hours.

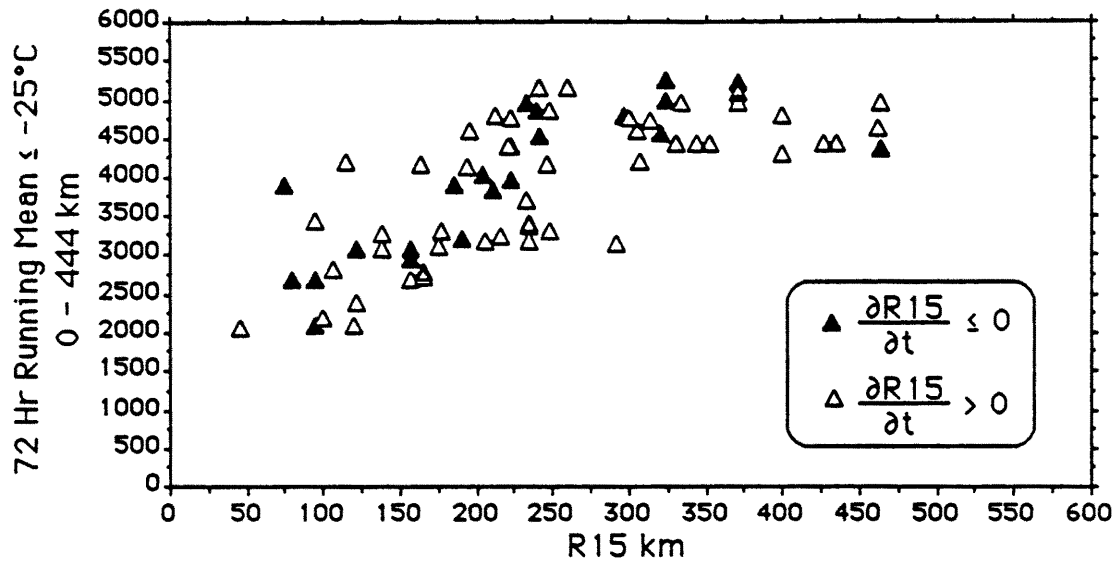


Figure 6.9: Same as Fig. 6.7 except for running mean -25°C pixel areas over the prior 72 hours.

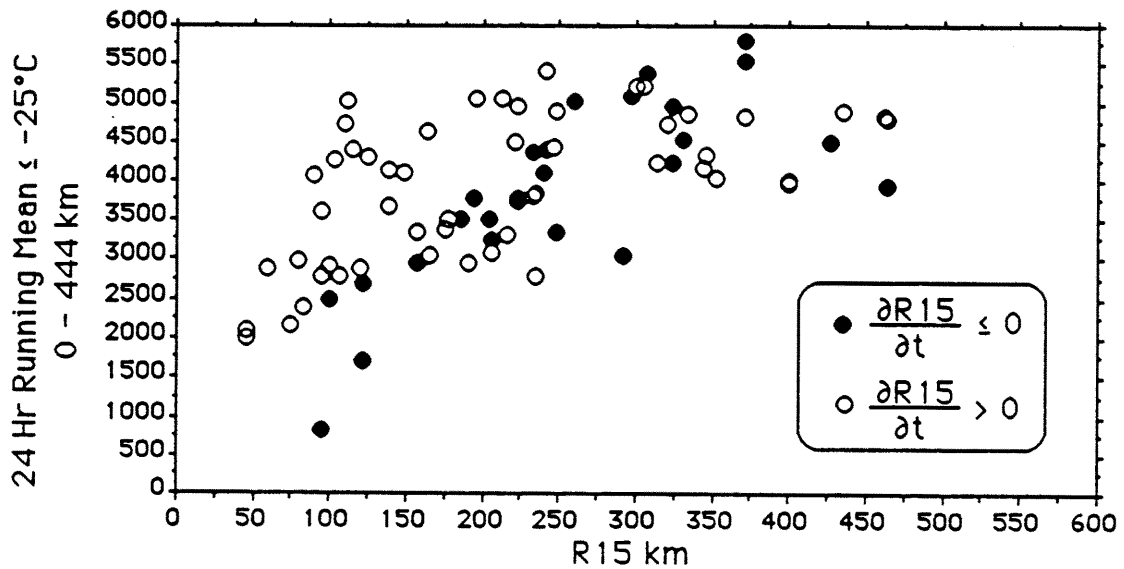


Figure 6.10: Stratification of R15 for subsequent 24 hour change compared to prior 24 hour running mean pixel area for -25°C convection. Again, considerable overlap occurred between cases where R15 was decreasing and increasing.

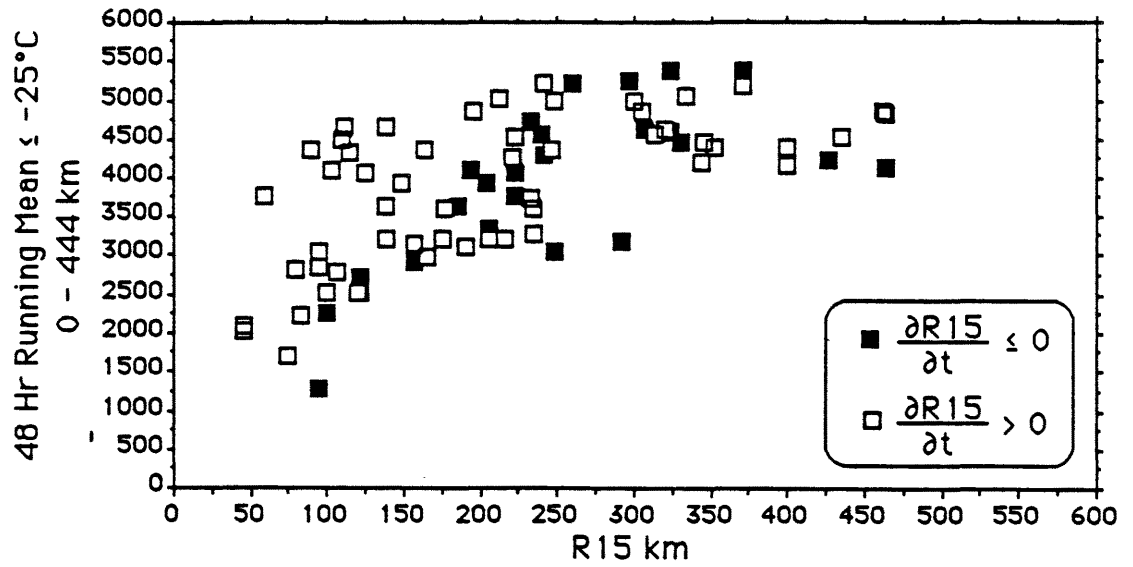


Figure 6.11: Same as Fig. 6.10 except for running mean -25°C pixel areas over the prior 48 hours.

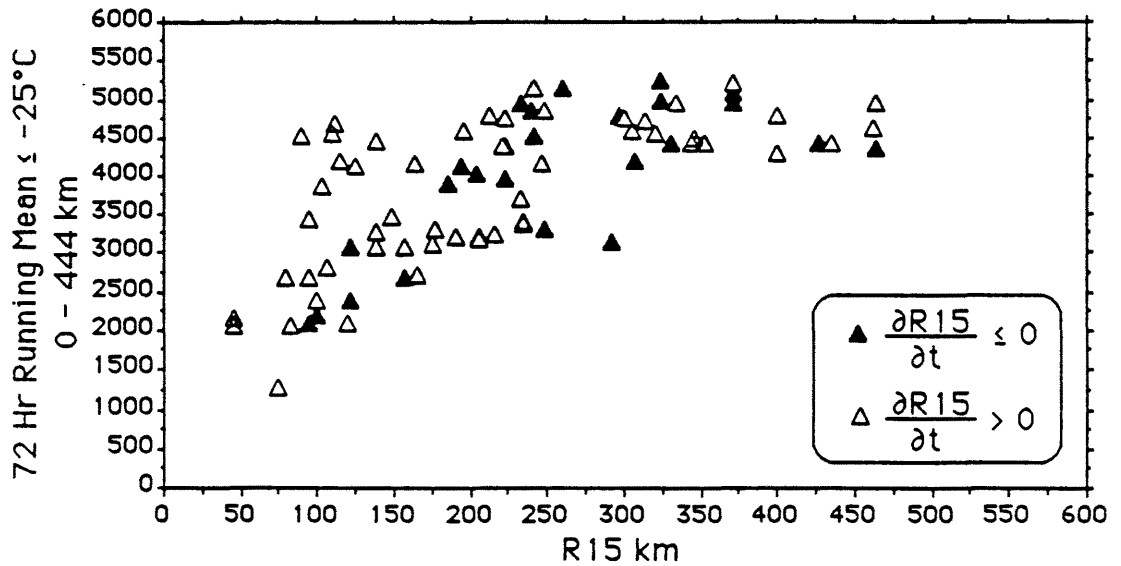


Figure 6.12: Same as Fig. 6.10 except for running mean -25°C pixel areas over the prior 72 hours.

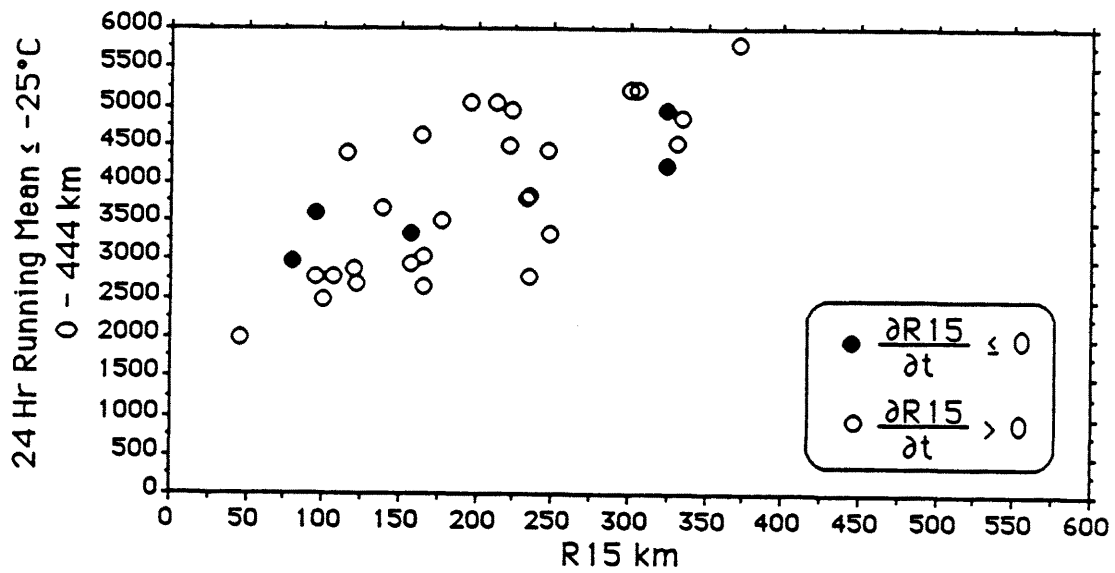


Figure 6.13: Cases of increasing (open) and decreasing (solid) 24 hour changes of R15 compared to prior 24 running mean -25°C convection.

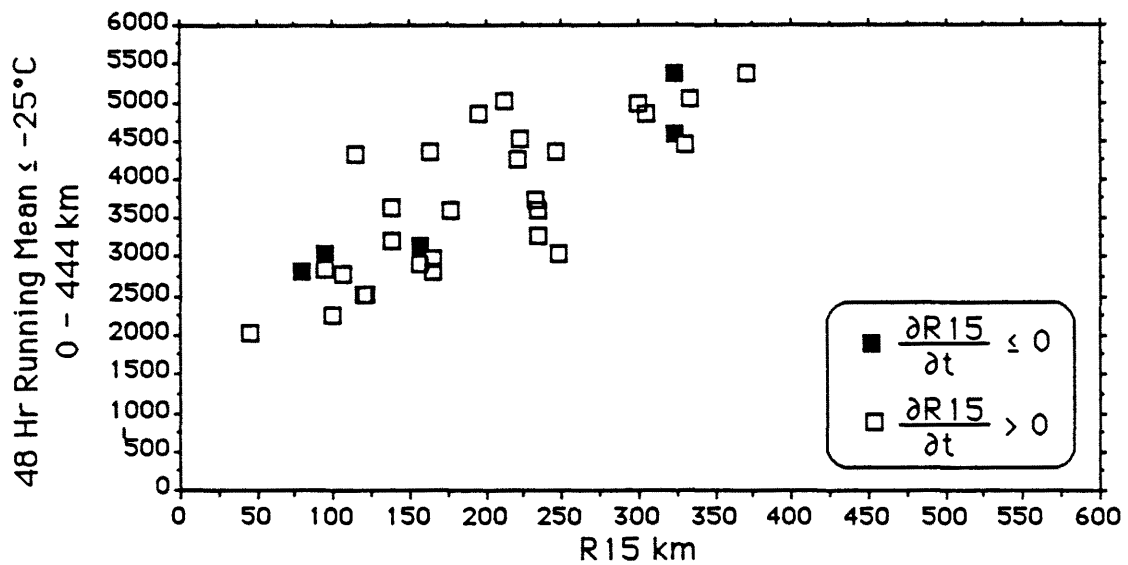


Figure 6.14: Same as Fig. 6.13 except for running mean -25°C pixel areas over the prior 48 hours.

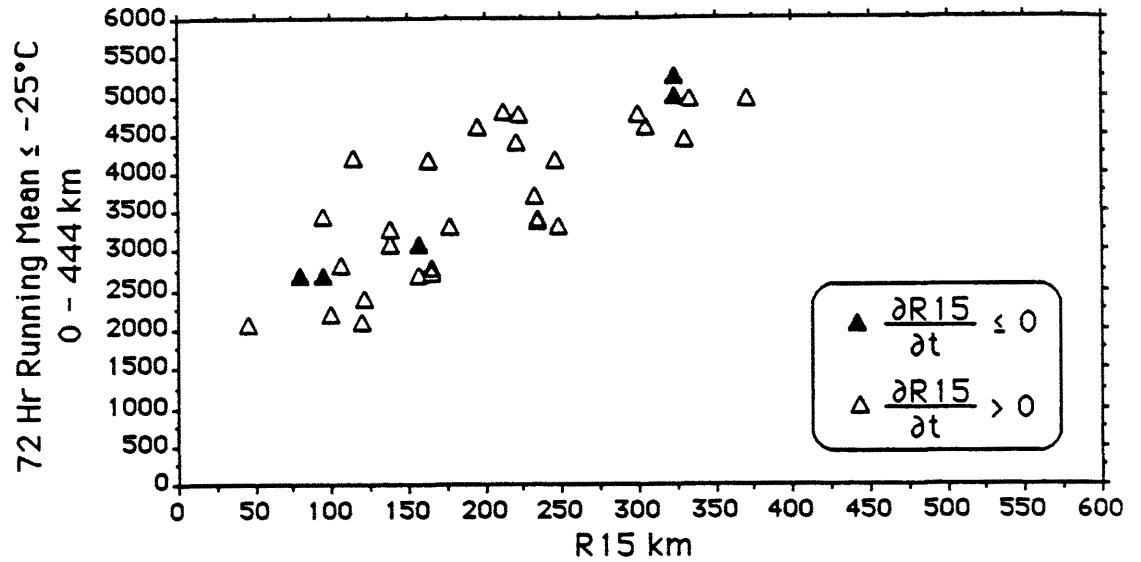


Figure 6.15: Same as Fig. 6.13 except for running mean -25°C pixel areas over the prior 72 hours.

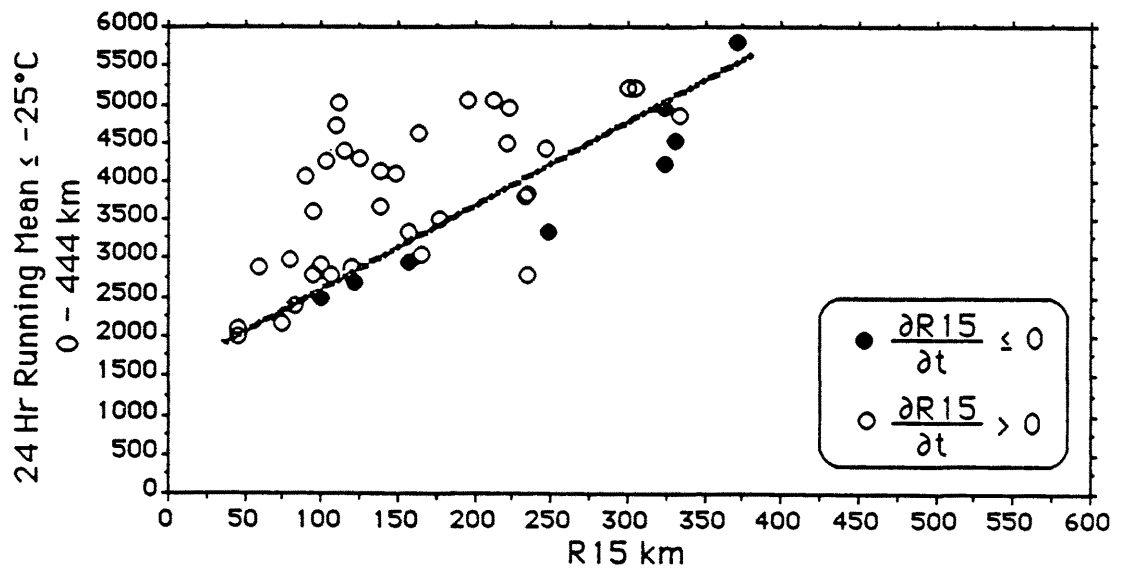


Figure 6.16: Stratification by subsequent 24 hour R15 change for intensifying TCs in comparison to the prior 24 hour running mean pixel counts. Overlap is much reduced in this analysis and it is possible to determine an approximate line of division between cases where R15 was decreasing and increasing.

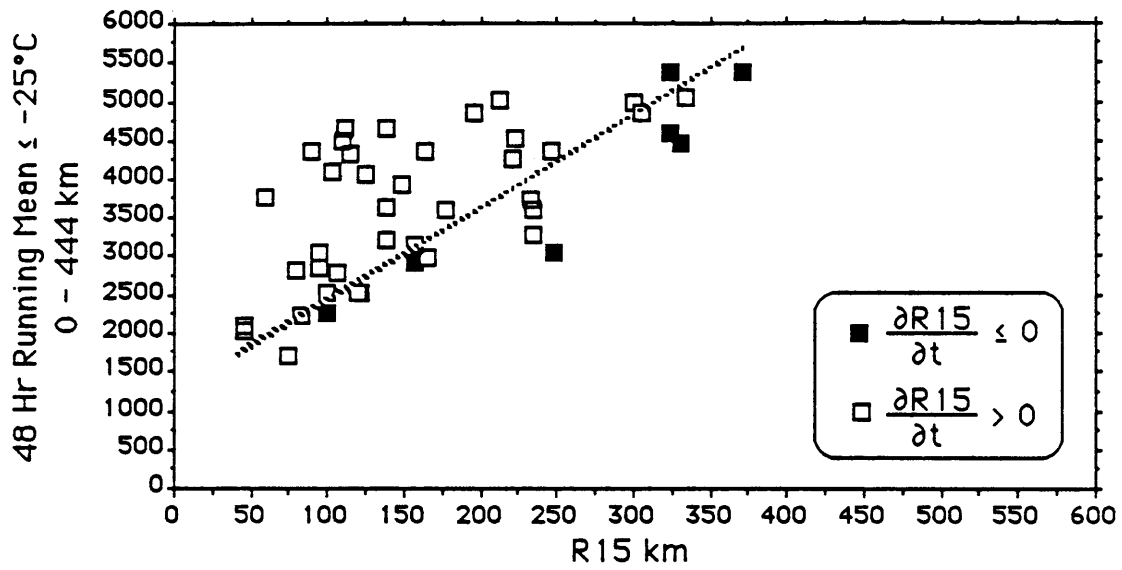


Figure 6.17: As in Fig. 6.16 except for running mean -25°C pixel areas over the prior 48 hours.

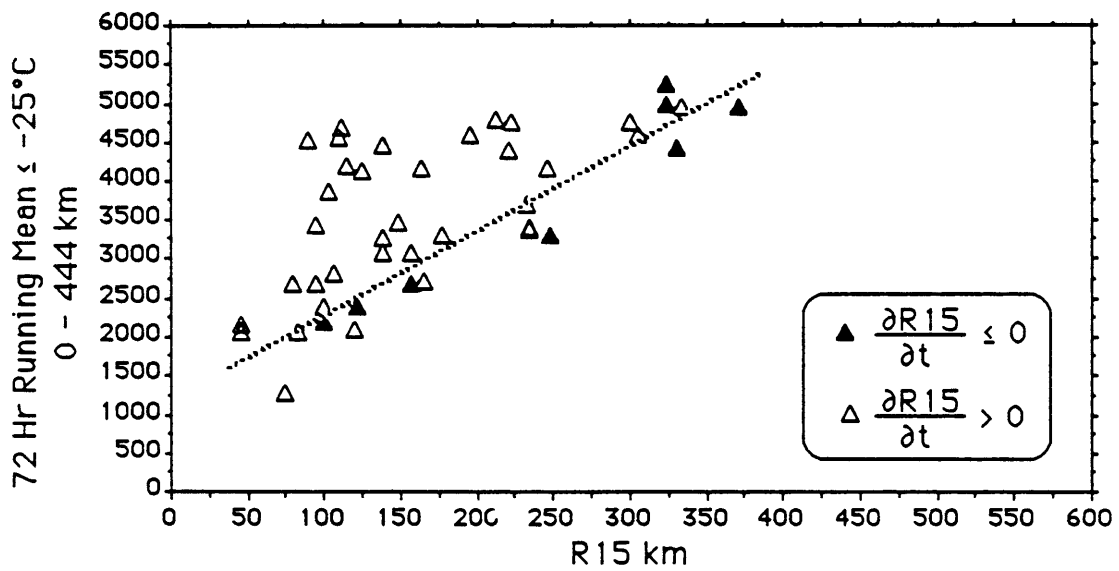


Figure 6.18: As in Fig. 6.16 except for running mean -25°C pixel areas over the prior 72 hours.

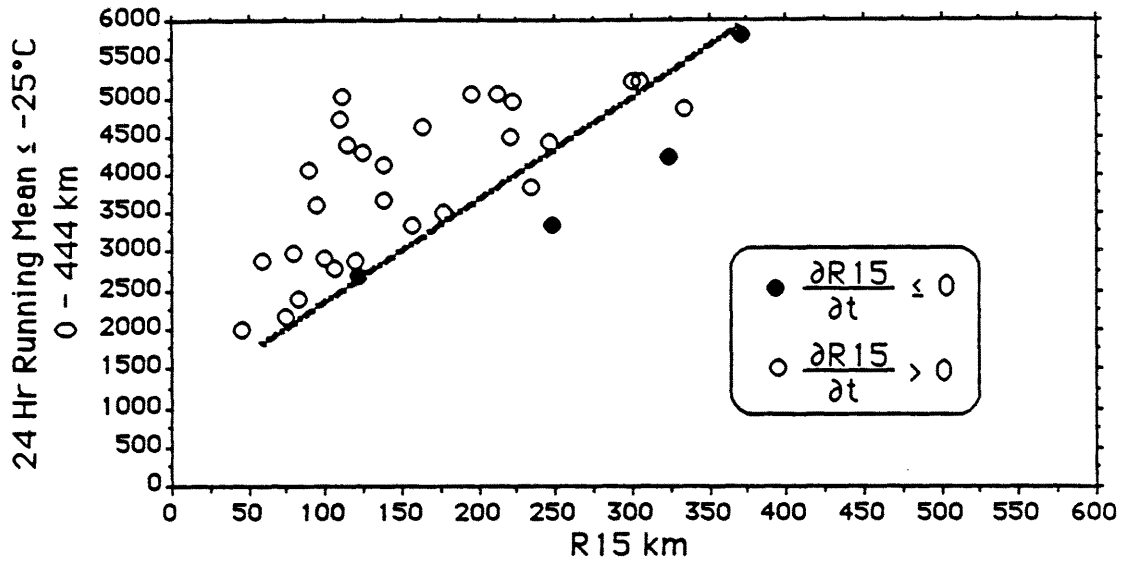


Figure 6.19: Stratification by subsequent 24 hour R15 change for intensifying TCs omitting all cases with net R15 changes of less than 20 km. This stratification again reduces overlap between cases where R15 was increasing or decreasing. A line which approximately separates these groups of points has been drawn.

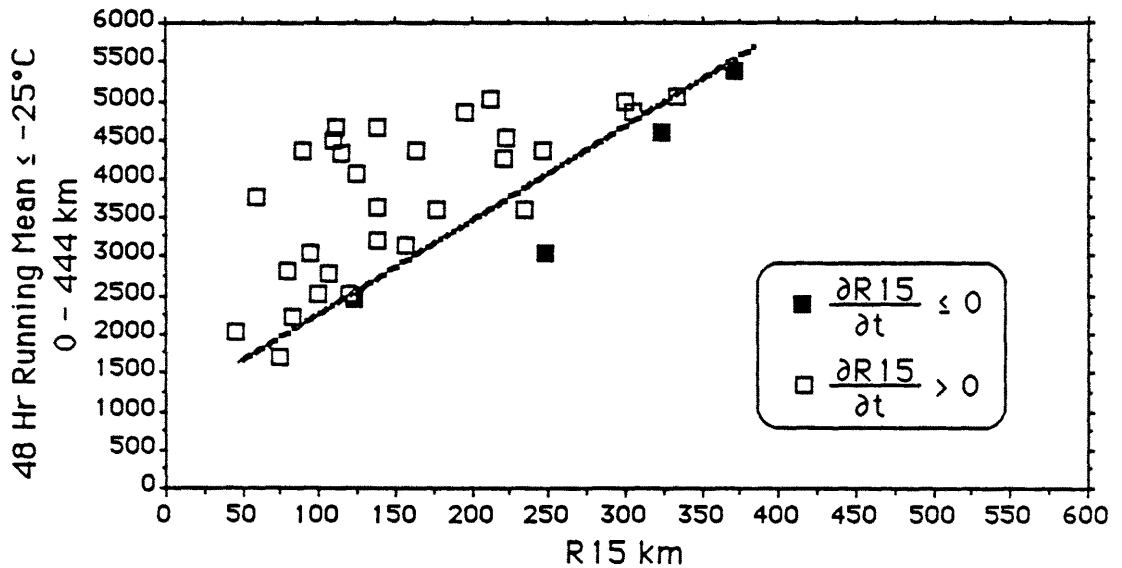


Figure 6.20: As in Fig. 6.19 except for running mean -25°C pixel areas for the prior 48 hours.

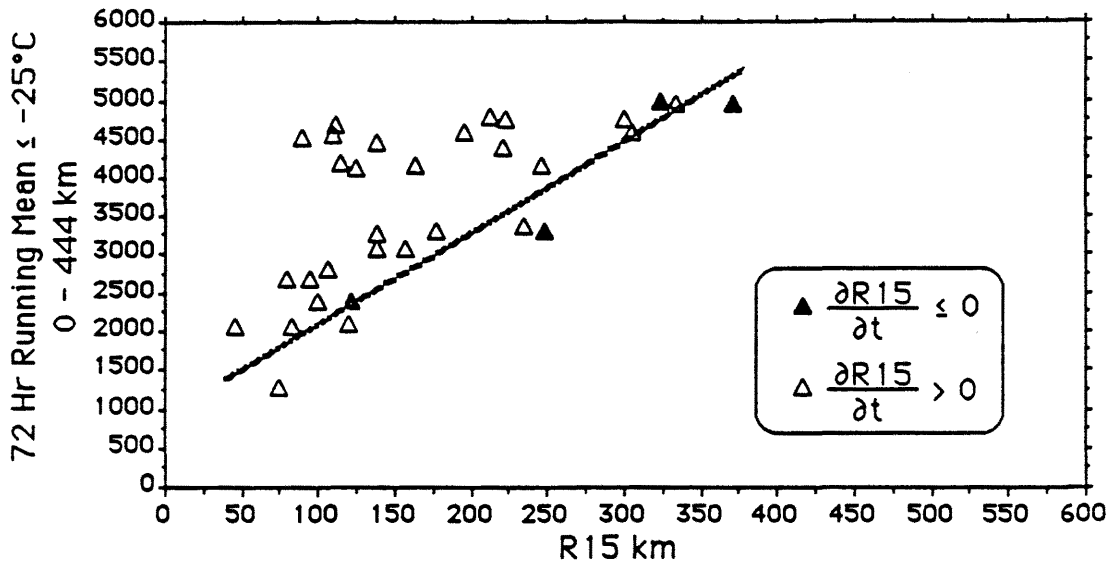


Figure 6.21: As in Fig. 6.19 except for running mean -25°C pixel areas over the prior 72 hours.

from the hypothetical equilibrium curve. Figures 6.22 through 6.24 suggest that there is a tendency for the greatest changes of R15 to be displaced farther from the main sequence of data points. The sample is small however and there is appreciable scatter for these results. It is nevertheless important to forecasters to be able to recognize that, for a given R15, a TC with appreciably greater than average convection has a greater potential for R15 to increase rapidly. This relationship is especially helpful in the early TC stages when rates of R15 increase can be very large.

The lack of correlation between convection and R15 during filling was also investigated further. The twelve storms were stratified according to whether they were delayed or simultaneous and R15 and convection were again compared, both for cases wherein R15 was increasing and for which it was decreasing. No distinction could be made for filling delayed cyclones due to considerable overlap between increasing and decreasing values of R15 (Fig. 6.25). Delayed TCs apparently do not have a relationship between convection and R15 following maximum intensity. Merrill (1982) compared small and large cyclones and determined that large cyclones may grow larger due to increased convergence of angular momentum which was forced by the large scale environment. Large scale forcing of

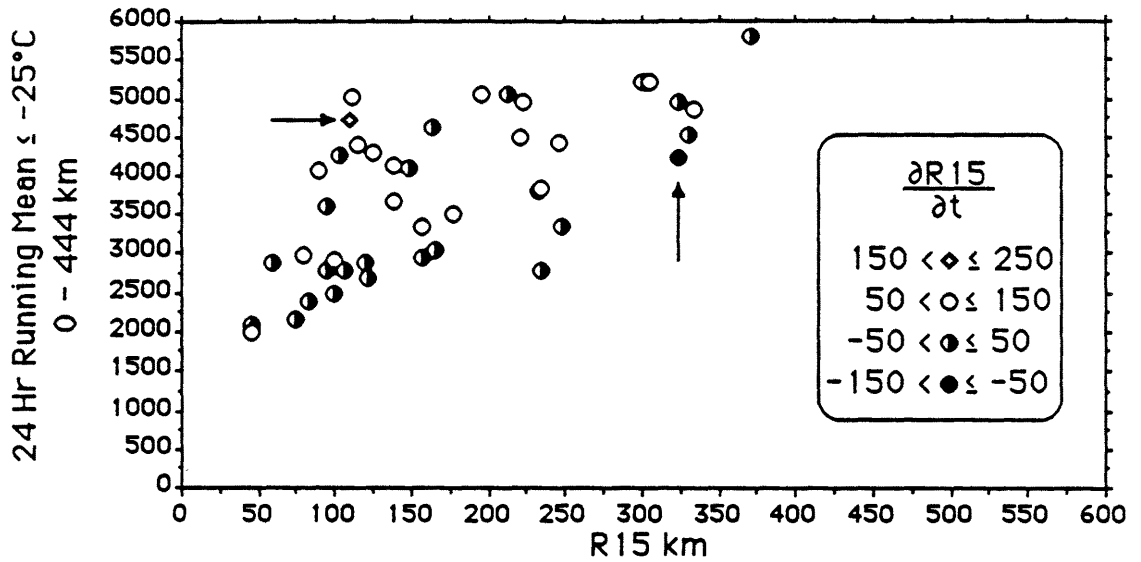


Figure 6.22: Stratification by subsequent R15 change for intensifying TCs in relation to 24 hour running mean pixel area, stratified by the rate of R15 change. There is a tendency for those observations with the greatest R15 changes to deviate farthest from the principal sequence of data points. Arrows point to observations with the greatest change values.

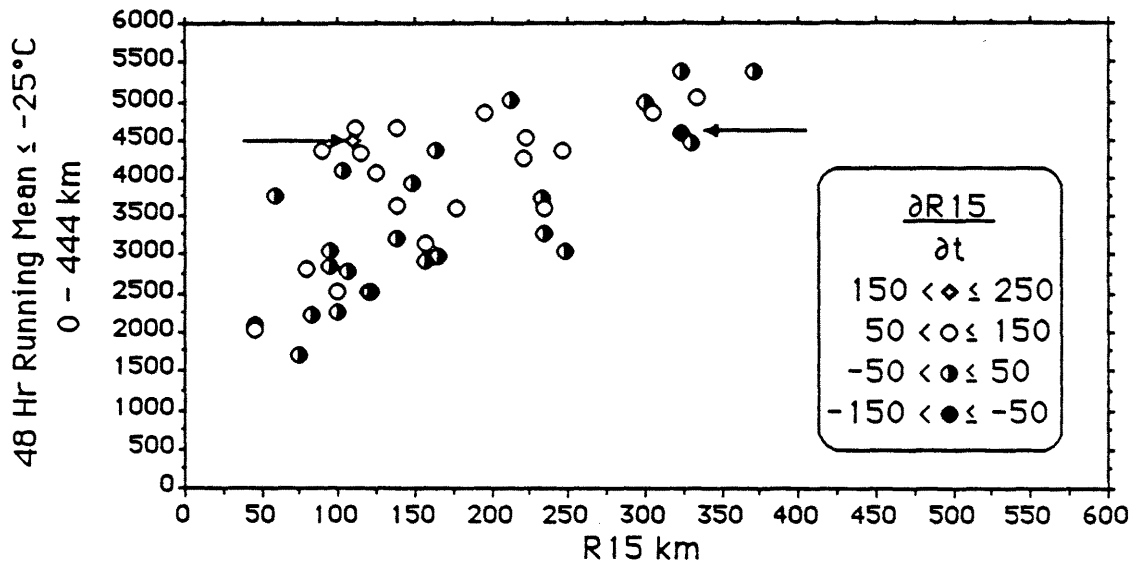


Figure 6.23: As in Fig. 6.22 except for running mean -25°C pixel counts over the prior 48 hours. Although convection amounts for both observations (indicated by arrows) are similar, R15 change was most positive for smaller R15, and most negative for larger R15.

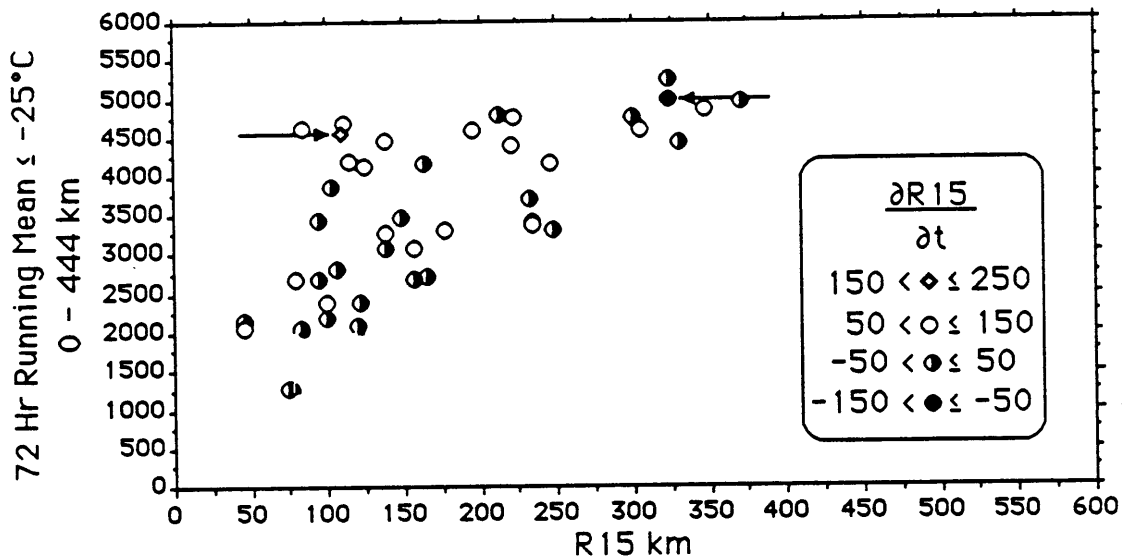


Figure 6.24: As in Fig. 6.12 except for running mean -25°C pixel areas for the prior 72 hours.

this sort is not accounted for in the hypothesis proposed here and other studies would be required to assess the effects of large scale circulations on the outer wind profile of these delayed TCs.

6.3 Forecasting R15 Decrease

No cases were observed wherein R15 increased during filling of simultaneous TCs. This observation simply confirms that these TCs are weakening as they fill. The simultaneous TCs shown in Fig. 6.26 appear to have a linear distribution of convection and it may be possible to use 24 hour running mean values of convection colder than -25°C for first guess values of R15. This process could be accomplished using convection amounts obtained from satellite images. Obviously, more observations need to be examined to see if this relationship is sufficiently accurate for forecasting purposes.

An empirical relationship for estimating rates of R15 decrease was also developed. Typically weakening TCs were caught in westerly currents and accelerating out of aircraft range or were dying away from land and no flights were necessary. Hence, few weather reconnaissance missions were flown after TCs began weakening. Nevertheless, rates of R15

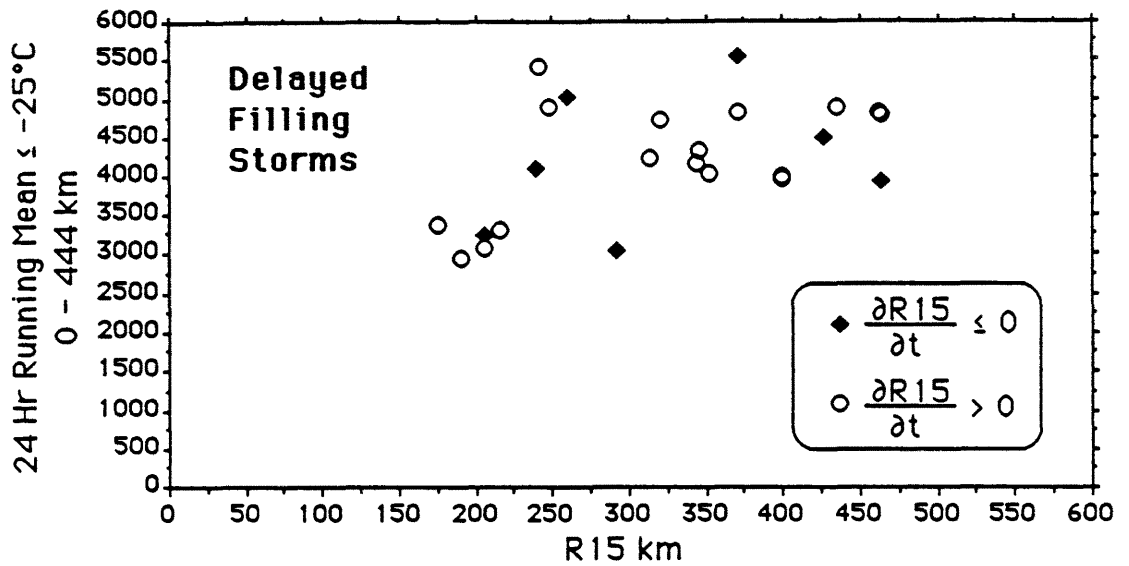


Figure 6.25: R15 change values for delayed type TCs in the filling stage.

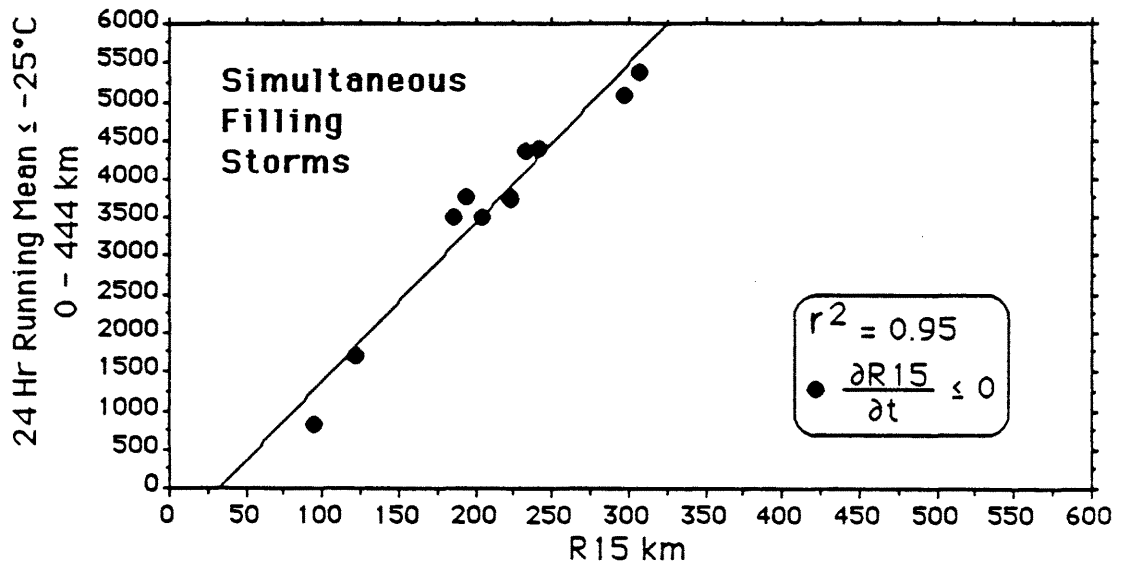


Figure 6.26: Relationship between R15 change and convection values for simultaneous TCs.

decrease were determined for those TCs for which sufficient data was available. Equation 6.1 gives the empirical rate of R15 decrease observed in these data.

$$R15 \text{ Decrease} = 48 \text{ km } d^{-1} \quad (6.1)$$

One standard deviation for this relationship is $15 \text{ km } d^{-1}$ indicating that approximately 15 percent of these TCs will have R15 decrease rates greater than $63 \text{ km } d^{-1}$, and 15 percent will have R15 decrease rates less than $33 \text{ km } d^{-1}$. It must be stressed that this is a purely empirical relationship and assumes that the TCs are dissipating at sea and have no major land (frictional) influences.

6.4 Specification of R15 from Observations of Intensity and Convection

The intensities of developing tropical cyclones may be estimated using Dvorak's (1975) Current Intensity (CI) number which is obtained using a procedure based on cloud pattern matching techniques. Table 6.1 gives the Dvorak CI numbers corresponding to maximum wind speed and MSLP for Northwest Pacific TCs. Dvorak's technique has proven accurate and is used operationally at JTWC.

It has also been shown that the rate of increase of R15 may be inferred from convection if an initial value of R15 is known. Because values of R15 have been shown to be poorly correlated with intensity, a reliable initial value of R15 cannot simply be specified for a given CI based intensity value. For example, the average R15 value for intensifying TCs in the 988 to 994 hPa MSLP intensity range was observed to be 124 km with a standard deviation of 38 km. Hence, a more reliable current value of R15 must be known for knowledge of the likely rate of R15 increase to be useful to forecasters.

A conceptual relationship between intensity (MSLP), convection amounts and R15 values was shown in Fig. 3.8. It was hypothesized that more convection for a given MSLP might be associated with larger R15 values. In this section the prospects for determining useful initial estimates of R15, given various measurements of convection and MSLP, are examined. Figures 6.27 through 6.32 show that intensity is reasonably well correlated with convection, explaining up to one half of the variance. However, Figs. 6.27-6.32 also

Table 6.1: Dvorak (1975) current intensity number (CI), maximum sustained wind speeds, and MSLP.

Dvorak CI Number	Max Wind Speed Meters per Second	MSLP NW Pacific
0.0	< 13	–
0.5	13	–
1.0	13	–
1.5	13	–
2.0	15	1000
2.5	18	997
3.0	23	991
3.5	28	984
4.0	33	976
4.5	40	966
5.0	46	953
5.5	52	941
6.0	59	927
6.5	65	914
7.0	72	898
7.5	80	879
8.0	87	858

show that this relationship is not likely to be very useful to forecasters in that for more intense TCs (especially those with MSLP less than 960 hPa) wherein there is little change of convection over a rather broad intensity range.

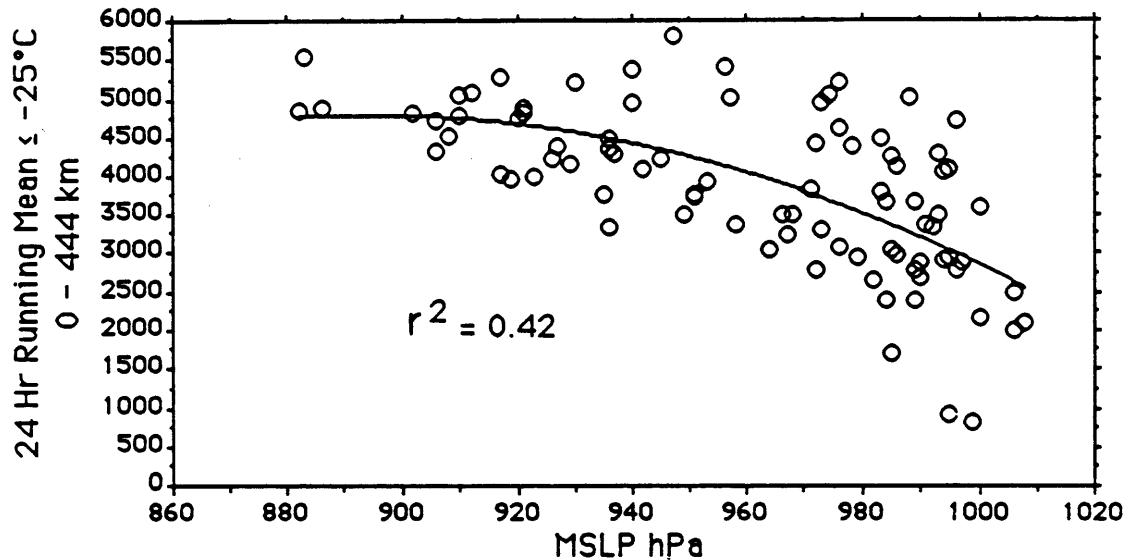


Figure 6.27: Analysis of intensity (MSLP) in comparison to running mean -25°C convection over the prior 24 hours. Similar convection amounts tend to correspond to a wide range of intensities for more intense TCs.

Differences in convection were examined for less intense TCs (i.e., MSLP greater than 960 hPa) to see if, for a given intensity, larger values of convection could be systematically linked to larger R15 values. Convection amounts were compared to MSLP and stratified by R15 for four size groups. Figure 6.33 shows that knowledge of MSLP convection does not always translate into a very close relationship with R15.

6.5 Summary

For intensifying cyclones, increases of R15 are highly correlated with the amount of sustained convection (represented by time averaged pixel counts) associated with the present R15 value. Larger increases of R15 are likely when convection is greater than the average value associated with a given value of R15. Decreases of R15 for simultaneous type TCs are also well correlated with convection. An empirical formula for R15 decrease was

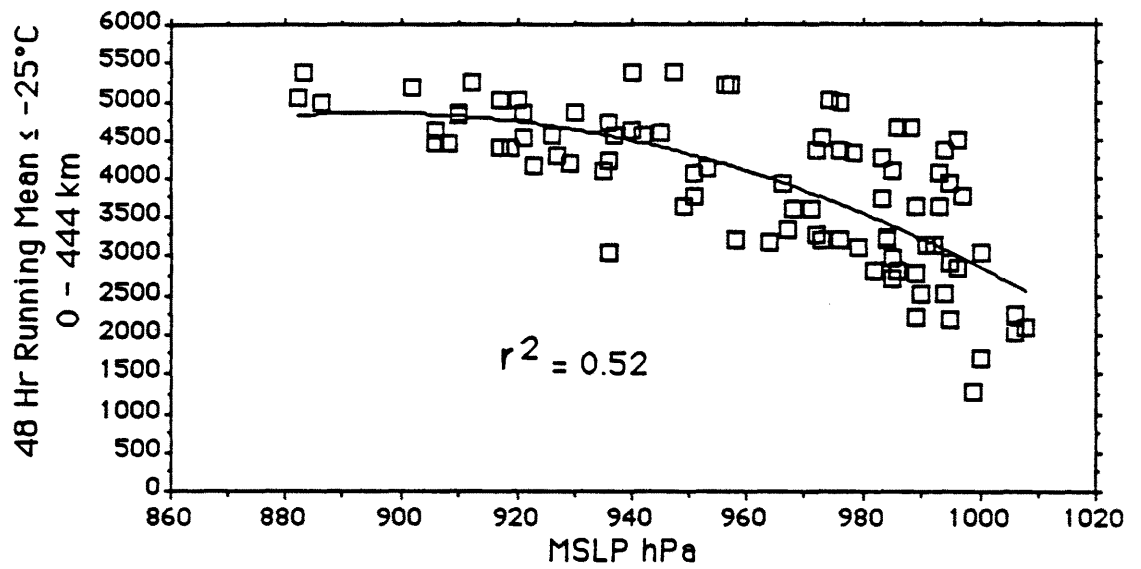


Figure 6.28: As in Fig. 6.27 except for 48 hour running mean pixel counts.

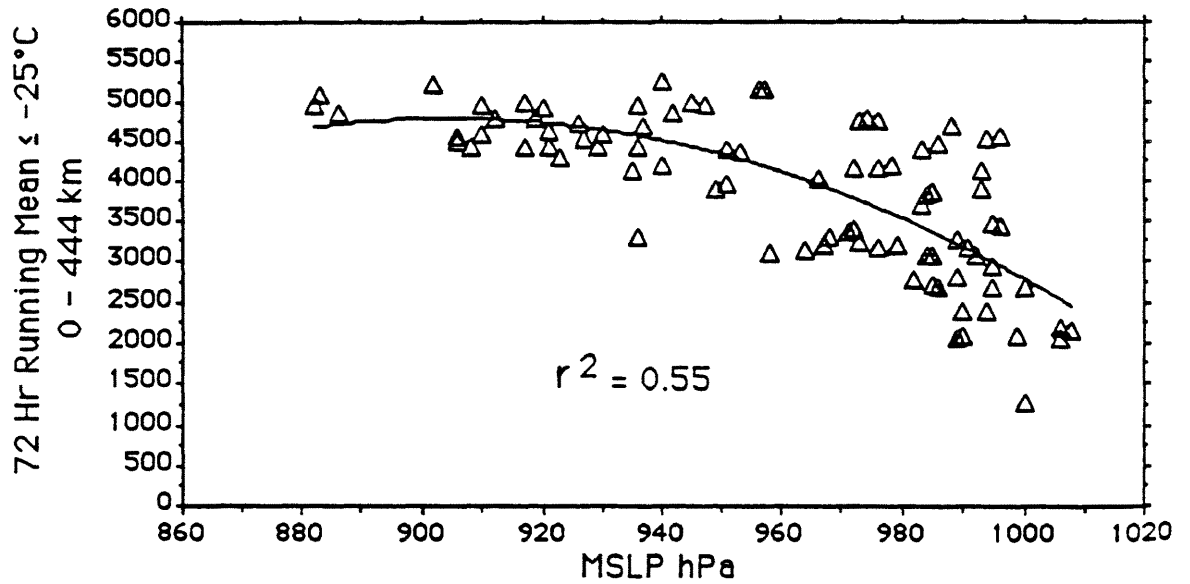


Figure 6.29: As in Fig. 6.27 except for 72 hour running mean pixel counts.

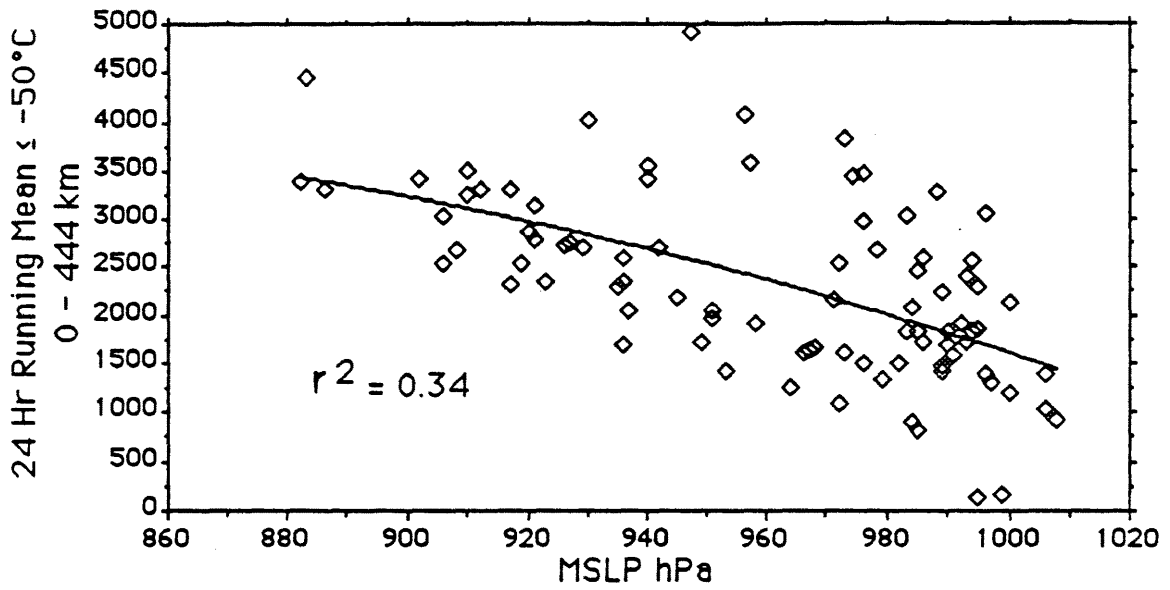


Figure 6.30: As in Fig. 6.27 except for -50°C convection.

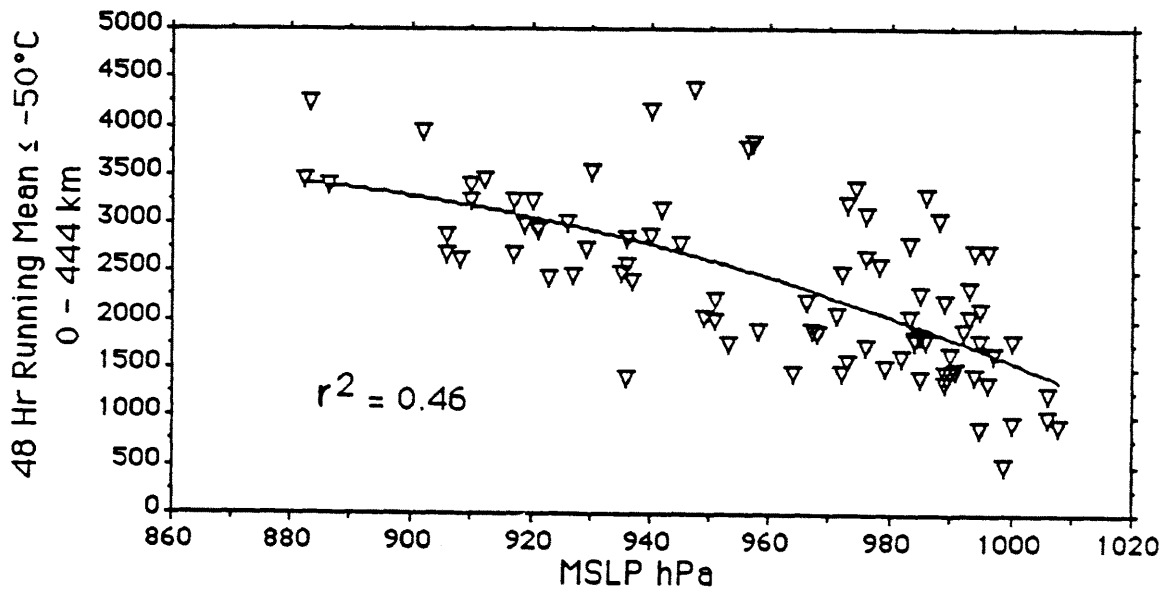


Figure 6.31: As in Fig. 6.28 except for -50°C convection.

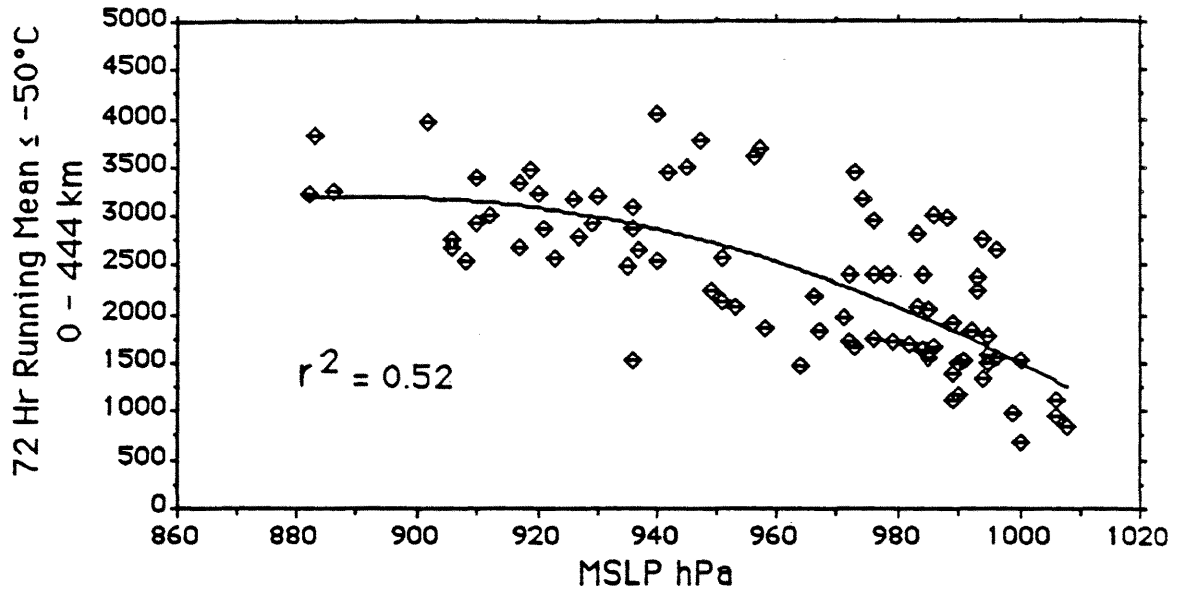


Figure 6.32: As in Fig. 6.29 except for -50°C convection .

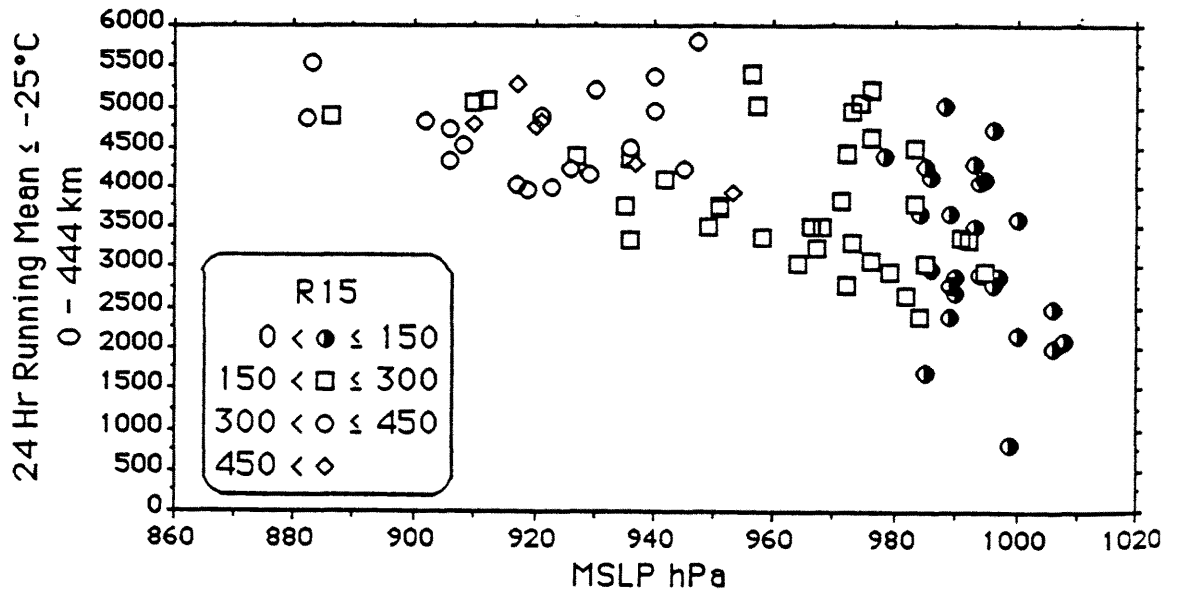


Figure 6.33: Comparisons between intensity (MSLP) and convection stratified for four classes of R15 values. Conceptually, the groupings of R15 values would slope from upper left to lower right if greater convection for a given intensity were in fact related to larger R15 values. This is not the case however, and it appears that R15 cannot be estimated from measurements of convection and intensity in this way.

developed which is valid for all TCs after maximum R15 has been reached. Unfortunately, efforts to specify initial R15 values from intensity and convection data were unsuccessful, thereby compromising the applicability of these rate of change associations.

Chapter 7

ASSOCIATIONS BETWEEN ASYMMETRIC CONVECTIVE BURSTS AND WIND FIELD ASYMMETRY

Values of R15 and R26 represent axially averaged quantities. Weather analysts and forecasters however, need to know the horizontal asymmetries in the tropical cyclone's wind profile. It was decided to examine quadrant scale asymmetries of R15 to determine if they were related to convective asymmetries. Specifically, could enhanced convection in a sector be used to predict a greater radial extent of R15 in that or any other sector?

7.1 Methodology

To accomplish this task, pixels were counted for all four temperature thresholds as described previously over the radius 0 to 444 km in four 90° sectors termed north, south, east, and west (N, S, E, W). These 90° sectors were centered on the compass headings of 0°, 90°, 180°, and 270°. Because convection within a TC varies in space and time, it was assumed that differences in convection between opposite sectors would best represent the effects of asymmetry. Opposite sector differences are defined here as the south sector pixel area minus the north sector pixel area (S-N) and similarly, the east minus west pixel area difference (E-W). Plots were made of the absolute values of S-N and E-W convection differences at the four temperature thresholds over time. Twenty-four hour running means of these differences were computed so as to smooth the plots.

7.2 Significance of Asymmetry

If the strength of convective asymmetries between opposite sectors were on the order of ten percent or less of the overall convection, they were not considered to be significant since the time variation of the asymmetries would then be a small percent of the total convection.

Therefore, the amount of asymmetry in comparison to average total sector convection was examined. Figures 7.1 to 7.8 show opposite sector differences in convection for Typhoon Abby as a function of average sector convection. Equation 7.1 gives the formula used for computing these differences which are expressed as percent. This expression represents the absolute value of sector differences (thereby avoiding negative percentage values) divided by the average sector convection. Hence, a difference value of 100 percent would mean an opposite sector difference in convection for a given threshold equivalent to the total average sector convection for that threshold. Significant convection differences at all temperature stratifications can be seen in Figs. 7.1 through 7.8, both in the S-N and E-W plots. The percentage differences become larger for the colder temperature thresholds because there is typically less net convection represented by colder temperature areas and corresponding sector average pixel areas (ie., denominator values in Fig. 7.1) are smaller. Also, deep convection appears to be more asymmetric in satellite images, making the asymmetries more pronounced at the colder temperature thresholds.

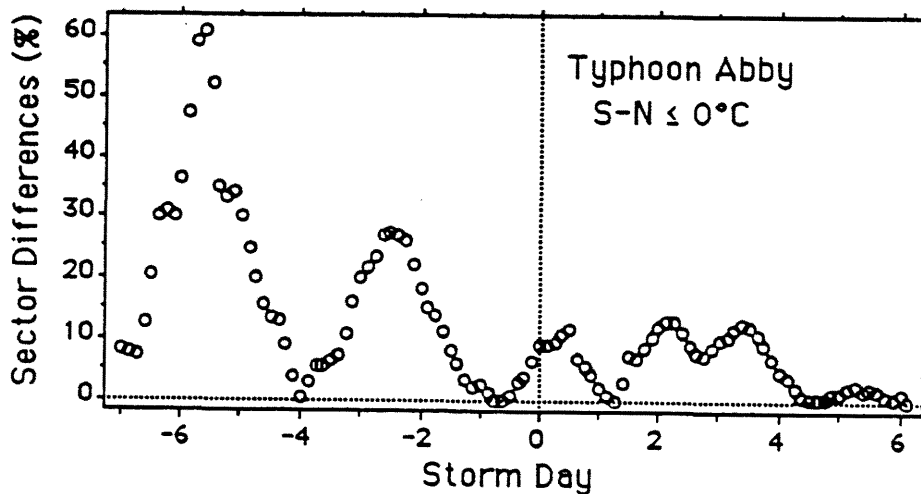


Figure 7.1: Absolute value of sector convection differences (south minus north, 0 to 444 km radius) expressed as a percentage of sector average total $< 0^{\circ}$ convection. See text for equation.

$$Diff(\%) = \frac{400 \times |S - N|}{(N + S + E + W)} \quad (7.1)$$

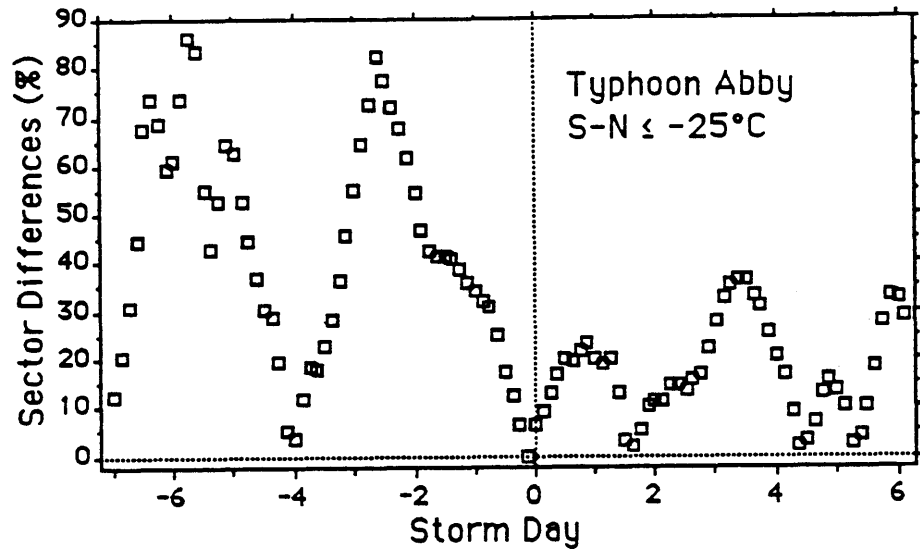


Figure 7.2: As in Fig. 7.1 except for -25°C convection.

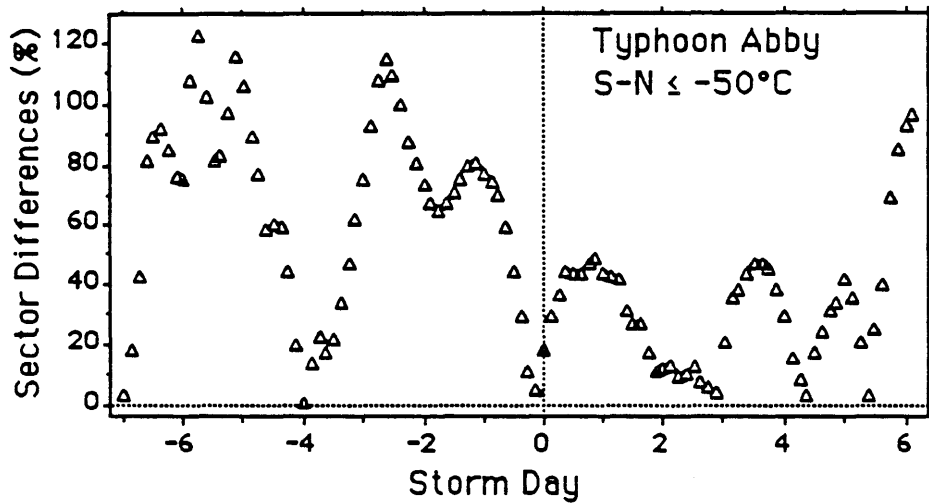


Figure 7.3: As in Fig. 7.1 except for -50°C convection.

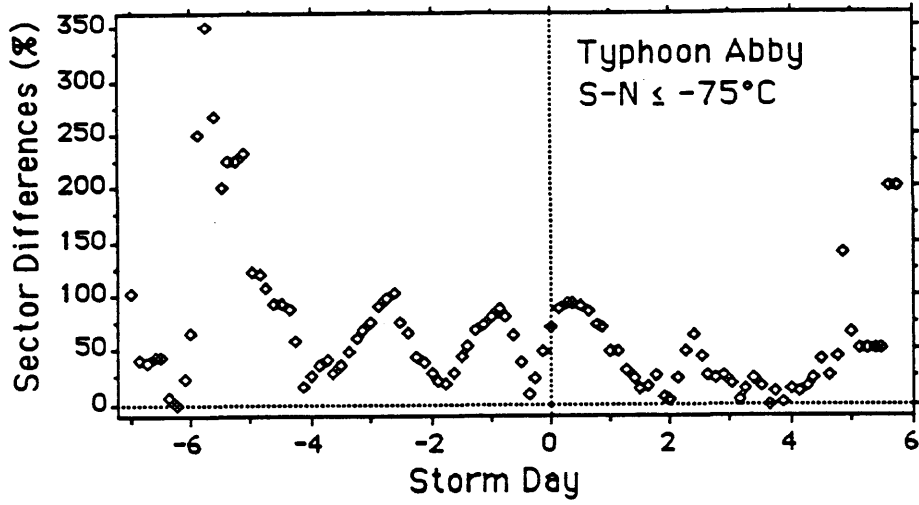


Figure 7.4: As in Fig. 7.1 except for -75°C convection.

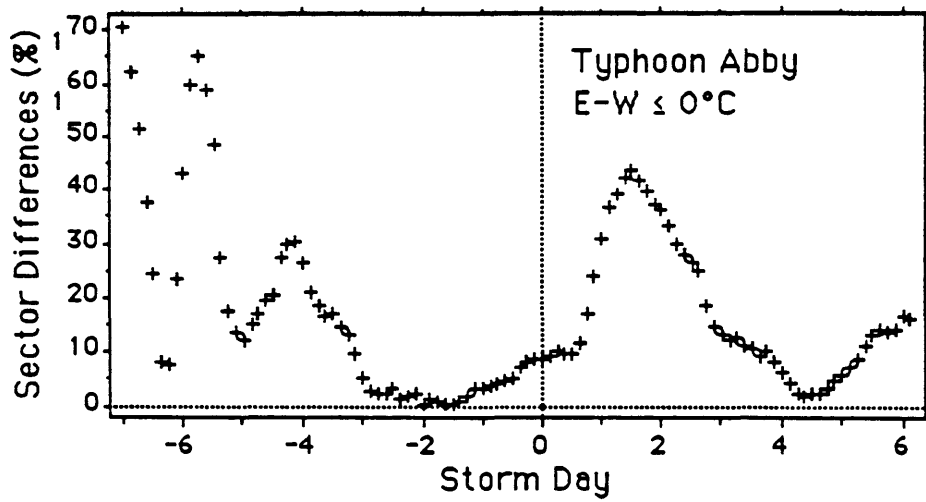


Figure 7.5: As in Fig. 7.1 except for east minus west 0°C convection.

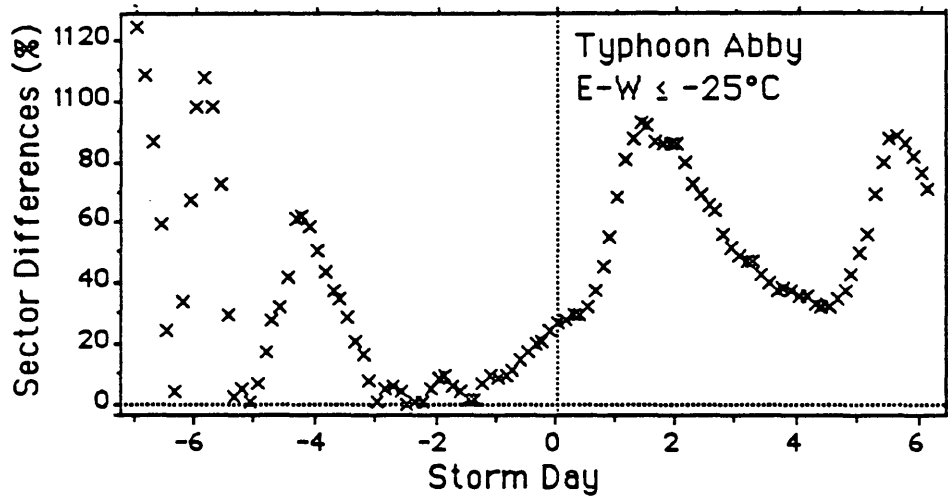


Figure 7.6: As in Fig. 7.5 except for -25°C convection.

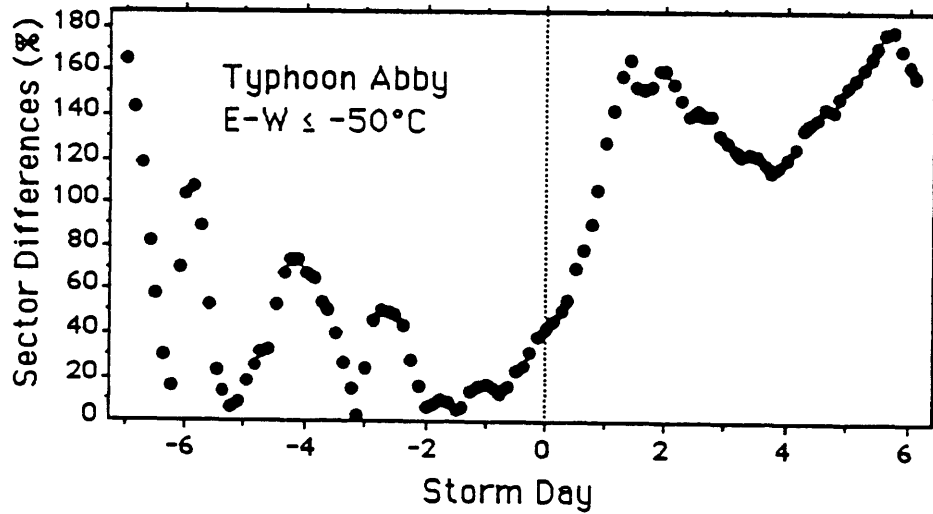


Figure 7.7: As in Fig. 7.5 except for -50°C convection.

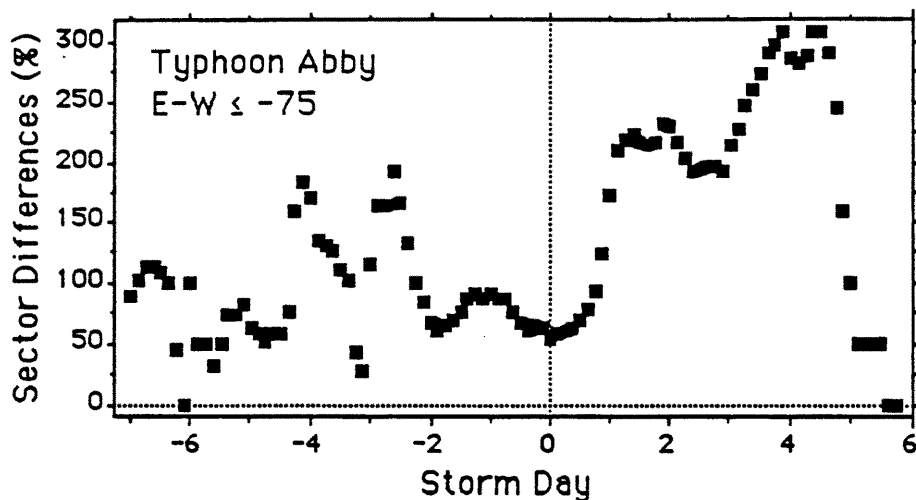


Figure 7.8: As in Fig. 7.5 except for -75°C convection.

Convective asymmetries were compared to analyses of aircraft winds. As described in Chapter 2 values of R_{15} in this study were obtained as a four quadrant average of the radial extent of 15m s^{-1} winds. Hence, for the analysis of asymmetries, values for individual quadrants were compared individually to plots of convection differences. These plots were examined in both the natural, Earth relative coordinate system (NAT) and in the TC motion relative coordinate system (MOT) wherein TC motion is subtracted out. Figures 7.9 and 7.10 show mission plots from Typhoon Abby for one day prior to maximum intensity in both of these coordinate systems. It can be observed that here and in most other TCs, wind asymmetry relative to the TC center largely disappears in MOT coordinates.

Results of the convective analyses show that TCs had significant convection asymmetries, especially in their early stages, regardless of whether or not pronounced wind asymmetries were present. Although Typhoon Ellen had fairly symmetric wind profiles throughout its lifetime, sector convection differences varied significantly (Figs. 7.11-7.18). In Fig. 7.12 it can be seen that convection favored the southern quadrant on day -8.5 while convection favored the northern quadrant quite strongly on day -2.5. However, at both of these times R_{15} values in the north quadrant were slightly larger in the NAT system while R_{15} profiles were very symmetrical in the MOT system. Similar results were obtained for the other TCs.

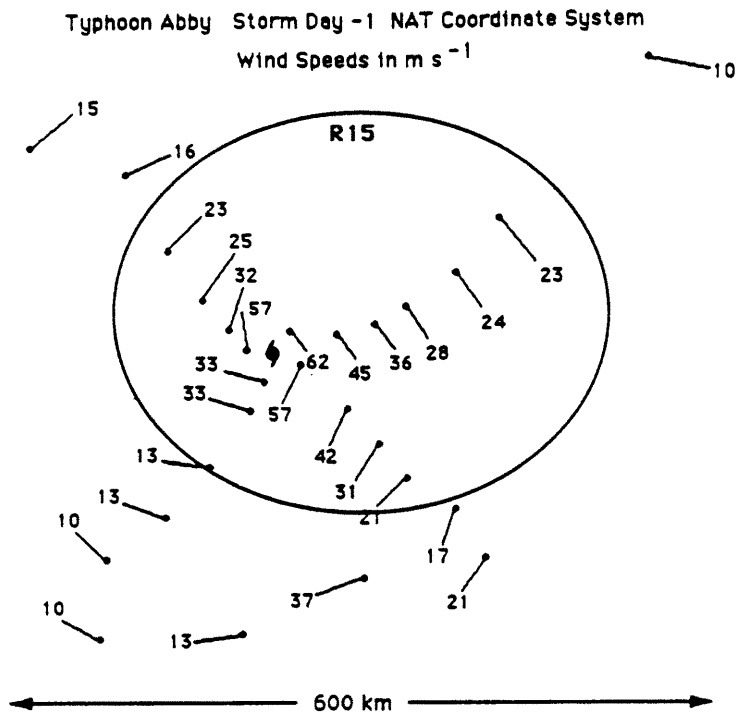


Figure 7.9: Wind plot in NAT coordinate system for Typhoon Abby on storm day -1. R15 is superimposed over the wind vector plot.

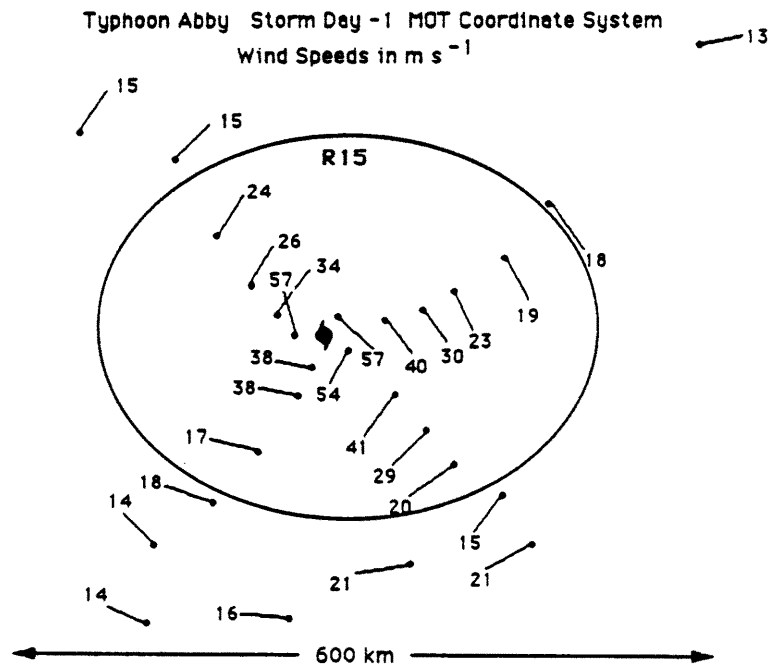


Figure 7.10: Wind plot in MOT coordinate system for Typhoon Abby on storm day 1. Note that R15 is much more symmetrical than in Fig. 7.9.

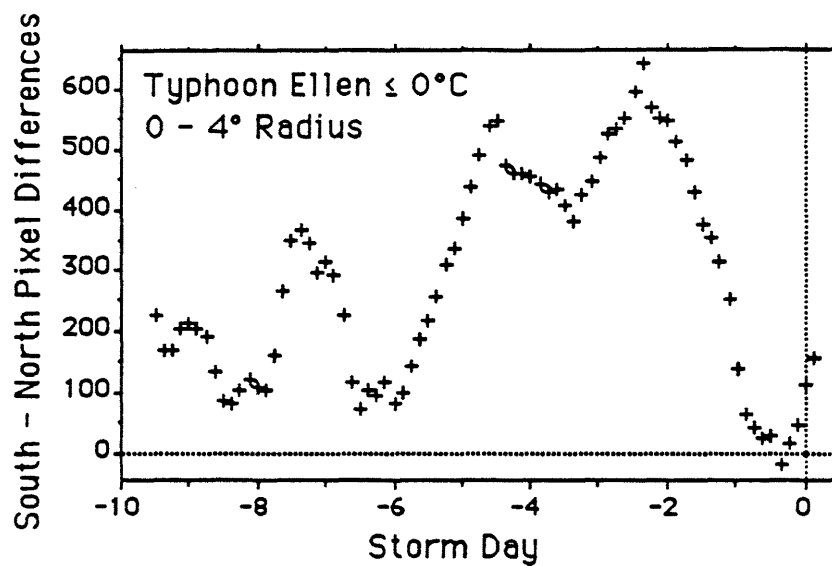


Figure 7.11: Time series of south minus north sector convection differences for Typhoon Ellen. The temperature threshold is 0°C .

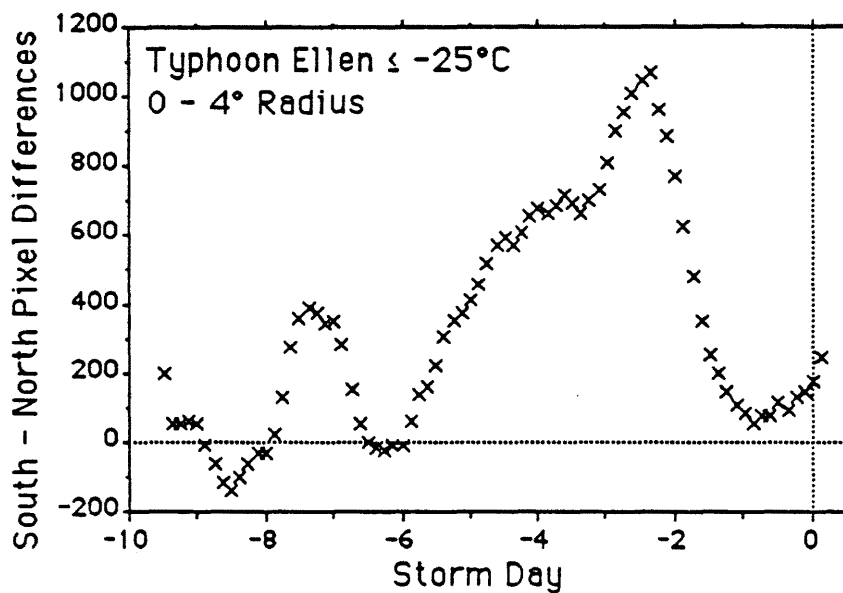


Figure 7.12: As in Fig. 7.11 except for -25°C convection.

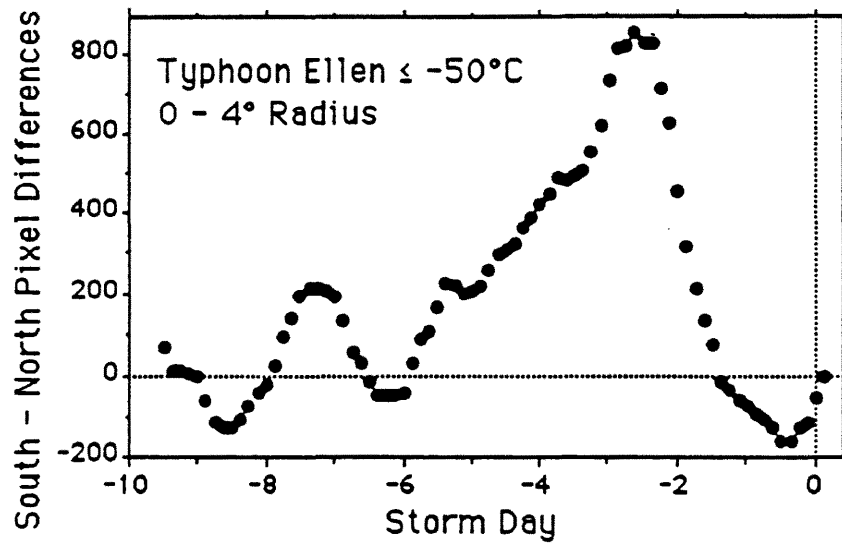


Figure 7.13: As in Fig. 7.11 except for -50°C convection.

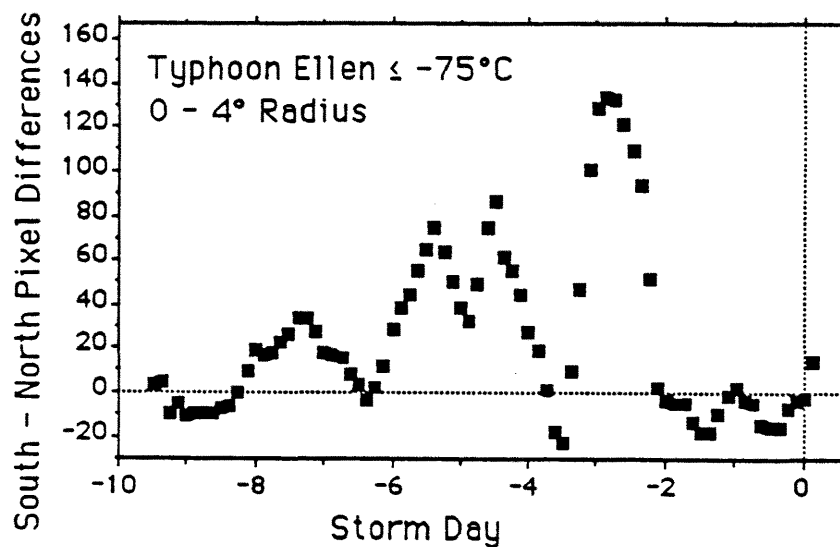


Figure 7.14: As in Fig. 7.11 except for -75°C convection.

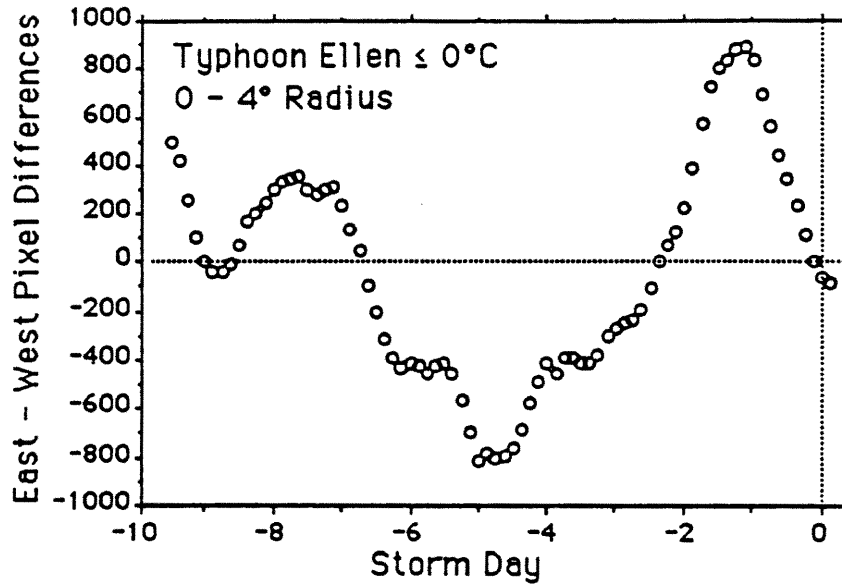


Figure 7.15: Time series of east minus west sector convection differences for Typhoon Ellen. The temperature threshold is 0°C .

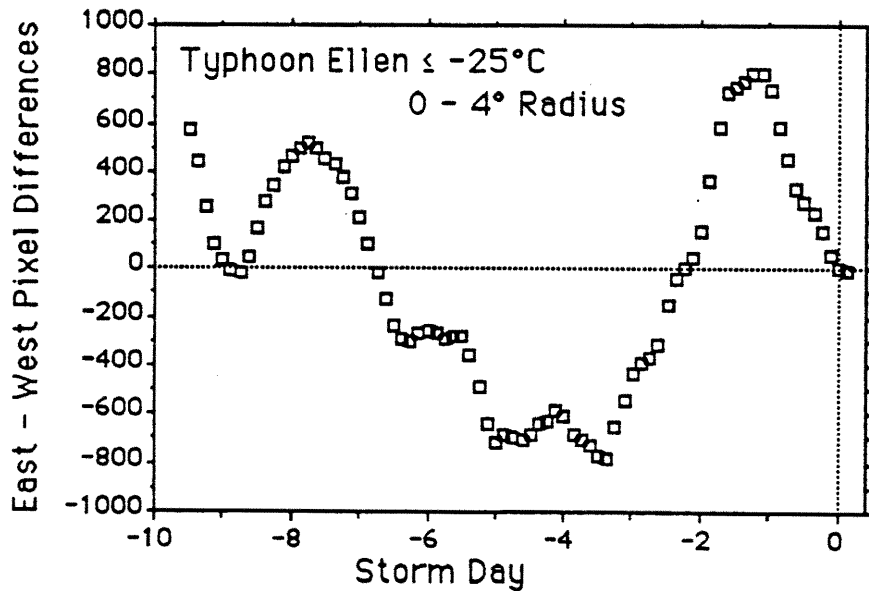


Figure 7.16: As in Fig. 7.15 except for -25°C convection.

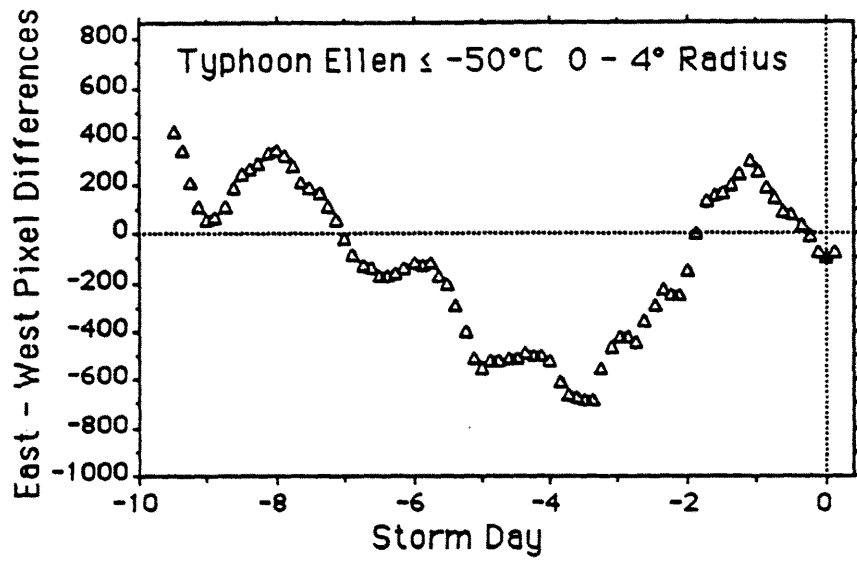


Figure 7.17: As in Fig. 7.15 except for -50°C convection.

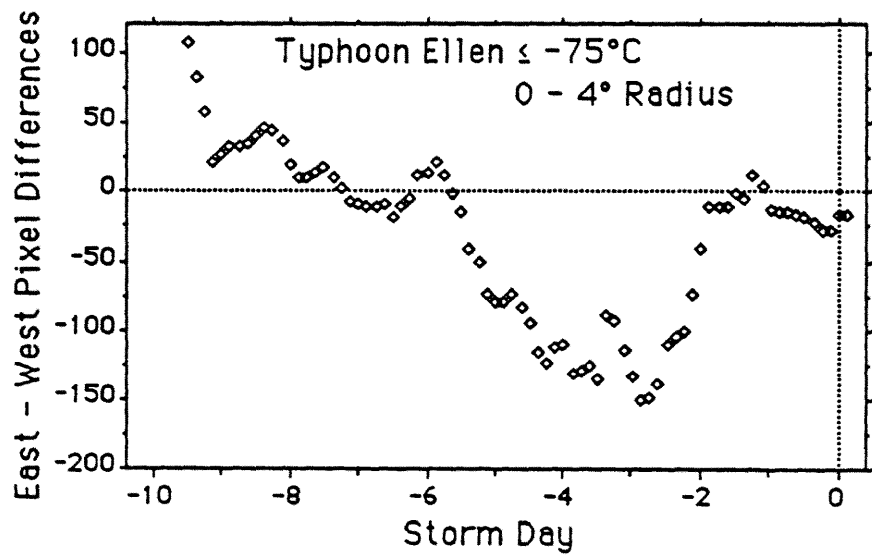


Figure 7.18: As in Fig. 7.15 except for -75°C convection.

Initially it was thought that asymmetric bursts of convection may simply rotate around the TC's center and thus would effect R15 in only the convective sector. Figure 7.19 shows that at day -5, convection differences in the east and west quadrants of Typhoon Abby were large while small differences occurred in the north and south quadrants. This situation then reverses on day -4 when convection differences in the east and west quadrants were much smaller than those in the north and south quadrants.

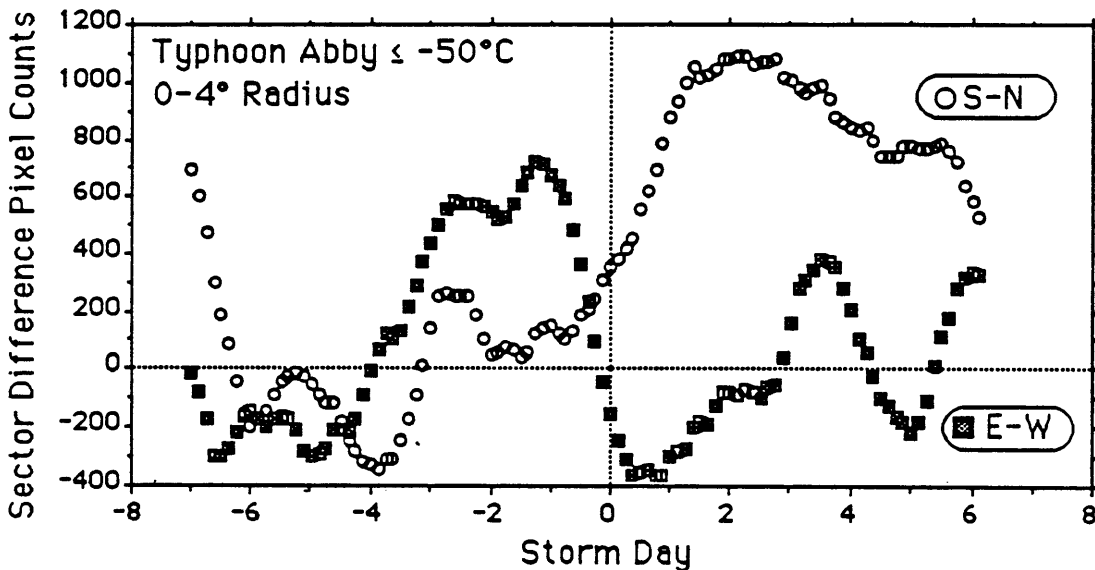


Figure 7.19: Time series of sector differences of -50° convection for Typhoon Abby. Note the phase difference from day -7 to day -4.

To more closely examine this apparent movement of asymmetry between sectors, image loops of the TCs were analyzed and compared to the plots at the corresponding times. The loops showed that the convective asymmetries were not propagating around the TC, but rather, were forming and dissipating at all times in all sectors. Thus, a convective outburst in the east quadrant could be followed by a similar outburst in the north quadrant. The east quadrant outburst would not necessarily move into the north quadrant. These asymmetric outbursts were more apparent when the TC was immature and disorganized and when convection was not well concentrated about the center.

7.3 Climatology of Asymmetry

It is possible that characteristic climatological distributions of convective asymmetries in tropical cyclones may occur or that convection in one sector may be favored over others because of current large scale environmental flow. To examine this possibility, inter-quadrant differences of convection were composited for those ten TCs for which three hourly images were available to see if any mean systematic differences could be observed. Because the TCs had different life spans, the asymmetries were temporally centered on the time of maximum intensity (storm day), as was done in Chapter Five when eye sizes were composited.

Twenty four hour average pixel count differences for all ten TCs at each temperature threshold were used to compute a mean difference time series for the area encompassed by 0 to 444 km. Results of this analysis are shown in Figs. 7.20-7.27. Those times when data for less than five storms were available to compute the mean (ie., at the beginning and end of the TCs time scale) were excluded from the analysis. These plots show that the intense convection favors the south and east sectors, possibly because of high dewpoints in equatorial air drawn into the southern quadrant. Drier air in the subtropical ridge generally lies to the north and is drawn into the north quadrant.

When comparing convective asymmetries of individual TCs against this composite, deviations from the average are of little apparent value for predicting wind asymmetries. For example, although convective sector differences in Typhoon Ellen were much greater than the observed average differences, tangential wind profiles in this TC were very symmetrical. Therefore, even though sector differences of convection may deviate considerably from the climatological average, it is not an indication of significant asymmetry of R15.

7.4 Summary

Asymmetries of convection appear to be unrelated to wind asymmetry because the effects of convective outbursts are quickly advected into the overall TC circulation. The lack of observed tangential wind changes due to large diurnal cycles of deep convection is further evidence of the need to maintain deep convection for an extended period in

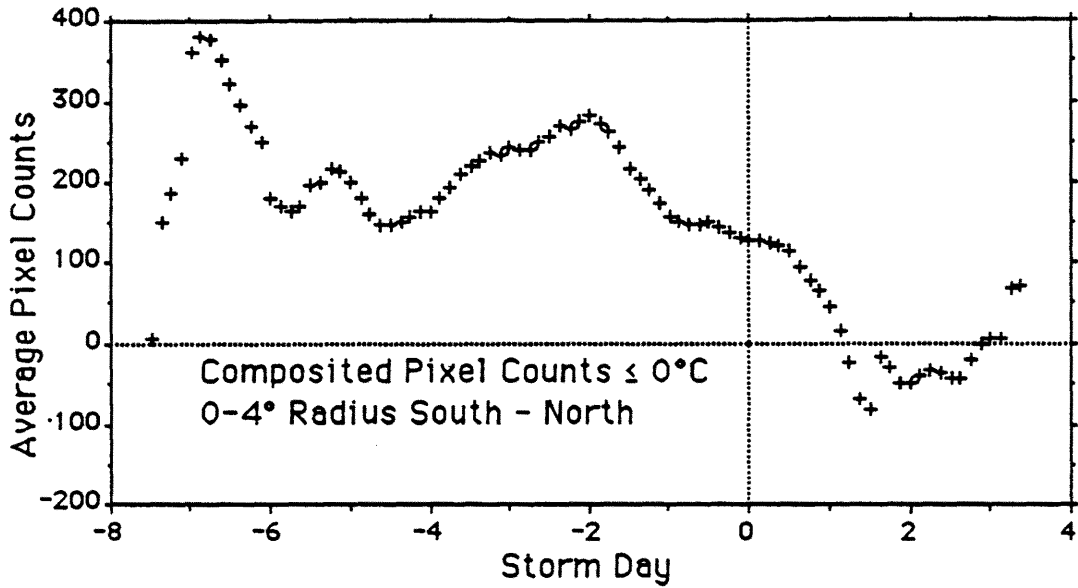


Figure 7.20: Composited south minus north convection differences. Ten storms were averaged, and only those points with five or more storms are displayed. The temperature threshold is 0°C .

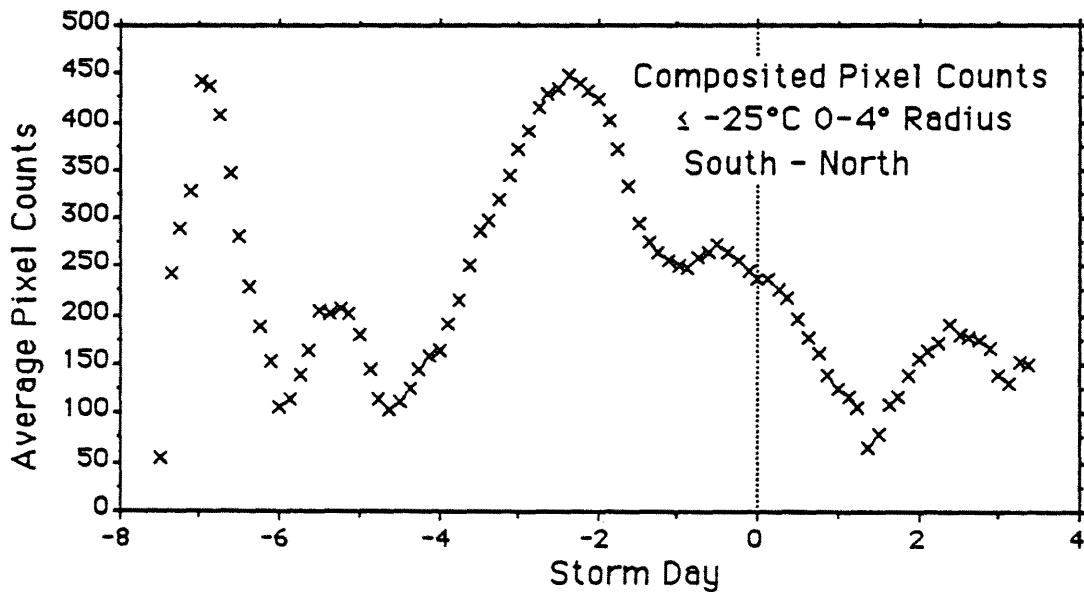


Figure 7.21: As in Fig. 7.20 except for -25°C convection.

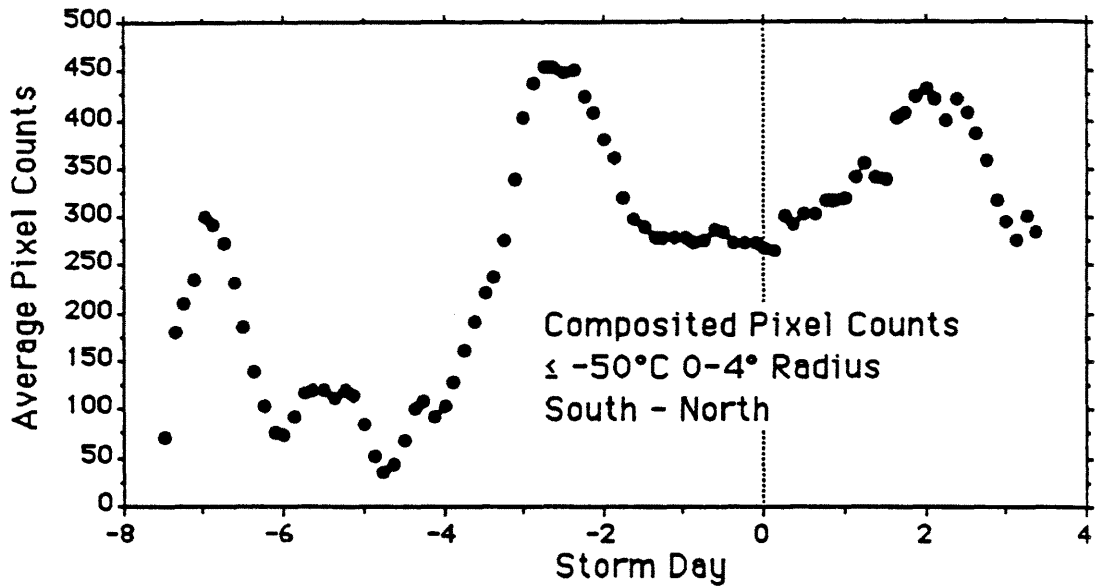


Figure 7.22: As in Fig. 7.20 except for -50°C convection.

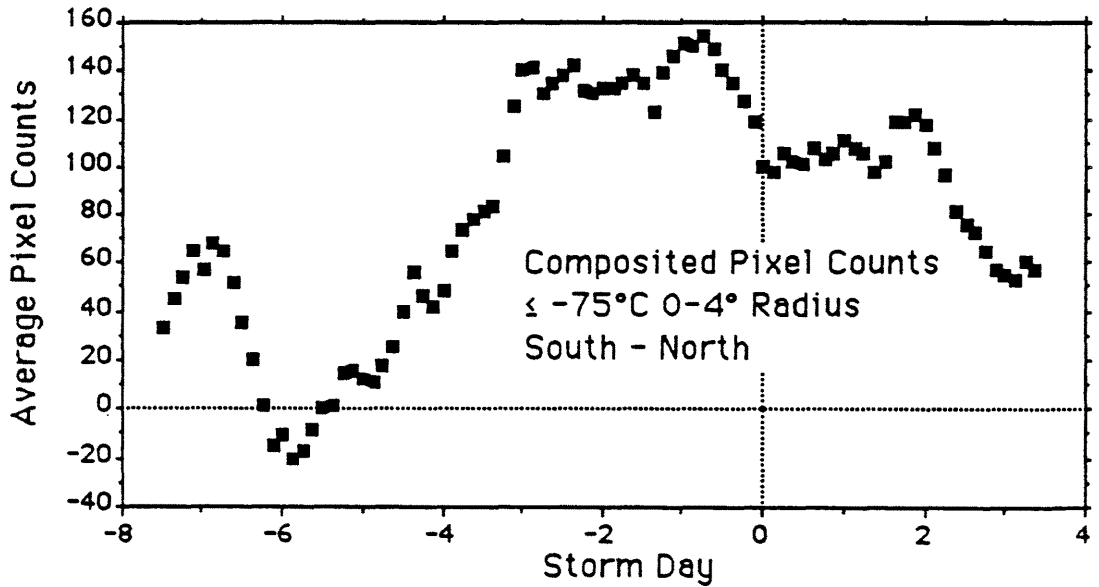


Figure 7.23: As in Fig. 7.20 except for -75°C convection.

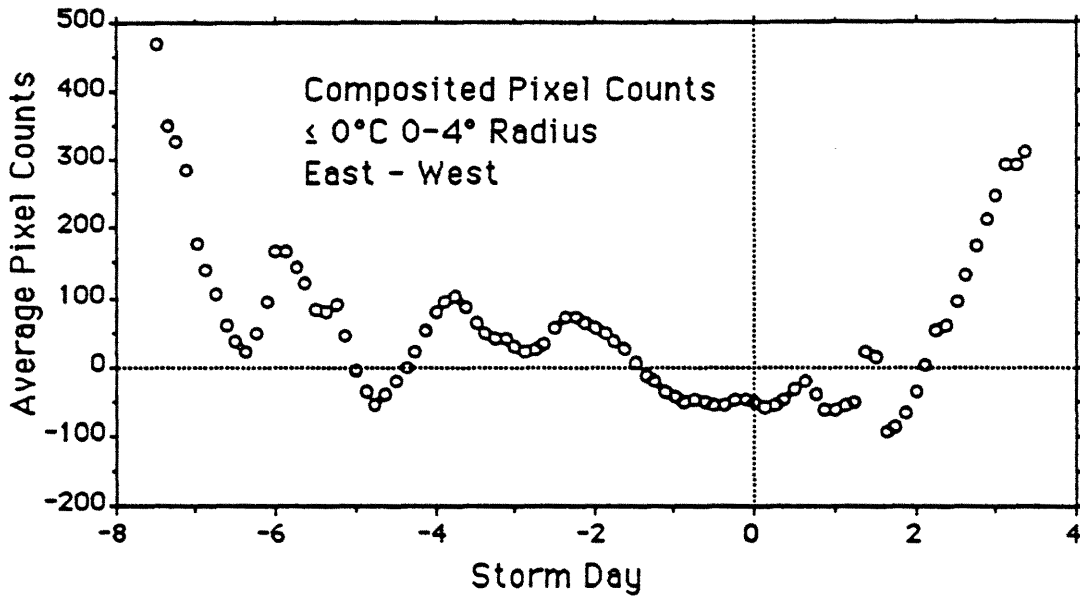


Figure 7.24: Composited east minus west convection differences. Ten storms were averaged, and only those points with five or more storms are displayed. The temperature threshold is 0°C .

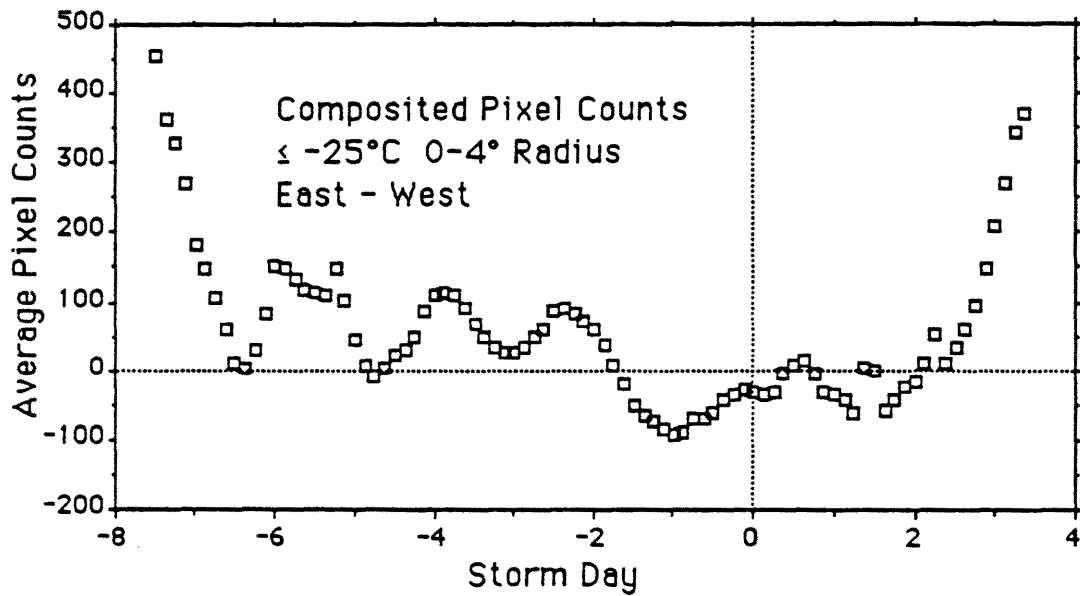


Figure 7.25: As in Fig. 7.24 except for -25°C convection.

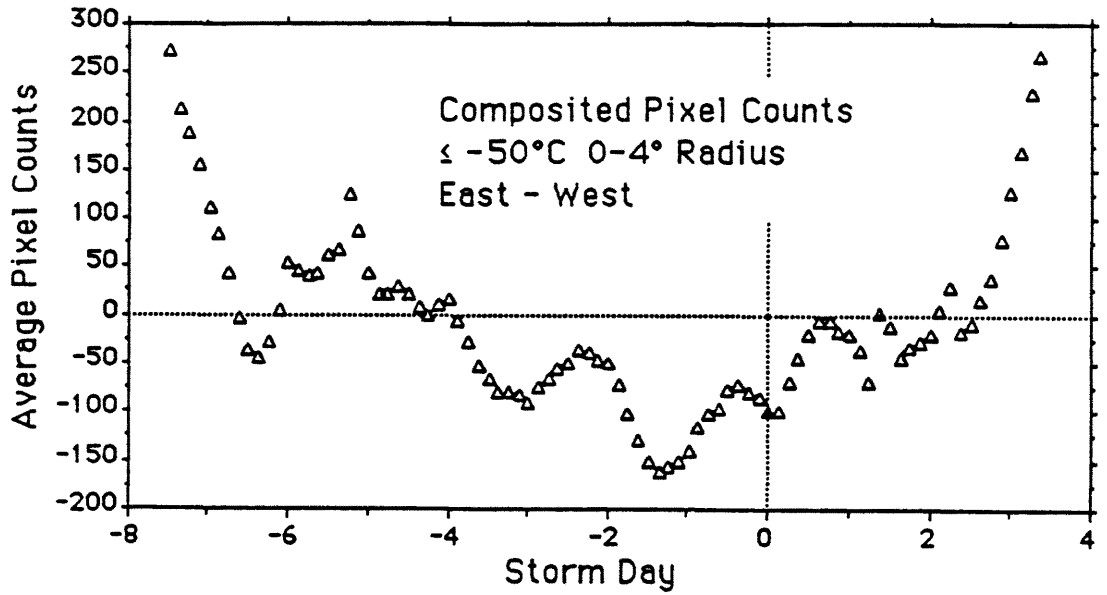


Figure 7.26: As in Fig. 7.24 except for -50°C convection.

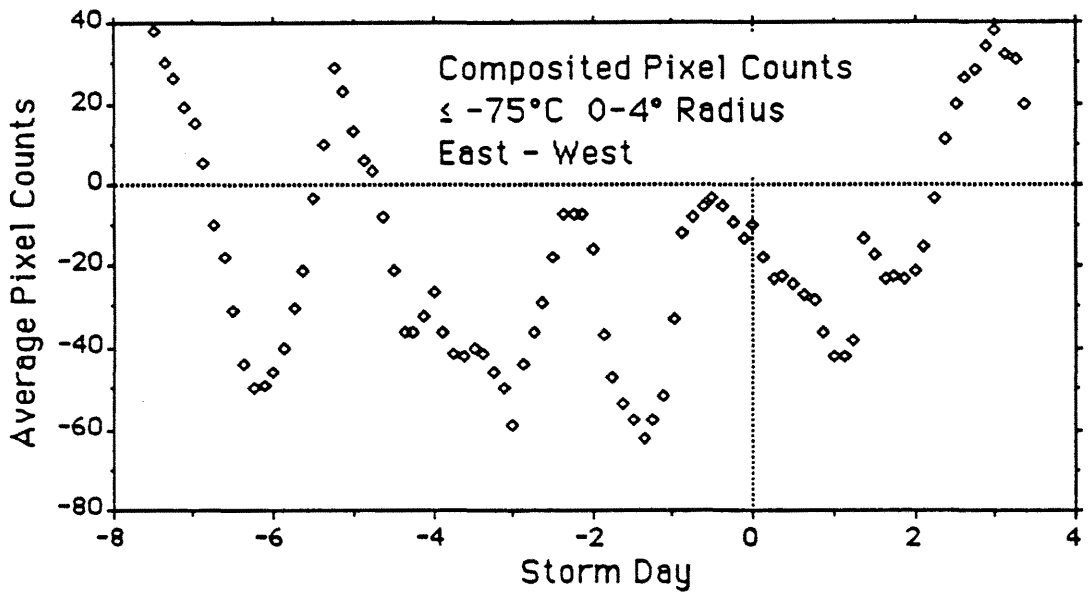


Figure 7.27: As in Fig. 7.24 except for -75°C convection.

order to bring about strengthening of winds. Small perturbations in the pressure field are apparently smoothed out quickly so as not to influence winds in just one quadrant. Asymmetric convection contributes to the entire wind field and thus the entire R15 profile, but no predictive signal for wind asymmetries is found. Currently, forecasters at JTWC are constructing symmetrical wind profiles and then adding TC motion vectors to predict wind asymmetries (personal communication with JTWC). This procedure has proven useful in the past and should continue to do so because TC motion is the primary cause of first order asymmetry in the wind field. In the future, archived synoptic data will become available to researchers and further study may identify causes of wind asymmetry in larger scale environmental features.

Chapter 8

SUMMARY AND CONCLUSIONS

8.1 Summary

The end of aircraft reconnaissance in the NWP in 1987 eliminated the best tool for measurement of R15 and R26 which are needed for warnings of rough seas and damaging winds. It is essential that new, satellite based techniques be developed and made available to forecasters for predicting R15. This study has attempted to initiate research on development of procedures which will immediately begin to fill the gap left by the loss of aircraft reconnaissance. Although limited in scope by the availability of only two years of concurrent aircraft and satellite data, and thus based on relationships which are not as tested as one might like, there appear to be some predictive signals in satellite data which correlate with certain aspects of the outer wind structure of TCs.

It was proposed that sustained deep convection is related to radial winds through continuity which is then related to changes of tangential winds. In this way, a physical basis was set for correlating convection with the extent of strong tangential winds in TCs. Running mean convection over 24, 48, and 72 hours, represented by cloud temperatures colder than -25°C within 444 km of the TC center, was shown to provide insight as to when R15 might be expected to either increase rapidly or decrease for intensifying TCs. The empirical rate of R15 decrease for filling storms was derived from the average rate of R15 decrease for a number of storms. A possible linear relationship for determining R15 using convection amounts for filling TCs was also examined.

Investigation of R15 throughout the lives of twelve TCs with good data continuity led to the identification of two types of cyclone evolution in the NWP. Values of R15 for "delayed" type TCs continue to increase after maximum intensity is reached. The R15 of

“simultaneous” type TCs follows intensity more closely and reaches its maximum value (MR15) within twelve hours of maximum intensity. Deep convection colder than -75°C in the 222 to 444 km annulus can be used in conjunction with satellite intensity measurements (Dvorak, 1975) to predict or observe when MR15 will occur for both delayed and simultaneous storms. Delayed TCs typically have a two day lead time following the end of the deep convection until maximum R15 occurs. For simultaneous TCs, MR15 occurs within twelve hours of the end of the deep convection, as does maximum intensity. Other attempts to use satellite radiance measurements to improve R15 specification and prediction were less successful. No relationships were found between concurrent values of convection and R15 or recent R15 change. There was also no correlation between convection asymmetry and R15 asymmetry. The Holland-Martin technique for determining outer wind profiles requires knowledge of the radius of maximum winds (personal communication with JTWC). In the absence of other measurements, R26 was shown to be correlated to R15 values and forecasters may derive approximate R26 values if R15 can be obtained. This technique may be advantageous when the radius of maximum winds is not known for a particular TC.

8.2 The Future

Improved satellite microwave imagery with better algorithms for determining surface wind speeds will add much needed data to the analysis of radial wind extent in tropical cyclones. More coverage from an increased number of platforms is needed to fill data gaps. Microwave derived winds with adequate areal coverage and timely availability to the forecaster would enhance the schemes developed here by providing more accurate initial data. Wind asymmetries would also become more apparent and new relationships could then be developed.

Other research that would be beneficial to forecasters includes an examination of the large scale synoptic data in relation to tangential winds. Studies of this nature might provide more insight into differences between delayed and simultaneous type TCs. Also, large scale vorticity values derived from this synoptic data may show correlations with R15

for formative storms. Relationships between convection and intensity, as well as intensity change, may become apparent.

Data sets which will allow such studies are currently being procured by Professor Gray's project at CSU and will be available for research in the future. The aircraft-satellite data set will be doubled to contain four years of concurrent data. This may be the most important portion of the data sets for developing additional satellite based TC forecasting techniques. There are many more procedures, techniques and rules that can be developed to maximize the use of satellite data in forecasting TCs and it is hoped that this paper stimulates more research that can be directly applied by tropical cyclone forecasters.

ACKNOWLEDGEMENTS

The author would like to thank Professor William M. Gray for his encouragement of my research on this subject of likely applicability to forecasters. I am indebted to him for his insights, suggestions, and help. Raymond Zehr provided the satellite data through NOAA/NESDIS/CIRA and gave invaluable advice. Thanks also go to: Todd Massey, Debra Lubich and William Thorson who wrote the programs which processed the satellite images and aircraft data. John Sheaffer made many valuable contributions to the editing and review of this manuscript. Thanks also to the project members for their discussions at our many meetings. Ms. Barbara Brumit was responsible for the final draft. Thanks also go to my wife, Vicki Griffeth, for her support on the home front. None of this would have been done without her.

The Air Force Institute of Technology sponsored my graduate studies at Colorado State University. Funding for this research was provided by the Air Force Geophysical Laboratory, Bedford, MA, Grant No. N00014-87- K-0203.

REFERENCES

- Arnold, C. P., 1977: Tropical cyclone cloud and intensity relationships. Dept. of Atmos. Sci. Paper No. 277, Colo. State Univ., Fort Collins, CO, 154 pp.
- Dunn and Miller, 1960. Atlantic hurricanes. Louisiana State Press, Baton Rouge, LA, 377 pp.
- Dvorak, V. F., 1975: Tropical cyclone intensity analysis and forecasting from satellite imagery. *Mon. Wea. Rev.*, 103, 420-430.
- Frank, W. M. and W. M. Gray, 1980: Radius and frequency of 15ms^{-1} (30 kt) winds around tropical cyclones. *J. Appl. Meteor.*, 19, 2, 219-223.
- Gray, W. M., 1981: Recent advances in tropical cyclone research from rawinsonde composite analysis. World Meteorological Organization Publication, Geneva, Switzerland, 407 pp.
- Holland, G. J., 1983: Angular momentum transports in tropical cyclones. *Quart. J. Roy. Meteor. Soc.*, 109, 187-209.
- Joint Typhoon Warning Center (JTWC), 1983: Annual tropical cyclone report. US Naval Oceanography Command Center, Joint Typhoon Warning Center, COMNAVMAR- IANAS Box 17, FPO, San Francisco, 96630.
- Joint Typhoon Warning Center (JTWC), 1984: Annual tropical cyclone report. US Naval Oceanography Command Center, Joint Typhoon Warning Center, COMNAVMAR- IANAS Box 17, FPO, San Francisco, 96630.
- McBride, J. L. and W. M. Gray, 1980a: Mass divergence and vertical velocity in tropical weather systems, Part I: Diurnal variation. *Quart. J. Roy. Meteor. Soc.*, 106, 449, 501-516.
- McBride, J. L. and W. M. Gray, 1980b: Mass divergence and vertical velocity in tropical weather systems, Part II: Large-scale controls on convection. *Quart. J. Roy. Meteor. Soc.*, 106, 449, 517-538.
- Merrill, R. T., 1982: A comparison of large and small tropical cyclones. Dept. of Atmos. Sci. Paper No. 352, Colo. State Univ., Ft. Collins, CO, 75 pp.
- Merrill, R. T., 1984: A comparison of large and small tropical cyclones. *Mon. Wea. Rev.*, 112, 7, 1408-1418.
- Statview 512+, 1986: Brainpower Inc., 24009 Ventura Blvd., Calabasas, CA, 91302.
- Weatherford, C., 1985: Typhoon structural variability. Dept. of Atmos. Sci. Paper No. 391, Colo. State Univ., Ft. Collins, CO, 77 pp.

- Weatherford, C., 1989: The structural evolution of typhoons. Dept. of Atmos. Sci. Paper No. 446, Colo. State Univ., Ft. Collins, CO, 198 pp.
- Weatherford, C., and W. M. Gray, 1988: Typhoon structure as revealed by aircraft reconnaissance: Part I: Data analysis and climatology. *Mon. Wea. Rev.*, Vol. 116, 5, 1032-1043.
- Weatherford, C., and W. M. Gray, 1988: Typhoon structure as revealed by aircraft reconnaissance: Part II: Structural variability. *Mon. Wea. Rev.*, Vol. 116, 5, 1044-1056.
- Wei, D., W. M. Gray, 1984: Estimation of typhoon outer wind strength from satellite imagery. Forthcoming Dept. of Atmos. Sci. Paper, Colo. State Univ., Fort Collins, CO.
- World Climate Programme, 1985: International satellite cloud climatology project—Description of reduced resolution radiance data. World Meteorological Organization/T.D., No. 58, Geneva, Switzerland.
- Zehr, R., 1987: The diurnal variation of deep convective clouds and cirrus with tropical cyclones. Paper presented at the 17th Technical Conference on Hurricanes and Tropical Meteorology, April 7-10, Miami, FL, 4 pp.
- Zehr, R., 1987: The diurnal variation of deep convective clouds and cirrus with tropical cyclones. Paper submitted to *Mon. Wea. Rev.*

W. M. GRAY'S FEDERALLY SUPPORTED RESEARCH PROJECT
REPORTS SINCE 1967

CSU Dept. of
Atmos. Sci.

<u>Report No.</u>	<u>Report Title, Author, Date, Agency Support</u>
104	The Mutual Variation of Wind, Shear and Baroclinicity in the Cumulus Convective Atmosphere of the Hurricane (69 pp.). W. M. Gray. February 1967. NSF Support.
114	Global View of the Origin of Tropical Disturbances and Storms (105 pp.). W. M. Gray. October 1967. NSF Support.
116	A Statistical Study of the Frictional Wind Veering in the Planetary Boundary Layer (57 pp.). B. Mendenhall. December 1967. NSF and ESSA Support.
124	Investigation of the Importance of Cumulus Convection and ventilation in Early Tropical Storm Development (88 pp.). R. Lopez. June 1968. ESSA Satellite Lab. Support.
Unnumbered	Role of Angular Momentum Transports in Tropical Storm Dissipation over Tropical Oceans (46 pp.). R. F. Wachtmann. December 1968. NSF and ESSA Support.
Unnumbered	Monthly Climatological Wind Fields Associated with Tropical Storm Genesis in the West Indies (34 pp.). J. W. Sartor. December 1968. NSF Support.
140	Characteristics of the Tornado Environment as Deduced from Proximity Soundings (55 pp.). T. G. Wills. June 1969. NOAA and NSF Support.
161	Statistical Analysis of Trade Wind Cloud Clusters in the Western North Pacific (80 pp.). K. Williams. June 1970. ESSA Satellite Lab. Support.
—	A Climatology of Tropical Cyclones and Disturbances of the Western Pacific with a Suggested Theory for Their Genesis/Maintenance (225 pp.). W. M. Gray. NAVWEARSCHFAC Tech. Paper No. 19-70. November 1970. (Available from US Navy, Monterey, CA). US Navy Support.
179	A diagnostic Study of the Planetary Boundary Layer over the Oceans (95 pp.). W. M. Gray. February 1972. Navy and NSF Support.
182	The Structure and Dynamics of the Hurricane's Inner Core Area (105 pp.). D. J. Shea. April 1972. NOAA and NSF Support.
188	Cumulus Convection and Larger-scale Circulations, Part I: A Parametric Model of Cumulus Convection (100 pp.). R. E. Lopez. June 1972. NSF Support.
189	Cumulus Convection and Larger-scale Circulations, Part II: Cumulus and Meso-scale Interactions (63 pp.). R. E. Lopez. June 1972. NSF Support.

CSU Dept. of
Atmos. Sci.

<u>Report No.</u>	<u>Report Title, Author, Date, Agency Support</u>
190	Cumulus Convection and Larger-scale Circulations, Part III: Broadscale and Meso-scale Considerations (80 pp.). W. M. Gray. July 1972. NOAA-NESS Support.
195	Characteristics of Carbon Black Dust as a Tropospheric Heat Source for Weather Modification (55 pp.). W. M. Frank. January 1973. NSF Support.
196	Feasibility of Beneficial Hurricane Modification by Carbon Black Seeding (130 pp.). W. M. Gray. April 1973. NOAA Support.
199	Variability of Planetary Boundary Layer Winds (157 pp.). L. R. Hoxit. May 1973. NSF Support.
200	Hurricane Spawned Tornadoes (57 pp.). D. J. Novlan. May 1973. NOAA and NSF Support.
212	A Study of Tornado Proximity Data and an Observationally Derived Model of Tornado Genesis (101 pp.). R. Maddox. November 1973. NOAA Support.
219	Analysis of Satellite Observed Tropical Cloud Clusters (91 pp.). E. Ruprecht and W. M. Gray. May 1974. NOAA/NESS Support.
224	Precipitation Characteristics in the Northeast Brazil Dry Region (56 pp.). R. P. L. Ramos. May 1974. NSF Support.
225	Weather Modification through Carbon Dust Absorption of Solar Energy (190 pp.). W. M. Gray, W. M. Frank, M. L. Corrin, and C. A. Stokes. July 1974.
234	Tropical Cyclone Genesis (121 pp.). W. M. Gray. March 1975. NSF Support.
—	Tropical Cyclone Genesis in the Western North Pacific (66 pp.). W. M. Gray. March 1975. US Navy Environmental Prediction Research Facility Report. Tech. Paper No. 16-75. (Available from the US Navy, Monterey, CA). Navy Support.
241	Tropical Cyclone Motion and Surrounding Parameter Relationships (105 pp.). J. E. George. December 1975. NOAA Support.
243	Diurnal Variation of Oceanic Deep Cumulus Convection. Paper I: Observational Evidence, Paper II: Physical Hypothesis (106 pp.). R. W. Jacobson, Jr. and W. M. Gray. February 1976. NOAA-NESS Support.
257	Data Summary of NOAA's Hurricanes Inner-Core Radial Leg Flight Penetrations 1957-1967, and 1969 (245 pp.). W. M. Gray and D. J. Shea. October 1976. NSF and NOAA Support.
258	The Structure and Energetics of the Tropical Cyclone (180 pp.). W. M. Frank. October 1976. NOAA-NHEML, NOAA-NESS and NSF Support.

CSU Dept. of
Atmos. Sci.

<u>Report No.</u>	<u>Report Title, Author, Date, Agency Support</u>
259	Typhoon Genesis and Pre-typhoon Cloud Clusters (79 pp.). R. M. Zehr. November 1976. NSF Support.
Unnumbered	Severe Thunderstorm Wind Gusts (81 pp.). G. W. Walters. December 1976. NSF Support.
262	Diurnal Variation of the Tropospheric Energy Budget (141 pp.). G. S. Foltz. November 1976. NSF Support.
274	Comparison of Developing and Non-developing Tropical Disturbances (81 pp.). S. L. Erickson. July 1977. US Army Support.
—	Tropical Cyclone Research by Data Compositing (79 pp.). W. M. Gray and W. M. Frank. July 1977. US Navy Environmental Prediction Research Facility Report. Tech. Paper No. 77-01. (Available from the US Navy, Monterey, CA). Navy Support.
277	Tropical Cyclone Cloud and Intensity Relationships (154 pp.). C. P. Arnold. November 1977. US Army and NHEML Support.
297	Diagnostic Analyses of the GATE A/B-scale Area at Individual Time Periods (102 pp.). W. M. Frank. November 1978. NSF Support.
298	Diurnal Variability in the GATE Region (80 pp.). J. M. Dewart. November 1978. NSF Support.
299	Mass Divergence in Tropical Weather Systems, Paper I: Diurnal Variation; Paper II: Large-scale Controls on Convection (109 pp.). J. L. McBride and W. M. Gray. November 1978. NOAA-NHEML Support.
—	New Results of Tropical Cyclone Research from Observational Analysis (108 pp.). W. M. Gray and W. M. Frank. June 1978. US Navy Environmental Prediction Research Facility Report. Tech. Paper No. 78-01. (Available from the US Navy, Monterey, CA). Navy Support.
305	Convection Induced Temperature Change in GATE (128 pp.). P. G. Grube. February 1979. NSF Support.
308	Observational Analysis of Tropical Cyclone Formation (230 pp.). J. L. McBride. April 1979. NOAA-NHEML, NSF and NEPRF Support.
—	Tropical Cyclone Origin, Movement and Intensity characteristics Based on Data Compositing Techniques (124 pp.). W. M. Gray. August 1979. US Navy Environmental Prediction Research Facility Report. Tech. Paper No. CR-79-06. (Available from the US Navy, Monterey, CA). Navy Support.

CSU Dept. of
Atmos. Sci.

Report No.

Report Title, Author, Date, Agency Support

- Further Analysis of Tropical Cyclone Characteristics from Rawinsonde Compositing Techniques (129 pp.). W. M. Gray. March 1981. US Navy Environmental Prediction Research Facility Report. Tech. Paper No. CR-81-02. (Available from the US Navy, Monterey, CA). Navy Support.
- 333 Tropical Cyclone Intensity Change—A Quantitative Forecasting Scheme. K. M. Dropco. May 1981. NOAA Support.
- Recent Advances in Tropical Cyclone Research from Rawinsonde Composite Analysis (407 pp.). WMO Publication. W. M. Gray. 1981.
- 340 The Role of the General Circulation in Tropical Cyclone Genesis (230 pp.). G. Love. April 1982. NSF Support.
- 341 Cumulus Momentum Transports in Tropical Cyclones (78 pp.). C. S. Lee. May 1982. ONR Support.
- 343 Tropical Cyclone Movement and Surrounding Flow Relationships (68 pp.). J. C. L. Chan and W. M. Gray. May 1982. ONR Support.
- 346 Environmental Circulations Associated with Tropical Cyclones Experiencing Fast, Slow and Looping Motions (273 pp.). J. Xu and W. M. Gray. May 1982. NOAA and NSF Support.
- 348 Tropical Cyclone Motion: Environmental Interaction Plus a Beta Effect (47 pp.). G. J. Holland. May 1982. ONR Support.
- Tropical Cyclone and Related Meteorological Data Sets Available at CSU and Their Utilization (186 pp.). W. M. Gray, E. Buzzell, G. Burton and Other Project Personnel. February 1982. NSF, ONR, NOAA, and NEPRF Support.
- 352 A Comparison of Large and Small Tropical Cyclones (75 pp.). R. T. Merrill. July 1982. NOAA and NSF Support.
- 358 On the Physical Processes Responsible for Tropical Cyclone Motion (200 pp.). Johnny C. L. Chan. November 1982. NSF, NOAA/NHRL and NEPRF Support.
- 363 Tropical Cyclones in the Australian/Southwest Pacific Region (264 pp.). Greg J. Holland. March 1983. NSF, NOAA/NHRL and Australian Government Support.
- 370 Atlantic Seasonal Hurricane Frequency, Part I: El Nino and 30 mb QBO Influences; Part II: Forecasting Its Variability (105 pp.). W. M. Gray. July 1983. NSF Support.
- 379 A Statistical Method for One- to Three-Day Tropical Cyclone Track Prediction (201 pp.). Clifford R. Matsumoto. December, 1984. NSF/NOAA and NEPRF support.
- Varying Structure and Intensity Change Characteristics of Four Western North Pacific Tropical Cyclones. (100 pp.). Cecilia A. Askue and W. M. Gray. October 1984. US Navy Environmental Prediction Research Facility Report No. CR 84-08. (Available from the US Navy, Monterey, CA). Navy Support.

CSU Dept. of
Atmos. Sci.

<u>Report No.</u>	<u>Report Title, Author, Date, Agency Support</u>
—	Characteristics of North Indian Ocean Tropical Cyclone Activity. (108 pp.). Cheng-Shang Lee and W. M. Gray. December 1984. US Navy Environmental Prediction Research Facility Report No. CR 84-11. (Available from the US Navy, Monterey, CA). Navy Support.
391	Typhoon Structural Variability. (77 pp.). Candis L. Weatherford. October, 1985. NSF/NOAA Support.
392	Global View of the Upper Level Outflow Patterns Associated with Tropical Cyclone Intensity Change During FGGE. (126 pp.). L. Chen and W. Gray. October, 1985. NASA support.
394	Environmental Influences on Hurricane Intensification. (156 pp.). Robert T. Merrill. December, 1985. NSF/NOAA Support.
403	An Observational Study of Tropical Cloud Cluster Evolution and Cyclogenesis in the Western North Pacific. (250 pp.). Cheng-Shang Lee. September, 1986. NSF/NOAA support.
—	Factors Influencing Tropical Cyclone Genesis as Determined from Aircraft Investigative Flights into Developing and Non-Developing Tropical Disturbances in the Western North Pacific. Michael Middlebrooke. October, 1986 (70 pp.). NSF/NOAA support.
—	Recent Colorado State University Tropical Cyclone Research of Interest to Forecasters. (115 pp.). William M. Gray. June, 1987. US Navy Environmental Prediction Research Facility Contractor Report CR 87-10. Available from US Navy, Monterey, CA. Navy support.
428	Tropical Cyclone Observation and Forecasting With and Without Aircraft Reconnaissance. (105 pp.) Joel D. Martin. May, 1988. USAF, NWS, ONR support.
429	Investigation of Tropical Cyclone Genesis and Development Using Low-level Aircraft Flight Data. (94 pp.) Michael G. Middlebrooke. May, 1988. USAF, NSF support.
436	Environmental and convective influence on tropical cyclone development vs. non-development. (105 pp.) Patrick A. Lunney. December, 1988.
446	The structural evolution of typhoons. (198 pp.). Candis Weatherford. July, 1989. NSF/NOAA and ONR Support